CHROMOSPHERIC EFFECTS ON GLOBAL SOLAR OSCILLATIONS

Alan Johnston

A Thesis Submitted for the Degree of PhD
at the
University of St Andrews

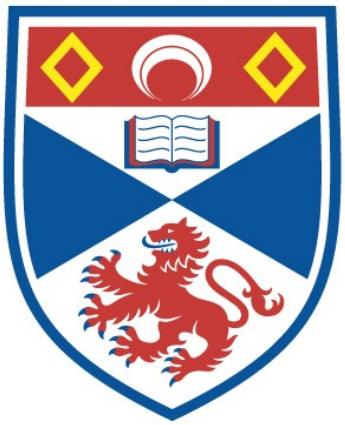

1994

Chromospheric Effects on Global Solar Oscillations

Alan Johnston

A thesis submitted for the degree of Doctor of Philosophy
at the University of St. Andrews.

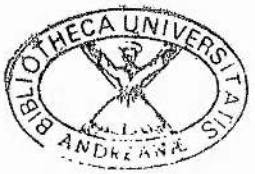

ProQuest LLC.
789 East Eisenhower Parkway
P.O. Box 1346
Ann Arbor, MI 48106 – 1346

Abstract

A study has been made of the global solar oscillations known as p-modes. The Sun is represented by a plane-parallel stratified plasma. Solutions are found to the magnetohydrodynamic equations of motion in such a plasma, and normal mode frequencies are calculated by applying realistic boundary conditions to these solutions. The normal modes model solar p-modes.

For a model consisting of an isothermal chromosphere with a uniform horizontal magnetic field, it is demonstrated that modes may form at all frequencies. Consideration is also given to the related problem of vertical propagation of fast magnetoacoustic waves in a uniform magnetic field.

An investigation is carried out into the observed solar cycle variations in the frequencies of p-modes in the classical, low frequency range (1–5 mHz). A possible mechanism for the observed "turnover" effect is discussed. Through the use of a modified Bohr-Sommerfeld condition, the effect of a non-isothermal chromosphere is also considered, and a physical description of chromospheric effects on p-mode frequencies is given.

The formation of modes above the acoustic cut-off frequency is investigated. The theoretically calculated forms of frequency shift curves in this high frequency range agree well with observations.

The special case of modes of degree zero is also briefly examined. A mathematical formulation for such modes is constructed, and frequency shifts are determined for a simple chromospheric model atmosphere.

I, Alan Thomas Frederick Reilly Johnston, hereby certify that this thesis has been composed by myself, that it is a record of my own work, and that it has not been accepted in partial or complete fulfilment of any other degree or professional qualification.

Signed

Date 13/1/94

I was admitted to the Faculty of Science of the University of St. Andrews under Ordinance General No. 12 on October 1st 1990 and as a candidate for the Degree of Ph.D. on October 1st 1991.

Signed ..... Date 13/1/95

I hereby certify that the candidate has fulfilled the conditions of the Resolution and Regulations appropriate to the degree of Ph.D.

Signature of Supervisor . ... Date 13/1/94

In submitting this thesis to the University of St. Andrews I understand that I am giving permission for it to be made available for use in accordance with the regulations of the University Library for the time being in force, subject to any copyright vested in the work not being affected thereby. I also understand that the title and abstract will be published, and that a copy of the work may be made and supplied to any *bona fide* library or research worker.

Acknowledgements

I would like to record my thanks to my supervisor, Bernard Roberts, for all his assistance and advice during my time as a post-graduate student. Rarely have I left his office without some light having been shed on my seemingly hopeless problem! My gratitude is also due to Andy Wright for his patience and help at a crucial stage of my degree.

I have been lucky to work in such a friendly and relaxed environment as the St. Andrews solar group, and for this my appreciation is due to all my fellow students. I would particularly like to mention my office-mates, Partha Joarder, Richard Ireland, Robert Walsh and Graham Forster — thanks, it's been a lot of fun.

Finally, I would like to thank my wife, Karen, for all the love and support she has given me over the last three (and a bit) years; it is having Karen to return home to after a long day's work that makes everything worthwhile. To her I dedicate this thesis.

Contents

Chapter 1

Introduction

1.1 The Sun

Throughout history, the Sun has occupied a central position in philosophy and science. Primitive peoples worshipped the Sun as a god, and the earliest astronomers used the relative motions of the Sun and the Earth to form the basis of our calendar. The idea that the Earth revolved around the Sun, or that the Sun itself was not a 'flawless' object, challenged the philosophical and religious beliefs of the time; and to this day, scientific study of the Sun gives unique insights into universal physical processes.

The Sun is an average star, of unexceptional mass and luminosity, in the middle of a relatively stable phase of its evolution. What makes it exceptional to us is obviously its proximity. It is the only star which we can resolve as a disc, and whose light we can study in great detail. We can measure the total energy it produces, and calculate its mass from observations of planetary motions. We can observe the many surface features it displays, and note how they vary in form and in number over the years. But the opacity of the material which makes up the Sun prevents us from directly observing its interior: the light we receive on Earth can only tell us about the very outermost layers of the Sun. In the past, descriptions of the solar interior have necessarily been based on conjecture and inference; we shall see, however, that a new method of solar observation promises to give us unique information about the solar interior.

The intention of this introduction is firstly to describe, in general terms, the relevant properties of both the Sun (section 1.1) and its global oscillations (section 1.2). In doing this we will briefly introduce some of the problems we wish to tackle in the later chap-

ters of the thesis. We go on to introduce the basic physical laws governing these oscillations (section 1.3), and introduce some of the mathematical models we shall use (sections 1.4 and 1.5). The chapter concludes with an outline of the thesis (section 1.6).

1.1.1 Solar structure

In basic terms, the Sun is a ball of matter, which is thought to have formed at some stage in the past due to the mutual gravitational attraction of its constituents. As the embryonic Sun condensed, the temperature at its centre rose, until nuclear reactions could commence. From this point, the Sun settled into an equilibrium where the outflow of energy from the centre balanced the centrally directed force of gravity. We will assume that the Sun is in such an equilibrium state, and can vary only in the short term.

The total mass of the Sun is around 1.99×10^{30} kg, which would balance with over 300 000 Earths, and its radius is 696 000 km, or over 100 times that of the Earth. The Sun is largely composed of two elements, hydrogen and helium, with the former comprising 90% of the total mass. Throughout the bulk of the Sun, matter exists in the form of a *plasma*, that is to say an ionised gas.

The energy generation referred to above takes place in the *core* of the Sun; temperatures in the core are given by models to be around 15 000 000 K. The photons produced through these processes are at very high energies, but the great opacity of the interior of the Sun ensures that they are not immediately released into space. Instead, as they venture outwards from the core, they are repeatedly absorbed and re-radiated by ions at progressively lower temperatures; this region is known as the *radiative zone*. This process lowers the energies, and thus increases the wavelengths, of the emitted photons. Those eventually emitted by the outermost layer, the *photosphere*, are of wavelengths lying within the optical range.

Immediately below the photosphere lies a region in which radiation alone cannot transport energy efficiently enough. The process of *convection*, or bulk motion of plasma in a characteristic cellular pattern, takes over as the major energy transport process, and so this region is known as the *convection zone*.

The photosphere is thin compared with the solar radius, with a thickness of only around 500km. However, this region is the source of the bulk of the emitted light. Within the spectrum of light received at the Earth, it is possible to detect dark *absorption lines*, where

light of a particular wavelength has been absorbed or scattered by particles in the upper photosphere, and thus inhibited from reaching the Earth. At the top of the photosphere, the temperature drops to a minimum value of around 4170K; this point is referred to as the *temperature minimum*. This is also taken as the dividing line between the solar interior and the solar atmosphere, which we now describe.

Immediately above the temperature minimum lies the region known as the *chromosphere*. The temperature rises gradually throughout the chromosphere, which has a height of around 2000km. Like the photosphere, the chromosphere is responsible for various absorption lines; indeed, the chromosphere is so named because of its colourful appearance in eclipses, caused by the scattering of light at certain wavelengths. The upper limit of the chromosphere is formed by the *transition region*, where the temperature jumps abruptly to several hundred thousand Kelvin; above the transition region lies the *corona*, which extends outwards into space.

1.1.2 Solar magnetism and the solar cycle

The brief outline of solar structure given above omits any mention of one of the Sun's most fundamental features: its magnetic field. Any plasma element will suffer electromagnetic forces due to other plasma elements, and these forces can be described in terms of electric and magnetic fields. For most processes occurring on the Sun, we find that the magnetic field acts as if it were 'frozen in' to the plasma, so configurations of the magnetic field are of the utmost importance in describing and modelling the solar features described below. The magnetic field is particularly important when our interest lies in any of the atmospheric features displayed by the Sun.

A commonly used concept is that of the *plasma* β, which is usually defined as the ratio of the gas pressure to the magnetic pressure at a point. Thus a low-β plasma will be dominated by the magnetic field, while a high-β plasma will act virtually as if no magnetic field were present. In the interior of the Sun, the intense gas pressure means that the plasma β is very high; in the chromosphere and corona, however, the relatively strong magnetic fields and rarefied atmosphere ensure a low value for β.

It is believed that magnetic fields are generated at the base of the convection zone in the form of *flux tubes*. These are self-contained 'strings' of intense magnetic flux, which rise through the convection zone to eventually emerge at the solar surface. The cellular

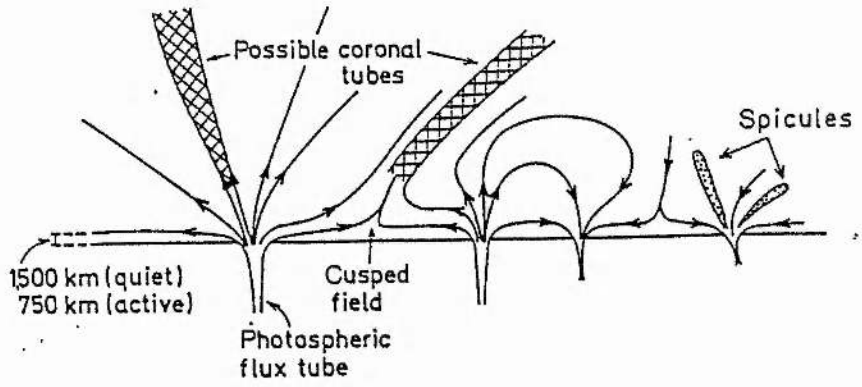

Figure 1.1: Schematic form of the chromospheric magnetic field, reproduced from Spruit and Roberts (1983).

nature of convective motion acts to aggregate flux tubes at the cell boundaries. At the emergent points of the tube structures, the intense magnetic fields create *sunspots*, dark areas on the solar surface. Sunspots are cooler than the surrounding solar surface, as the strong magnetic fields locally inhibit convection.

In the chromosphere, the magnetic flux fans out to occupy the entire atmosphere. The magnetic field takes up many forms, as depicted in Figure 1.1, but above a certain height in the chromosphere, the magnetic field is approximately horizontal in alignment. We say that the magnetic field exists in the form of a *magnetic canopy*. Below the canopy, the atmosphere is largely devoid of magnetic field, except where sunspots or intense flux tubes are emerging. This picture is necessarily a simple one; there will be many local variations in the magnetic field topology, and the height of the canopy will itself vary. However, there is some observational evidence for this form of magnetic field (Giovanelli, 1980; Giovanelli and Jones, 1982; Jones and Giovanelli, 1983), and it provides a useful basis for mathematical modelling of the chromosphere.

In the corona, a variety of interesting features such as prominences, flares and mass ejections result from the configurations of the magnetic field. The magnetic field is also thought to play an important role in the heating of the corona, by such processes as the damping of Alfvén waves. It is observed that solar magnetic features tend to cluster into definite regions of increased activity; these areas are known as *active regions*. The size and number of active regions visible on the Sun varies, as we shall now describe.

For several hundred years it has been observed that the Sun undergoes a cycle of activity. For some years it will be quiet, with few active regions and few sunspots. Gradually the activity will increase, with the solar latitude at which the active regions are found following a distinctive pattern. After a period of maximum activity, the level of which varies from cycle to cycle, the activity will decrease rapidly, and the cycle will start again. This process is known as the *solar cycle*. The average period of the cycle is around 10–11 years, and the last maximum occurred around the year 1989. The overall luminosity of the Sun does not vary significantly over the cycle; it is simply those features which we customarily associate with the solar magnetic field which undergo marked cyclical changes. Thus the solar cycle is considered to be fundamentally a magnetic effect.

This has been a necessarily brief description of solar structure and magnetism. For a more detailed account, see Priest (1982).

1.2 Global solar oscillations

It is over thirty years since the first report of global solar oscillations was published (Leighton, 1960). Since then, a vast quantity of observation has confirmed that the surface of the Sun is oscillating, not randomly, but in a regular way. Analysis of the surface velocity fluctuations reveals thousands of individual oscillations, each with its own distinct frequency (Libbrecht, Woodard and Kaufman, 1990; Elsworth, Howe, Isaak, McLeod and New, 1990). The Sun is a violent, noisy object; there are many processes which could conceivably disturb the solar surface. But how do these disturbances organise themselves to create such regular motions? And what determines the individual frequencies of these oscillations?

1.2.1 Formation

The fundamental explanation was provided by Ulrich (1970) and later Leibacher and Stein (1971). They postulated that the surface motions are the visible effect of the trapping of sound waves inside the Sun. Given a disturbance in the solar interior, sound waves will propagate outwards in all directions. A wave directed towards the centre of the Sun will encounter progressively higher temperatures, and thus sound speeds, causing the end of the wavefront nearer the centre of the Sun to travel faster than the end nearer the surface. This has the effect of turning the wave around, through the horizontal, until the wave is propagating outwards, as depicted in Figure 1.2. Eventually the outward-

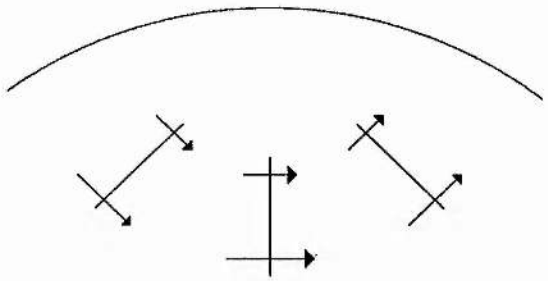

Figure 1.2: Schematic diagram depicting refraction of plane wavefront propagating in a region of radially stratified sound speed.

propagating wave will reach the solar surface. For waves with frequencies less than a critical value, the rapid decrease in density at the surface acts to reflect the wave; higher frequency waves can propagate through the surface without significant reflection. The frequency which is classically taken as the dividing line between these two cases is called the *acoustic cut-off frequency*. This was first formulated mathematically for a generally stratified gas by Lamb (1932); this frequency has a value of around 5.3mHz at the temperature minimum.

The conclusion is that waves of a sufficiently low frequency can be trapped by refraction within a finite volume in the solar interior. For a particular wave, we call the region in which it is trapped its *cavity*; it is the dimensions and properties of this cavity which select the distinct frequencies observed. In essence, a standing wave is set up within the cavity, and we call a particular configuration of the standing wave with respect to the cavity a *mode*.

The process which selects the frequencies of each mode is constructive interference, which operates as follows. For certain waves, the repeated processes of refraction and reflection will act in such a way that the wave can return to retrace its original ray path, as in Figure 1.3. This is a first requirement for constructive interference to occur; the consequence of this requirement is the introduction of the integer l, called the *degree* of a mode. This is equivalent to the number of occasions on which the wave undergoes reflection during its transit of the Sun, so Figure 1.3 depicts a mode of degree l=4. Remembering that the Sun is a sphere, we see that this corresponds to the number of great circles on the solar surface which are nodal lines for the standing wave.

The mode depicted in Figure 1.3 penetrates deep within the Sun. Higher degree

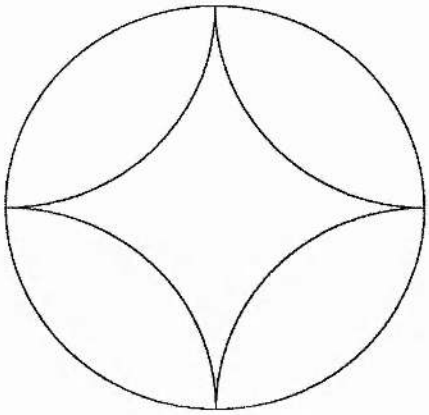

Figure 1.3: Schematic ray path for mode of degree l=4

modes will not, however, be able to travel far from the solar surface. For such modes, we can effectively ignore the spherical nature of the Sun, and treat the solar surface as a plane. This approach is described further in section 1.4.1.

The second requirement is that once the wave has returned to its original ray path, the wave will actually be in phase with the original disturbance. This condition chooses the frequency of the mode. Obviously, overtones will exist; these are classified by the whole number n, called the *radial order*. This number corresponds to the number of nodes of the standing wave on a radius of the Sun.

Thus for our purposes, an individual mode is defined by a pair of numbers, the degree, l, and the radial order, n. A third number, the azimuthal order m, tells us how many of the surface nodal lines are perpendicular to the equator. Since we ignore the effect of solar rotation, however, this number is not invoked in our later analysis.

Note that the description given above is only adequate for modes of non-zero degree. There also exist modes for which $l = 0$, that is to say for which the whole solar surface is oscillating in phase. Since the wavefront of those waves responsible for these modes must be spherical, the process of refraction described above cannot provide a base to the cavity within the solar interior. This special case is investigated in Chapter 6.

The oscillations we have just described are termed *p-modes*, a notation introduced by Cowling (1941). This reflects the fact that pressure is the driving force behind the sound waves which form the modes. Other forms of mode exist, in particular the fundamental

mode or *f-mode*, which can be viewed as the $n = 0$ case of p-modes, and gravity modes or *g-modes*, for which the driving force is the buoyancy force upon a displaced plasma element. However, it is p-modes which make up the subject of this thesis.

1.2.2 Properties

What are the specific properties of p-modes, as revealed by observations? Since the first detailed observations of p-modes, most reports have given the range of frequencies observed as being from around 1mHz to around 5mHz, with the peak of power at around 3.3mHz. This has led to the name '5-minute oscillations' being applied to p-modes. Since the acoustic cut-off frequency is around 5.3mHz at the temperature minimum, and since in "classical" p-mode theory only waves with frequencies less than the cut-off can form standing waves, this upper limit of the observed range is much as expected. However, recent observations (Libbrecht, 1988; Duvall Jr., Harvey, Jefferies and Pomerantz, 1991; Fernandes, Scherrer, Tarbell and Title, 1992; Ronan, Cadora and LaBonte, 1993) have found modes, of a similar character to p-modes, with frequencies up to around 10mHz and beyond. Such high-frequency modes are discussed in Chapter 5.

Classification of p-modes by their l and n numbers leads to an important observation. If, for each of a set of modes of various l and n, the cyclic frequency ν is plotted against the degree l, an interesting pattern emerges (Deubner, 1975). For each value of n, the frequencies lie along near-perfect parabolic curves, as seen in Figure 1.4, which has been constructed from data supplied by K.G. Libbrecht. The lowest parabola consists of modes with $n = 0$ (the f-mode), the highest with $n = 26$; the frequency is measured in mHz. The discovery that a simple mathematical application of the mode-formation theory given above could reproduce the parabolic character of the observations was a crucial step in the acceptance of the cavity theory for p-mode formation. We give such a simple application in section 1.4.4 below.

The theory above predicts that p-mode properties will depend on the sound speed, and thus the temperature, of the solar interior. Thus we can invert the problem, and, by observing many different modes, deduce the form of temperature variation within the Sun. This idea is the basis of the subject of *helioseismology*, named for its correspondence to seismology, the study of the interior of the Earth through observations of waves produced by earthquakes. Detailed descriptions of helioseismological techniques and problems are

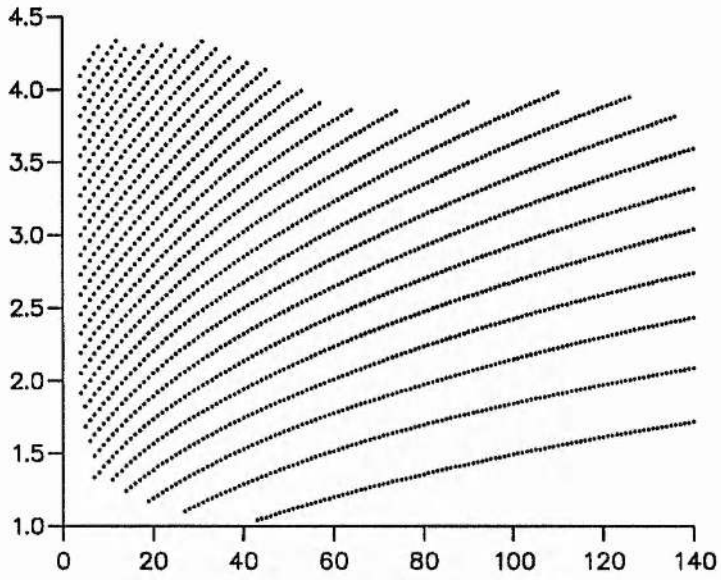

Figure 1.4: Frequency (in mHz) vs. degree l for a total of 1840 observed modes, from data supplied courtesy of K.G. Libbrecht, and published in Libbrecht, Woodard and Kaufman (1990). The lowest curve corresponds to order n=0 (the f-mode); higher curves are p-modes of increasing order from n=1 to n=26.

given in such reviews as Deubner and Gough (1984).

1.2.3 Solar cycle variations in p-mode frequencies

Frequencies of individual p-modes can be measured to great accuracy, with an error of around one part in ten thousand. This precision has allowed observers to detect slight but systematic changes in the frequencies of p-modes over the solar cycle.

Figure 1.5 shows the change in frequency, in μHz, between observing sessions in the years 1986 and 1989, for the same 1840 modes depicted in Figure 1.4; between 1986 and 1989, the Sun's magnetic activity increased greatly. The frequency shift of each mode is plotted against the frequency of the mode in 1986. The scatter of mode shifts forms a "trumpet" shape, the frequency uniformly increasing for modes up to around 3.5mHz, but then becoming less certain above this value. Some high frequency modes show a significant drop in frequency.

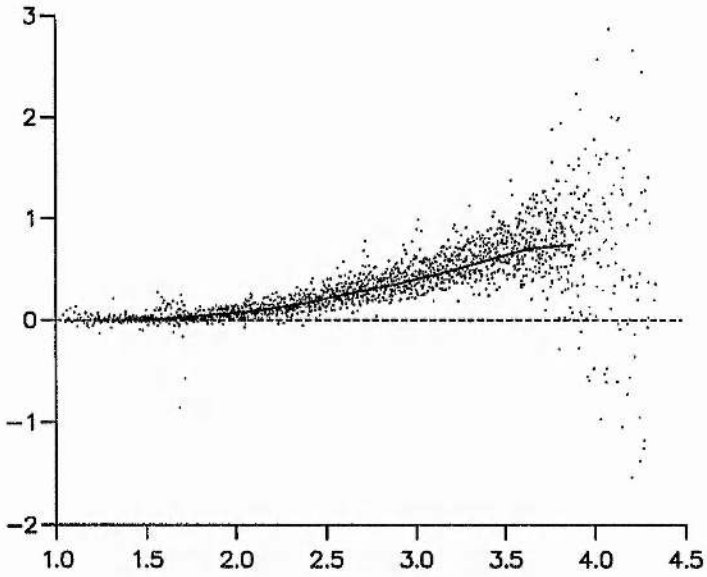

Figure 1.5: Frequency shift (in μHz) vs. original frequency (in mHz), for the 1840 modes depicted in Figure 1.4. The shift is determined by comparing mode frequencies for the' year 1986 (solar minimum) with those for 1989 (solar maximum). Data supplied courtesy of K.G. Libbrecht. The solid curve depicts the averaged frequency shift.

The frequency shift of a mode is approximately linearly dependent on the degree of the mode. Taking this l-dependence into account, we can average over all the available modes to find a frequency shift curve for modes of degree 50. This is the solid curve in Figure 1.5. This shows a gradual rise in frequency shift to around 3.5mHz, followed by a slight levelling-off of the curve. Beyond about 4mHz, there is insufficient information in this dataset to form reliable conclusions. However, other observational reports (Libbrecht and Woodard, 1991; Ronan et al., 1993) confirm that the frequency shift averaged over all observed modes drops sharply above 4mHz, as shown in Figure 1.6, which is reproduced from Libbrecht and Woodard (1991). This figure shows the averaged frequency shift, plotted against mode frequency, and compares observing sessions in the years 1986, 1988 and 1989; the circles show frequency shifts between 1986 and 1988, the squares between 1986 and 1989.

The conclusions we can draw are as follows. Associated with an increase in solar activity, there is a definite, systematic rise in p-mode frequencies for modes up to around

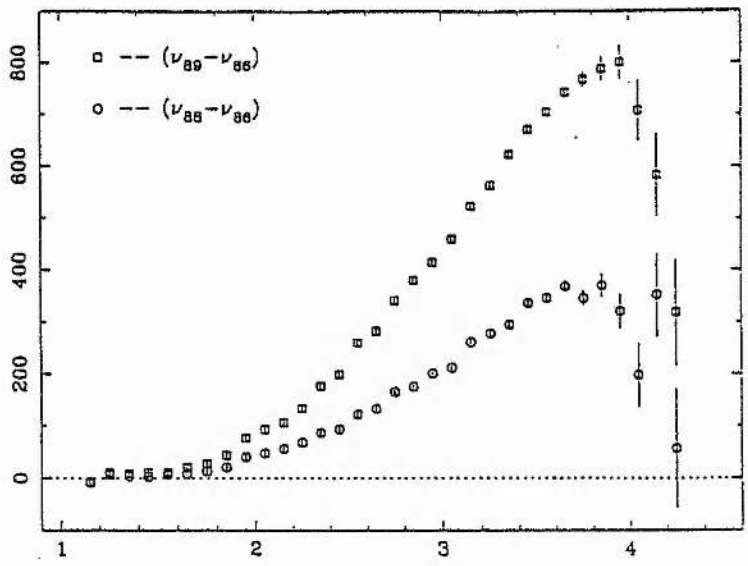

Figure 1.6: Averaged frequency shift plotted against original mode frequency; circles represent changes in frequency between 1986 and 1988, squares the change between 1986 and 1989. Reproduced from Libbrecht and Woodard (1991).

3.5 mHz. Beyond that frequency, a secondary effect appears to inhibit this frequency increase, lowering the average frequency shift of the modes and giving some modes a negative frequency shift. We call the effect observed at around 4mHz 'turnover'; this feature is the subject matter of Chapters 3 and 4.

Separate datasets exist describing changes in p-mode frequencies at high frequencies, that is to say above 5mHz (Ronan et al., 1993). This subject is discussed in Chapter 5.

1.3 Elementary equations

In section 1.2 we gave a descriptive account of the formation and character of global oscillations of the Sun, and introduced some of the fundamental problems we wish to tackle. To do this, we must now examine quantitatively the physical processes which govern the motions of a plasma such as that found in the Sun.

In general, any plasma element within the Sun will encounter both fluid and magnetic forces. In consequence, the equations describing the motion of such a plasma element belong to the intersection of two fields of physics: fluid mechanics and electromagnetism.

This specific field is known as magnetohydrodynamics, or MHD.

1.3.1 The fundamental equations of MHD

The basic equations of MHD are formed by grouping together Maxwell's equations and the basic laws of fluid dynamics, along with an equation of motion which takes account of both fluid and magnetic forces acting on a plasma element (Priest, 1982). At this point we are interested in a general, plane-parallel stratified atmosphere. We will link this to a solar model at a later stage.

We consider a continuous plasma of density ρ, pressure p and temperature T, moving with a general motion $\boldsymbol{v}$ in a magnetic field $\boldsymbol{B}$, subject to a gravitational acceleration $\boldsymbol{g}$. Firstly we have the equation of mass continuity, which is given by

$$\frac{D\rho}{Dt} + \rho \boldsymbol{\nabla}.\boldsymbol{v} = 0, \tag{1.1}$$

where $\frac{D}{Dt}$ represents the convectional derivative, that is

$$\frac{D}{Dt} \equiv \frac{\partial}{\partial t} + \boldsymbol{v}.\boldsymbol{\nabla}\,.$$

We assume that all motions are isentropic: that is, there is no heat exchange between a moving plasma element and its surroundings. This allows us to state that

$$\frac{D}{Dt}\left(\frac{p}{\rho^{\gamma}}\right) = 0, \tag{1.2}$$

where γ is the adiabatic index, which we take to equal 5/3.

We also assume that the plasma acts as an ideal gas, so that

$$p = \rho R T, \tag{1.3}$$

where R denotes $k_B/\hat{m}$, where k_B is Boltzmann's constant and $\hat{m}$ is the mean particle mass.

The neglect of resistivity in Maxwell's equations gives us the following equation for magnetic induction:

$$\frac{\partial \boldsymbol{B}}{\partial t} = \boldsymbol{\nabla} \times (\boldsymbol{v} \times \boldsymbol{B})\,. \tag{1.4}$$

This implies that the magnetic field is 'frozen-in' to the plasma.

Our equation of motion takes into account the pressure, magnetic and gravitational forces on the plasma element as follows:

$$\rho \frac{D\boldsymbol{v}}{Dt} = -\boldsymbol{\nabla} p + \boldsymbol{j} \times \boldsymbol{B} + \rho \boldsymbol{g}, \tag{1.5}$$

where the current density $\boldsymbol{j}$ is given by $\mu_0 \boldsymbol{j} = \boldsymbol{\nabla} \times \boldsymbol{B}$ and μ_0 is the magnetic permeability of free space. The $\boldsymbol{j} \times \boldsymbol{B}$ term can be expanded by means of a vector identity to give

$$\boldsymbol{j} \times \boldsymbol{B} = (\boldsymbol{B}.\boldsymbol{\nabla})\boldsymbol{B}/\mu_0 - \boldsymbol{\nabla}(B^2/2\mu_0);$$

for this reason we identify the quantity $B^2/2\mu_0$ as the *magnetic pressure*, p_M. The sum of the gas pressure and the magnetic pressure is known as the *total pressure*, p_T.

Finally, the magnetic field $\boldsymbol{B}$ is subject to the constraint that

$$\boldsymbol{\nabla}.\boldsymbol{B} = 0. \tag{1.6}$$

We wish to examine the motions of a plasma element, governed by equations (1.1-1.6), as it undergoes a small velocity perturbation. We align gravity with the z-axis such that $\boldsymbol{g} = g\hat{\mathbf{z}}$, and assume that all equilibrium quantities are functions of z alone. Equilibrium quantities are denoted by the subscript 0: for example, $\rho_0(z)$ denotes the equilibrium gas density and $p_0(z)$ the equilibrium gas pressure. The background magnetic field is considered to be horizontal and aligned with the x-axis, so that

$$\boldsymbol{B}_0 = \Big(B_0(z), 0, 0\Big).$$

Thus for the plasma to be in equilibrium in its unperturbed state, equation (1.5) requires that

$$\frac{d}{dz}\left(p_0 + \frac{B_0^2}{2\mu_0}\right) = \rho_0 g. \tag{1.7}$$

We introduce two-dimensional velocity perturbations by

$$\boldsymbol{v} = \Big(v_x(z), 0, v_z(z)\Big)e^{i(\omega t - k_x x)}, \tag{1.8}$$

where ω is the angular frequency and k_x is the horizontal wavenumber. The angular frequency, ω, and the cyclic frequency, ν, are related by $\omega = 2\pi\nu$; in calculation, we shall generally use the angular frequency ω, but in displaying the actual frequency of a mode, we shall use the cyclic frequency ν.

The density, pressure and magnetic field will now have the forms

$$\begin{aligned}
\rho &= \rho_0 + \rho_1(z)e^{i(\omega t - k_x x)}, \\
p &= p_0 + p_1(z)e^{i(\omega t - k_x x)}, \\
\mathbf{B} &= \Big(B_0(z), 0, 0\Big) + \Big(B_{1x}(z), 0, B_{1z}(z)\Big)e^{i(\omega t - k_x x)}.
\end{aligned} \tag{1.9}$$

We substitute the above expressions into equations (1.1-1.6) and assume that all perturbations are small, so terms formed from products of perturbed quantities can be neglected. Terms of the order of the unperturbed quantities drop out through the equilibrium, leaving us with a set of equations containing terms of the order of the perturbed quantities. These are as follows:

$$i\omega B_{1x} = -\frac{dB_0}{dz}v_z - B_0\frac{dv_z}{dz}; \tag{1.10}$$

$$i\omega B_{1z} = -ik_x B_0 v_z; \tag{1.11}$$

$$i\omega\rho_1 + v_z\frac{d\rho_0}{dz} = -\rho_0\nabla.\boldsymbol{v}; \tag{1.12}$$

$$i\omega\rho_0 v_x = ik_x p_1 + \frac{B_{1z}}{\mu_0}\frac{dB_0}{dz}; \tag{1.13}$$

$$i\omega\rho_0 v_z = -\frac{dp_1}{dz} - \frac{B_{1x}}{\mu_0}\frac{dB_0}{dz} - \frac{ik_x}{\mu_0}B_0 B_{1z} - \frac{B_0}{\mu_0}\frac{dB_{1x}}{dz} + \rho_1 g; \tag{1.14}$$

$$-ik_x B_{1x} + \frac{dB_{1z}}{dz} = 0; \tag{1.15}$$

$$i\omega p_1 + v_z\frac{dp_0}{dz} = -\gamma p_0\nabla.\boldsymbol{v}; \tag{1.16}$$

$$\nabla.\boldsymbol{v} = -ik_x v_x + \frac{dv_z}{dz}. \tag{1.17}$$

From this set of equations, we can eliminate all perturbed variables other than the velocity to give us the two equations

$$\frac{dv_z}{dz} + \frac{gk_x^2}{\omega^2}v_z = \frac{\omega^2 - k_x^2 c_s^2}{\omega^2}\nabla.\boldsymbol{v} \tag{1.18}$$

and

$$\frac{d}{dz}\left[\rho_0 v_A^2\frac{dv_z}{dz}\right] + \rho_0 g\frac{dv_z}{dz} + \rho_0\left(\omega^2 - k_x^2 v_A^2\right)v_z = -\frac{d}{dz}\left[\rho_0 c_s^2\nabla.\boldsymbol{v}\right] + \rho_0 g\nabla.\boldsymbol{v}, \tag{1.19}$$

where c_s, the local sound speed, and v_A, the Alfvén speed, are defined by

$$c_s^2(z) = \frac{\gamma p_0}{\rho_0}, \qquad v_A(z)^2 = \frac{B_0^2}{\mu_0\rho_0}.$$

In the absence of a magnetic field ($v_A = 0$), equations (1.18) and (1.19) tell us that v_z can be written as a function of $\nabla.\boldsymbol{v}$ by the alternative expression

$$(\omega^4 - g^2k_x^2)v_z = g(k_x^2c_s^2 - \gamma\omega^2)\nabla.\boldsymbol{v} - \omega^2 c_s^2\frac{d}{dz}(\nabla.\boldsymbol{v}). \tag{1.20}$$

Given equations (1.18) and (1.19), we may form a second-order differential equation for the velocity of the plasma element; this we now do.

1.3.2 Forms of the wave equation

We can write the wave equation in terms of either v_z, the vertical velocity, or $\nabla.\boldsymbol{v}$, the divergence of the velocity. The differential equation in terms of v_z is given by (Goedblood, 1971; Adam, 1977; Roberts, 1985)

$$\frac{d}{dz}\left[P\frac{dv_z}{dz}\right] = Qv_z, \tag{1.21}$$

where

$$P = \frac{\rho_0(c_s^2+v_A^2)(\omega^2-k_x^2c_T^2)}{\omega^2-k_x^2c_s^2},$$

and

$$Q = \frac{\rho_0 g^2 k_x^2}{\omega^2-k_x^2c_s^2} - \rho_0(\omega^2-k_x^2v_A^2) - gk_x^2\left(\frac{\rho_0 c_s^2}{\omega^2-k_x^2c_s^2}\right)',$$

and c_T, which we call the tube speed, is defined by

$$c_T^2 = \frac{c_s^2v_A^2}{c_s^2+v_A^2}.$$

The dash ($'$) denotes differentiation with respect to z.

The differential equation in terms of $\nabla.\boldsymbol{v}$ is cumbersome for a non-uniform magnetic field. The general form is given by

$$\frac{d^2}{dz^2}(\nabla.\boldsymbol{v}) + a\frac{d}{dz}(\nabla.\boldsymbol{v}) + b(\nabla.\boldsymbol{v}) = 0, \tag{1.22}$$

where a and b are given by

$$a = \frac{2\beta'}{\beta} - \frac{\alpha'}{\alpha}$$

and

$$b = \frac{\alpha}{\beta}\frac{\omega^2-k_x^2c_s^2}{\omega^2} + \frac{\beta''}{\beta} - \frac{\alpha'}{\alpha}\frac{\beta'}{\beta} + \frac{gk_x^2}{\omega^2}\frac{\alpha'}{\alpha} - \frac{g^2k_x^4}{\omega^4}.$$

Here α and β are defined by

$$\alpha = \frac{\rho_0(\omega^2-k_x^2v_A^2)(\omega^4-g^2k_x^2)}{\omega^4} - \frac{gk_x^2}{\omega^2}(\rho_0v_A^2)'$$

and

$$\beta = \frac{\rho_0(c_s^2+v_A^2)(\omega^2-k_x^2c_T^2)}{\omega^2}.$$

In the absence of a magnetic field, the general form (1.22) reduces to

$$\frac{d^2}{dz^2}(\nabla.\boldsymbol{v}) + \left[\frac{\gamma g}{c_s^2} + \frac{(c_s^2)'}{c_s^2}\right]\frac{d}{dz}(\nabla.\boldsymbol{v}) + \left\{\frac{\omega^2 - k_x^2 c_s^2}{c_s^2} + \frac{g k_x^2}{\omega^2}\left[(\gamma-1)\frac{g}{c_s^2} - \frac{(c_s^2)'}{c_s^2}\right]\right\}\nabla.\boldsymbol{v} = 0. \tag{1.23}$$

It proves convenient to cast the equation in $\nabla.\boldsymbol{v}$ in a form for which the coefficient of the first derivative is zero. This form is usually known as *canonical form.* In general we find an equation of the form

$$\frac{d^2Q}{dz^2} + \kappa^2(z)\,Q = 0, \tag{1.24}$$

where

$$Q = \frac{\beta}{\alpha^{1/2}}\nabla.\boldsymbol{v}.$$

The form of κ^2 depends on the form of magnetic field chosen. For example, in the presence of a *uniform* magnetic field, we find that

$$\kappa^2(z) = \frac{\omega^2}{(c_s^2+v_A^2)}\frac{\omega^2}{(\omega^2-k_x^2c_T^2)} + \frac{1-H'}{2H^2}\frac{\omega^2}{(\omega^2-k_x^2v_A^2)} - \frac{3}{4H^2}\frac{\omega^4}{(\omega^2-k_x^2v_A^2)^2}$$

$$-k_x^2 + \frac{k_x^2}{\omega^2}\frac{g}{H}\frac{\omega^2}{(\omega^2-k_x^2v_A^2)} - \frac{k_x^2}{\omega^2}\frac{g^2}{(c_s^2+v_A^2)}\frac{\omega^2}{(\omega^2-k_x^2c_T^2)}, \tag{1.25}$$

where H, the density scale height, is given by

$$H = \frac{\rho_0}{\rho_0'}.$$

In the absence of a magnetic field, equation (1.25) simplifies to give

$$\kappa^2 = \frac{\omega^2}{c_s^2} - \frac{1}{4H^2}(1+2H') - k_x^2 + \frac{k_x^2}{\omega^2}\left(\frac{g}{H} - \frac{g}{c_s^2}\right), \tag{1.26}$$

and Q is defined by

$$Q = \rho_0^{1/2}c_s^2\nabla.\boldsymbol{v}.$$

Equation (1.26) can be written in the form

$$\kappa^2 = \frac{\omega^2-\omega_a^2}{c_s^2} + k_x^2\left(\frac{\omega_g^2}{\omega^2} - 1\right), \tag{1.27}$$

where

$$\omega_a^2 = \frac{c_s^2}{4H^2}(1+2H') \tag{1.28}$$

and

$$\omega_g^2 = \frac{g}{H} - \frac{g^2}{c_s^2}. \tag{1.29}$$

We call ω_a the acoustic cut-off frequency; this is discussed further in section 1.4.3. We call ω_g the buoyancy frequency; this is a characteristic frequency of plasma oscillations whose restoring force is buoyancy. The buoyancy frequency is discussed further in section 1.4.1.

1.3.3 Behaviour of the wave equations

The equations (1.21), (1.22) and (1.24) describe the periodic motions of a plane-parallel, stratified plasma, subject to the perturbation given in equation (1.8). We have specified that the time and horizontal distance dependence of the motion is of the form $\exp[i(\omega t - k_x x)]$; this represents a wave which has a horizontal component of propagation. The vertical component of motion is unspecified. What we are effectively doing, then, is "firing off" a wave at some oblique angle to the gravitational acceleration, and attempting to examine how it behaves with varying z. Thus it is the vertical motion v_z, or its related quantity $\nabla.\boldsymbol{v}$, which we wish to calculate.

To do this, our usual procedure will be to specify some form of temperature and magnetic field variation, and calculate the equilibrium form of variables such as density and pressure from the equilibrium equation (1.7). We can then attempt to solve one or more of the wave equations, either exactly or in some asymptotic limit or approximate case. We can find a solution analytically, giving the functional form of v_z (or a related variable), or we may find it numerically, using some computational scheme.

The equations listed above are very general, and contain much information. It would be useful to form some basic ideas about their behaviour by considering first some simplified situations.

Firstly let us look at the case of a completely uniform, unstratified plasma. The gravitational acceleration is thus set to zero, and all quantities such as temperature, density and magnetic field strength are considered uniform. Under these conditions our differential equation (1.22) reduces to

$$\frac{d^2}{dz^2}(\nabla.\boldsymbol{v}) + \frac{(\omega^2 - k_x^2 v_A^2)(\omega^2 - k_x^2 c_s^2)}{(c_s^2 + v_A^2)(\omega^2 - k_x^2 c_T^2)}\nabla.\boldsymbol{v} = 0. \tag{1.30}$$

This is a constant-coefficient differential equation, so we can find a solution by writing

$$\nabla.\boldsymbol{v} \propto e^{ik_z z}, \tag{1.31}$$

where k_z is the vertical wavenumber. We then find that

$$\left[-k_z^2 + \frac{(\omega^2 - k_x^2 v_A^2)(\omega^2 - k_x^2 c_s^2)}{(c_s^2 + v_A^2)(\omega^2 - k_x^2 c_T^2)}\right] \nabla.\boldsymbol{v} = 0. \tag{1.32}$$

There are two ways in which equation (1.32) can be satisfied: either $\nabla.\boldsymbol{v}$ is zero or its coefficient is zero.

If $\nabla.\boldsymbol{v} = 0$, equation (1.18) tells us that dv_z/dz is zero also, and so from equation (1.19) we find that

$$(\omega^2 - k_x^2 v_A^2) v_z = 0. \tag{1.33}$$

Thus for a non-trivial solution we find the relationship

$$\omega^2 = k_x^2 v_A^2. \tag{1.34}$$

This form of wave motion is known as the *Alfvén wave.* A description of the wave's physical properties is given in Roberts (1985). However, from equations (1.12), (1.13) and (1.16) it can be seen that the motions of an Alfvén wave do not disturb the background values of density and pressure, and that the horizontal component of motion is zero.

If $\nabla.\boldsymbol{v} \neq 0$, equation (1.32) implies that the coefficient of $\nabla.\boldsymbol{v}$ is zero. This gives the result that

$$\omega^4 - \omega^2(c_s^2 + v_A^2)k^2 + k^2 k_x^2 c_s^2 v_A^2 = 0, \tag{1.35}$$

where $k^2 = k_x^2 + k_z^2$. There are two roots in ω^2 to this result; we can write them in the form

$$\omega_{1,2}^2 = \frac{k^2(c_s^2 + v_A^2)}{2}\left\{1 \pm \left[1 - \frac{4k_x^2 c_s^2 v_A^2}{k^2(c_s^2 + v_A^2)^2}\right]^{1/2}\right\}. \tag{1.36}$$

These two solutions are known as the *fast* and *slow magnetoacoustic waves.* If it is also true that $k_x^2 \ll k_z^2$, we can expand equation (1.36) for small k_x/k; we then find the results

$$\omega_1^2 \approx k^2(c_s^2 + v_A^2) \tag{1.37}$$

and

$$\omega_2^2 \approx k_x^2 c_T^2; \tag{1.38}$$

equation (1.37) gives the fast wave, equation (1.38) the slow wave. If k_x is identically zero, the slow wave disappears completely, and the fast wave propagates vertically at a phase speed c_f, the fast speed, given by

$$c_f^2 = c_s^2 + v_A^2. \tag{1.39}$$

Again, a fuller description of the properties of these waves is given in Roberts (1985).

Obviously we will generally be more interested in the behaviour of the wave equations when gravity is present. The simplest case we can examine now is that of an isothermal plasma, one in which the temperature is constant, without any magnetic field. In such a situation, equation (1.24) reduces to

$$\frac{d^2Q}{dz^2} + \kappa_0^2 Q = 0, \tag{1.40}$$

where

$$\kappa_0^2 = \frac{\omega^2}{c_0^2} - \frac{\gamma^2 g^2}{4c_0^4} - k_x^2 + (\gamma - 1)\frac{g^2 k_x^2}{\omega^2 c_0^2}. \tag{1.41}$$

We can again find solutions by setting $Q \propto \exp(ik_z z)$, which simply gives us that

$$k_z^2 = \kappa_0^2. \tag{1.42}$$

Now in general κ_0^2 can be positive or negative; the sign of κ_0^2 will determine the type of solutions found to equation (1.40).

If $\kappa_0^2 > 0$, we find that k_z is real and equal to κ_0, so the time and position dependence of Q will be given by

$$Q = c_1 e^{i(\omega t - k_x x + \kappa_0 z)} + c_2 e^{i(\omega t - k_x x - \kappa_0 z)}. \tag{1.43}$$

Thus one solution represents a wave with a component of propagation in the positive z-direction, the other a wave with a component of propagation in the negative z-direction.

If, on the other hand, $\kappa_0^2 < 0$, then k_z will be purely imaginary, and will be equal to $i\sqrt{-\kappa_0^2}$. In such a situation, the time and position dependence of Q will be given by

$$Q = e^{i(\omega t - k_x x)} \left\{ c_1 \exp\left[\sqrt{-\kappa_0^2} z\right] + c_2 \exp\left[-\sqrt{-\kappa_0^2} z\right] \right\}. \tag{1.44}$$

Both solutions are of an exponential form, one increasing and one decreasing in each z-direction. The conclusion is that waves in such an unbounded plasma cannot propagate in the z-direction.

Thus we conclude that in a region where κ^2 is constant and positive, we will find sinusoidal solutions for Q which represent propagating waves. Where κ^2 is constant and negative, we do not find propagatory solutions for Q; instead, solutions are found in terms of exponential functions of z. The precise nature of the solution in each case will depend on physical considerations; an example of this is given in section 1.5.2.

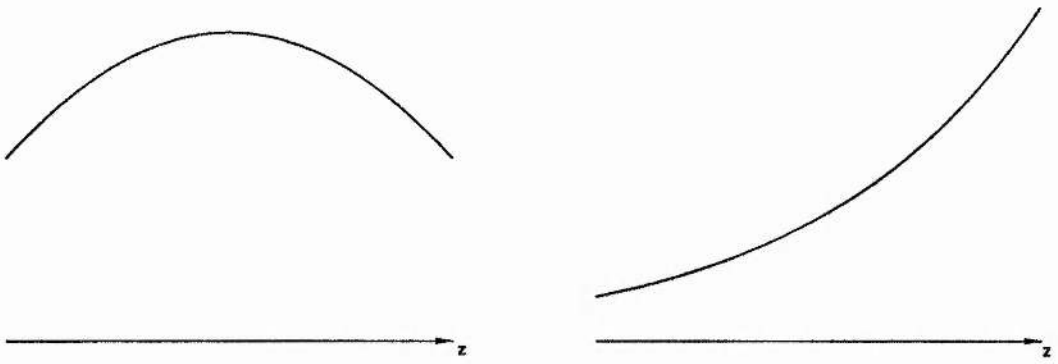

Figure 1.7: Form of Q which is a) convex and b) concave to the z-axis

We finish this section by looking at the general case where κ^2 is not constant. In this situation it is not generally possible to find simple solutions for Q in terms of sinusoidal or exponential functions. Solutions for Q may be found in terms of more involved functions, from which it may be difficult to infer the nature of plasma motions. In such a situation, we may still be able to form an approximate picture of the behaviour of the plasma as follows.

Firstly, we could consider a purely local analysis, which will be valid where the value of κ^2 is varying so slowly that at a particular point it may be treated as being constant. In such an instance we can again find a value for k_z, which we should now describe as the *local vertical wavenumber*. The reasoning then follows along similar lines to that for κ^2 constant. Positive κ^2 implies real k_z, and thus a propagating wave; negative κ^2 implies imaginary k_z, and thus non-propagatory motions. Regions where κ^2 changes sign correspond to a change in the nature of plasma motions, from propagatory to non-propagatory. This approach is the basis for WKB theory, which is described further in Chapter 3. We would not expect it to give a good representation of the problem where κ^2 changes rapidly with z.

A more general picture of plasma motions may be formed by again considering equation (1.24), our canonical equation in Q, where κ^2 is a general function of z. In a region where κ^2 is positive, we can state, without solving for Q, that

$$\frac{d^2Q}{dz^2} \Big/ Q < 0. \tag{1.45}$$

This immediately tells us something about the form of Q: it must be 'convex' to the z-axis, as shown in Figure 1.7a. If κ^2 is negative, however, we will find that

$$\frac{d^2Q}{dz^2} \Big/ Q > 0, \tag{1.46}$$

implying that Q is 'concave' to the z-axis, as shown in Figure 1.7b. Where κ^2 is zero, we must find a point of inflexion of Q. By considering the global range of κ^2 with z, we may thus form a picture of Q as a function of z. Often we will also be able to enlist asymptotic solutions to equation (1.24) in certain limits (e.g. large z) to help construct this picture, even when the full solution is inscrutable.

We describe the form of Q where κ^2 is positive as displaying *oscillatory-type* behaviour in z, because of its convex form, while in regions where κ^2 is negative, Q will be said to display *exponential-type* behaviour. Points where κ^2 is zero are described as *turning points.*

1.4 Modelling the solar interior

In section 1.3, we described the basic forms of the wave equation which will be used in the greater part of this thesis. We now describe how these equations can be applied to the problem of solar p-modes. We proceed by introducing some of the standard models which have been constructed to achieve this end.

In this section we describe a standard mathematical model for the interior of the Sun, and relate the behaviour of equation (1.24) for this model to our conceptual picture of p-mode formation. We then present an approximate treatment of the problem, which, though simple, is sufficient to display some basic properties of p-modes. Finally we give an exact solution to the wave equation for the standard model.

1.4.1 Linear polytrope model

A significant proportion of previous analytical investigation into chromospheric effects on p-mode frequencies has been based on one model for the solar interior (Campbell and Roberts, 1989; Evans and Roberts, 1990; Jain and Roberts, 1993). This is usually called the *linear polytrope* model, since the temperature is assumed to increase linearly with depth. Our aim is to find solutions to certain forms of the wave equation for this model.

The first step in constructing this model is to consider the Sun to be flat, allowing us to use the plane-parallel theory developed in section 1.3. This will be a good approximation for modes whose depth of penetration inside the Sun is much less than the radius

of the Sun. Since we will see that the base of the cavity is approximately at the depth at which $c_s = \omega/k_x$, this approach will be least accurate for modes of high frequency and, in particular, of low k_x.

We must also find some way of relating the degree of a p-mode, l, to the horizontal wavelength of a wave disturbance, k_x. In a spherical geometry, the derivation of the wave equation corresponding to equation (1.24) gives a similar result (Deubner and Gough, 1984):

$$\frac{d^2Q}{dr^2} + \kappa^2(r)Q = 0, \tag{1.47}$$

where

$$\kappa^2 = \frac{\omega^2}{c_s^2} - \frac{1}{4H^2}(1 + 2H') - \frac{l(l+1)}{r^2} + \frac{l(l+1)}{r^2}\frac{1}{\omega^2}\left(\frac{g}{H} - \frac{g^2}{c_s^2}\right). \tag{1.48}$$

Here r is the radial distance, $Q = \rho_0^{1/2} c_s^2 \nabla.\boldsymbol{v}$, and l is a whole number corresponding exactly to the degree of a p-mode. For modes which are confined to near the solar surface, the radial distance r will be approximately equal to $R_\odot$, the solar radius, throughout the mode cavity. For such modes we can see that the forms of κ^2 given in equations (1.26) and (1.48) are identical if we form the equivalence

$$k_x^2 \equiv \frac{l(l+1)}{R_\odot^2}, \tag{1.49}$$

where $R_\odot = 6.96 \times 10^8$m is the solar radius.

Thus we may represent a p-mode with degree l in spherical geometry by an oscillation in plane-parallel geometry with a horizontal wavenumber given by equation (1.49). As is true for our plane-parallel approximation, this will be a good approximation for high-l modes, but will be less accurate for modes which penetrate nearer to the centre of the Sun. In the greater part of this thesis, we will restrict ourselves to considering modes of order at least 50; the exception to this is Chapter 6, where we present a distinct description of modes of degree zero.

We place the solar surface at $z = 0$; we have already aligned gravity with the positive z-direction, so z represents the depth within the solar interior. Thus the entire solar interior is represented in this model by the region $z > 0$. The region $z < 0$, which will represent the solar chromosphere, will be modelled separately, as described in section 1.5.

We model the rise in temperature within the Sun by the temperature profile

$$T = T_0(1 + z/z_0), \tag{1.50}$$

T_0	4170.0K
p_{01}	86.82 $\mathrm{kgm^{-1}s^{-2}}$
R	6425.97 $\mathrm{m^2s^{-2}K^{-1}}$
g	274.0 $\mathrm{ms^{-2}}$
c_{0L}	6682.9 $\mathrm{ms^{-1}}$

Table 1.1: Standard parameter values for linear polytrope model

where T_0 is the temperature at $z = 0$ and z_0 is the temperature scale height at $z = 0$. In general, we set the magnetic field to zero within the solar interior. Thus, from equation (1.7), our equilibrium becomes

$$\frac{dp_0}{dz} = \rho_0 g. \tag{1.51}$$

Thus we can derive the following forms for the sound speed, density and pressure variation in $z > 0$:

$$\begin{aligned} c_s^2 &= c_{0L}^2(1 + z/z_0), \\ \rho_0 &= \rho_{01}(1 + z/z_0)^m, \\ p_0 &= p_{01}(1 + z/z_0)^{m+1}, \end{aligned} \tag{1.52}$$

where c_{0L}, ρ_{01} and p_{01} are the equilibrium values of the sound speed, density and pressure, respectively, at $z = 0$. The quantity m is called the *polytropic index*; its value is given by

$$m = \frac{\gamma g z_0}{c_{0L}^2} - 1. \tag{1.53}$$

Table 1.1 shows the parameter values we shall employ for the linear polytrope model. These are consistent with values previously used by Evans and Roberts (1990) and Jain and Roberts (1993). The value of the temperature scale height is generally picked to conform with the assumption of marginal stratification described below.

What forms do the differential equations above take for these forms of the sound speed and density? We look first at equation (1.24), with κ^2 given by equation (1.26). We find that κ^2 takes the form

$$\kappa^2 = \frac{\omega^2}{c_{0L}^2}\frac{1}{1 + z/z_0} - \frac{m(m+2)}{4z_0^2}\frac{1}{(1 + z/z_0)^2} - k_x^2 + \frac{g^2 k_x^2}{c_{0L}^2\omega^2}\left(\frac{m\gamma}{m+1} - 1\right)\frac{1}{1 + z/z_0}. \tag{1.54}$$

m	3/2
z_0	244.5 km

Table 1.2: Further parameter values for linear polytrope with marginal stratification

We can now introduce the concept of *marginal stratification.* The value of the polytropic index m depends on the value chosen for the temperature scale height; thus it is possible to select the value of z_0 such that the last term in equation (1.54) is identically zero. In effect we are specifying that the buoyancy frequency ω_g is identically zero. Then, for marginal stratification, the polytropic index m must satisfy

$$m = \frac{1}{\gamma - 1} = \frac{g z_0}{c_{0L}^2}. \tag{1.55}$$

Since we take $\gamma = 5/3$, this implies the values of m and z_0 given in Table 1.2.

Thus, under the assumption of marginal stratification, we can write κ^2 in the form

$$\kappa^2 = k_x^2 \left(\frac{A^2}{1 + z/z_0} - \frac{B^2}{(1 + z/z_0)^2} - 1 \right), \tag{1.56}$$

where

$$A^2 = \frac{\omega^2}{k_x^2 c_{0L}^2}, \qquad B^2 = \frac{m(m+2)}{4 k_x^2 z_0^2}. \tag{1.57}$$

1.4.2 Mode formation

We have specified the forms of variables such as the temperature, density and pressure in the solar interior. Motions of the plasma in such a model are governed by the differential equation

$$\frac{d^2 Q}{dz^2} + \kappa^2(z) Q = 0$$

with κ^2 given by equation (1.56) above. How does this relate to our picture of p-mode formation by successive reflection and refraction given in section 1.2.1 above? To see this, it is convenient to examine the form of κ^2 in our solar interior model.

As an example, we look at a mode with degree 50 and frequency 4.5mHz. For this mode, we find that the quantities A^2 and B^2 from equation (1.56) above are both large, of the order 10^3. Thus, near $z = 0$ we would expect the first two terms of κ^2 in equation (1.56) to dominate. As z increases, the second term will rapidly go to zero, because of its inverse square dependence on $1 + z/z_0$; we thus expect that for some intermediate range of z, the

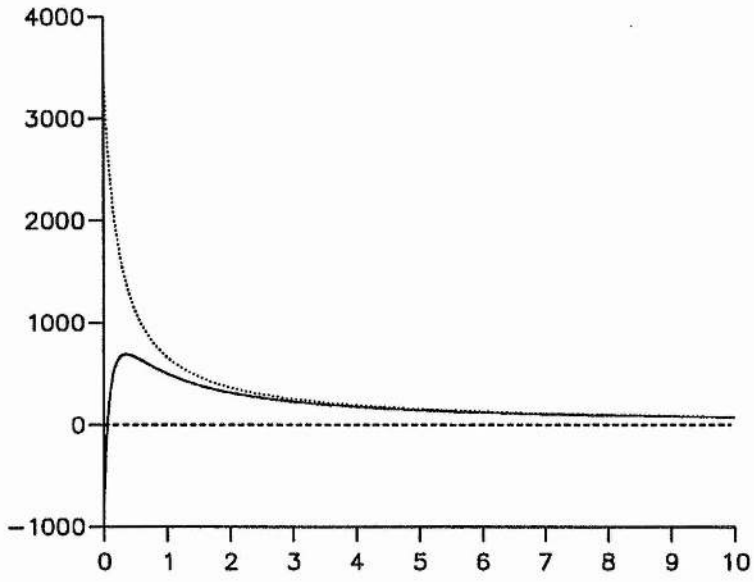

Figure 1.8: κ^2/k_x^2 (solid curve) vs. z (in Mm) near $z = 0$. The dotted curve shows the variation of the first term in κ^2 with z.

first term will be the sole dominant term. As z increases further, the first term will also decrease, until there will be some point at which κ^2 is equal to zero. Ultimately, as z tends to infinity, κ^2 will tend towards $-k_x^2$.

The solid curve in Figure 1.8 shows part of the variation of κ^2 (normalised to k_x^2) with depth, z, for this mode. The dotted curve depicts the variation of the first term of κ^2 in equation (1.56). We see that for the greater part of the range of z, the first term is the dominant term. Near $z = 0$, however, the second term can have a significant contribution, and acts to bring the value of κ^2 sharply down. Thus the overall form of κ^2 is that we have a region in which κ^2 is positive, sandwiched between two regions in which κ^2 is negative.

How does this relate to p-modes? We described in section 1.2.1 how p-modes are formed from the trapping of sound waves in a cavity below the solar surface. We also described, in section 1.3.3 above, how the nature of solutions to equation (1.24) depends on the sign of κ^2. We can now tie these together in a qualitative way. Figure 1.8 shows that for a large range of z, κ^2 is positive; thus we will expect wave-like solutions in this region. Outside this region, κ^2 is negative, and any motion will either grow or decay exponentially with height. Thus a wave instigated in the $\kappa^2 > 0$ region will not be able to travel into a

$\kappa^2 < 0$ region, but will be trapped. Thus our picture is of a cavity corresponding to the region in which $\kappa^2 > 0$.

We associate the zero of κ^2 at large z with the refraction of waves by the increasingly high temperatures within the solar interior. This will occur approximately at the depth z at which

$$\frac{\omega^2}{k_x^2 c_s^2(z)} = 1;$$

thus waves of lower horizontal wavenumber k_x will reach greater depths in the model, as will waves of higher angular frequency ω.

We associate the zero of κ^2 near $z = 0$ with the reflection of waves by the rapid drop-off in density near the solar surface; we now describe this process in greater detail.

1.4.3 Acoustic cut-off frequency

Above a certain frequency, the drop in κ^2 near $z = 0$ will not be sharp enough to create a zero of κ^2. In this case, the mode cavity will not be formed entirely within the interior model, and the formation of modes will depend on the behaviour of κ^2 in whatever model is eventually chosen for the chromosphere. This introduces the idea of the acoustic cut-off frequency.

Assuming marginal stratification, we can rewrite the form of κ^2 given in equation (1.27) as

$$\kappa^2(z) = \frac{\omega^2 - \omega_a^2}{c_s^2} - k_x^2, \tag{1.58}$$

where

$$\omega_a^2(z) = \frac{c_s^2}{4H^2}(1 + 2H'). \tag{1.59}$$

Following Lamb (1932), we identify ω_a as the acoustic cut-off frequency. For the linear polytrope, ω_a is given by

$$\omega_a^2 = \frac{m(m+2)c_{0L}^2}{4z_0^2}\frac{1}{1 + z/z_0}. \tag{1.60}$$

For $z > 0$, the acoustic cut-off frequency will take its maximum value at $z = 0$:

$$\omega_a\Big|_{z=0} = \frac{\sqrt{m(m+2)}c_{0L}}{2z_0}. \tag{1.61}$$

This value will be the theoretical upper limit for a zero of κ^2 to exist near $z = 0$, and thus for a cavity to be formed entirely within the solar interior for this model. For the parameters given in Tables 1.1 and 1.2, $\omega_a/2\pi$=4.98mHz.

Of course, it is not a necessary condition on the formation of modes that the cavity be formed entirely within the interior model. If the model of the chromosphere we eventually choose is such that a bounded cavity can be formed covering any finite range of z, then we would expect the formation of modes. This subject will be considered further in sections 1.5.2 and 1.5.3 and also in Chapter 2.

1.4.4 An approximate solution

At frequencies such that a cavity may form in our model, we can use an approximate method of solving equation (1.24) to find the frequencies of normal modes resident in the cavity. We use the Bohr-Sommerfeld condition (Nayfeh, 1983; Bender and Orszag, 1987), a result of WKB theory which provides an approximate solution to eigenvalue problems such as the above. This body of theory, and the Bohr-Sommerfeld condition in particular, are discussed in greater detail in Chapters 3 and 4; we restrict ourselves here to an illustration of its use.

For equation (1.24), the Bohr-Sommerfeld condition implies that the frequency of a mode trapped between the two turning points (or zeros of κ^2) is approximately given by

$$\int_{z_1}^{z_2} \kappa(z)\, dz = (n - \frac{1}{2})\pi, \tag{1.62}$$

where n is a positive integer equivalent to the order of a mode and z_1 and z_2 are the roots of $\kappa^2(z) = 0$. Equation (1.62) is an asymptotic result valid as $n \to \infty$. Since both these roots must lie in the interior model, we require that $\kappa^2(0) < 0$. Thus we are restricted to modes with frequencies below the acoustic cut-off frequency at the top of the interior model, as described in section 1.4.3 above. Carrying out the integration for $\kappa^2(z)$ given by equation (1.56) then gives (see Appendix A)

$$\frac{\omega^2}{gk_x} = -\frac{1}{m} + \left(1 + \frac{2}{m}\right)^{1/2} + \frac{2n}{m}. \tag{1.63}$$

Such an equation is known as a dispersion relation. Given the horizontal wavenumber k_x, such a dispersion relation tells us the frequencies at which normal modes will form for the given model. We see in this simple case that the square of the frequency, ω^2, is proportional to the horizontal wavenumber k_x, which is itself approximately proportional to the degree l; thus we have reproduced the parabolic form of the ω-l curves seen in Figure 1.4.

1.4.5 An exact solution

In section 1.4.4, we were effectively finding an approximate solution to our wave equation, giving us the form of motions in $z > 0$, and using boundary conditions to find a dispersion relation. It is also possible to find an exact solution to the wave equation for the linear polytrope model (Lamb, 1932). Introduce the quantity Ω^2, defined by

$$\Omega^2 = \frac{\omega^2}{gk_x}. \tag{1.64}$$

Setting $s = 2k_x z_0(1 + z/z_0)$ then transforms equation (1.24), with κ^2 given by equation (1.56), into

$$\frac{d^2Q}{ds^2} + \left[-\frac{1}{4} + \frac{m\Omega^2}{2}\frac{1}{s} - \frac{m(m+2)}{4}\frac{1}{s^2}\right] Q = 0. \tag{1.65}$$

This is in the form of Whittaker's equation, which is (Abramovitz and Stegun, 1967: 13.1.31)

$$\frac{d^2w}{dx^2} + \left[-\frac{1}{4} + \frac{\alpha}{x} + \frac{\frac{1}{4} - \beta^2}{x^2}\right] w = 0.$$

Whittaker's equation has the solutions

$$\mathrm{M}_{\alpha,\beta}(x) = e^{-x/2}x^{\beta+\frac{1}{2}}\mathrm{M}(\frac{1}{2} + \beta - \alpha, 1 + 2\beta, x)$$

and

$$\mathrm{W}_{\alpha,\beta}(x) = e^{-x/2}x^{\beta+\frac{1}{2}}\mathrm{U}(\frac{1}{2} + \beta - \alpha, 1 + 2\beta, x),$$

where M and U are the confluent hypergeometric functions (Abramovitz and Stegun, 1967).

For equation (1.65) these solutions are

$$\mathrm{M}_{\alpha,\beta}(z) = e^{-k_x(z+z_0)}(z + z_0)^{1+\frac{m}{2}}\mathrm{M}\Big(-a, m + 2, 2k_x(z + z_0)\Big)$$

and

$$\mathrm{W}_{\alpha,\beta}(z) = e^{-k_x(z+z_0)}(z + z_0)^{1+\frac{m}{2}}\mathrm{U}\Big(-a, m + 2, 2k_x(z + z_0)\Big),$$

where the parameter a is related to ω^2 by

$$a = \frac{m}{2}\Omega^2 - \frac{m}{2} - 1.$$

Remembering that $Q = \rho_0^{1/2}c_s^2\nabla.\boldsymbol{v}$, the general solution for $\nabla.\boldsymbol{v}$ is thus

$$\nabla.\boldsymbol{v} = e^{-k_x(z+z_0)}\Big\{c_1\mathrm{M}\Big(-a, m + 2, 2k_x(z + z_0)\Big) + c_2\mathrm{U}\Big(-a, m + 2, 2k_x(z + z_0)\Big)\Big\}, \tag{1.66}$$

where c_1 and c_2 are arbitrary constants.

This solution describes the form of the wave motion in $z > 0$. We can exploit this expression in two ways. We can form a dispersion relation by allowing the interior temperature to rise from zero at $z = 0$. For this situation it can be shown that the frequency of the mode is given by (Christensen-Dalsgaard, 1980; Campbell and Roberts, 1989)

$$\omega^2 = gk_x\left(1 + \frac{2n}{m}\right). \tag{1.67}$$

This simple result is often used as an approximate dispersion relation for p-mode frequencies.

Since we wish to examine the influence of the chromosphere on p-mode frequencies, we require a fuller treatment of the interface $z = 0$ than given above. For the solution given by equation (1.66) to be physically realistic, one condition must apply: that as z goes to infinity, the energy density must be finite. Since the M-function increases exponentially with z, we must set the constant c_1 to be zero. Thus our solution is given by

$$\nabla.\boldsymbol{v} = c_2 e^{-k_x(z+z_0)}\mathrm{U}\Big(-a, m+2, 2k_x(z+z_0)\Big). \tag{1.68}$$

Equation (1.20), along with the basic properties of the U-function, then leads to an expression for the form of v_z in $z > 0$ as follows:

$$(\omega^4 - g^2k_x^2)\exp\Big[k_x(z+z_0)\Big]v_z = c_2\Big\{\Big[k_xc_s^2(\omega^2 + gk_x) - \gamma g\omega^2\Big]\mathrm{U}\Big(-a, m+2, 2k_x(z+z_0)\Big)$$

$$- 2a\omega^2c_s^2k_x\mathrm{U}\Big(1-a, m+3, 2k_x(z+z_0)\Big)\Big\}. \tag{1.69}$$

The result (1.68) tells us the form of wave disturbances in $z > 0$ for given k_x and ω. It does not tell us the frequencies at which normal modes will form, as we have not yet considered our boundary condition at the interface $z = 0$, which we associate with the solar surface. Thus our attention now turns to modelling the solar surface and chromosphere.

1.5 Modelling the solar chromosphere

We now turn to the region above the temperature minimum, of which a brief description is given in section 1.1.1. Just as we associated the interior of the Sun with the interval $z > 0$ in our model, we associate the region above the temperature minimum with the interval $z < 0$. The interface $z = 0$ then represents the solar surface.

For the classical range of p-mode frequencies, we have seen that wave motions will generally be evanescent in this region, and we would expect that solutions to the wave

equation in $z < 0$ will have a very different character to those in $z > 0$. We would also expect the magnetic field to be a significant element in our chromospheric model. The fact that the motions will die out with height implies that the region nearest the temperature minimum will be the most significant. Thus in general we ignore the presence of high temperatures in the transition region and corona, and attempt simply to model the chromosphere.

The chromosphere is a complex region, and numerous models have attempted to describe its features. We will look in this section at two simple models, to allow us to introduce some of the concepts we will encounter later in the thesis. Since our ultimate aim is to examine the influence of the chromosphere on our oscillations in the interior, it is necessary to consider the means by which these influences are expressed. Thus our first point of investigation must be the interface between the interior model and the chromospheric model.

1.5.1 Interface conditions

We have constructed a model for the solar interior, and found the form of wave motions in that region. We aim to do the same for the chromosphere. For this treatment of the problem to be physically realistic, certain conditions must be met at the interface between the two regions.

A condition for equilibrium of the interface is that the unperturbed total pressure p_{T0}, given by

$$p_{T0} = p_0 + B_0^2/2\mu_0,$$

is the same on each side of the interface. The effect of this is simply to relate the values of the unperturbed density ρ_0 either side of the interface; this condition does not directly affect the matching of the solutions.

Now let us consider two plasma elements, in immediate juxtaposition across the interface. It is obvious that if one has a particular vertical velocity v_z, then so must the other. Thus our first condition on v_z is as follows:

$$v_z \text{ is continuous across the interface.} \tag{1.70}$$

The second condition on v_z is less straightforward. As our two plasma elements are perturbed, the total pressure perturbation of the moving elements must be the same, for pressure balance to be maintained. Thus we introduce the quantity p_L, called the

Lagrangian total pressure perturbation (Wright and Thompson, 1992), by

$$p_L = p_{T1} + (\boldsymbol{\xi}.\boldsymbol{\nabla})p_{T0}, \tag{1.71}$$

where p_{T0} and p_{T1} are, respectively, the unperturbed total pressure and the total pressure perturbation, and $\boldsymbol{\xi}$ is the displacement of the element. Consideration of the basic linearised equations gives

$$p_L = -\rho_0 \left[v_A^2 \frac{d\xi_z}{dz} + c_s^2 \boldsymbol{\nabla}.\boldsymbol{\xi} \right]. \tag{1.72}$$

This quantity must also be continuous across the interface. The time derivative of this quantity, which we will denote by p_{Lt}, must also be continuous, so our second continuity condition on v_z can be written as follows:

$$\rho_0 v_A^2 \frac{dv_z}{dz} + \rho_0 c_s^2 \boldsymbol{\nabla}.\boldsymbol{v} \quad \text{is continuous across the interface.} \tag{1.73}$$

Thus we have established our continuity conditions, namely the continuity of p_{T0}, v_z and p_{Lt}.

We can express the boundary condition (1.73) in a different form by substituting for $\boldsymbol{\nabla}.\boldsymbol{v}$ from equation (1.18), giving a boundary condition in terms of dv_z/dz and v_z; this condition can be written as follows:

$$\frac{\rho_0(c_s^2 + v_A^2)(\omega^2 - k_x^2 c_T^2)}{\omega^2 - k_x^2 c_s^2} \frac{dv_z}{dz} + \frac{\rho_0 c_s^2 g k_x^2}{\omega^2 - k_x^2 c_s^2} v_z \quad \text{is continuous across the interface.} \tag{1.74}$$

The condition (1.74) has been used in previous studies of chromospheric effects on p-mode frequencies; see, for example, Evans and Roberts (1990). There, the condition (1.74) was derived by integrating the equation (1.21) across the interface.

1.5.2 Isothermal non-magnetic model

In this most basic of models for the chromosphere, the temperature is taken to be the constant value T_0 throughout $z < 0$, and the atmosphere is assumed to be field-free. The equilibrium equation (1.7) then implies that the sound speed, density and pressure variations in $z < 0$ are as follows:

$$c_s^2(z) = c_0^2, \qquad \rho_0(z) = \rho_{00} \exp(z/H), \qquad p_0(z) = p_{00} \exp(z/H), \tag{1.75}$$

where $c_0^2 = \gamma R T_0$, $H = c_0^2/\gamma g$ and ρ_{00} and p_{00} are respectively the unperturbed density and pressure at the base of the chromosphere. Thus, the density and pressure drop off exponentially with height in the atmosphere.

For this model, equation (1.24) takes the form

$$\frac{d^2Q}{dz^2} + \kappa_0^2(z)Q = 0, \tag{1.76}$$

where

$$\kappa_0^2 = \frac{\omega^2}{c_0^2} - \frac{\gamma^2 g^2}{4c_0^4} - k_x^2 + (\gamma - 1)\frac{g^2 k_x^2}{\omega^2 c_0^2}.$$

This is a constant-coefficient differential equation, the nature of its solutions depending upon the sign of κ_0^2. If κ_0^2 is positive, solutions will be of the form

$$Q(z) = c_3 \exp[i\kappa_0 z] + c_4 \exp[-i\kappa_0 z]. \tag{1.77}$$

This gives the combined height and time dependence of Q as

$$Q(z,t) = c_3 \exp[i(\omega t + \kappa_0 z)] + c_4 \exp[i(\omega t - \kappa_0 z)]. \tag{1.78}$$

One solution represents an upward propagating wave, and the other a downward propagating wave.

If κ_0^2 is negative, solutions will be of the form

$$Q(z) = c_3 \exp\left[\sqrt{-\kappa_0^2}z\right] + c_4 \exp\left[-\sqrt{-\kappa_0^2}z\right]. \tag{1.79}$$

We can apply a boundary condition at infinity to this solution. We require that as $z \to -\infty$, the kinetic energy density $\frac{1}{2}\rho_0 v^2$, where $v^2 = v_x^2 + v_z^2$, must be bounded. This rules out the c_4 solution, so we are forced to set $c_4 = 0$. Thus the height dependence of our physically realistic solution is given by

$$Q(z) = c_3 \exp\left[\sqrt{-\kappa_0^2}z\right], \tag{1.80}$$

which tells us that motions die out, or *evanesce*, with height in the atmosphere. The combined height and time dependence of Q will thus be given by

$$Q(z,t) = c_3 \exp\left[\sqrt{-\kappa_0^2}z\right] \exp(i\omega t). \tag{1.81}$$

Equation (1.81) represents what we call an *evanescent standing wave.*

Since $Q = \rho_0^{1/2} c_s^2 \nabla.v$, we find the form of $\nabla.v$ in $z < 0$ to be given by

$$\nabla.v = \frac{c_3}{\rho_{00}^{1/2} c_0^2} \exp\left[\left(\sqrt{-\kappa_0^2} - \frac{\gamma g}{2c_0^2}\right) z\right], \tag{1.82}$$

and thus, from equation (1.20), the form of v_z is given by

$$(\omega^4 - g^2k_x^2)v_z = \frac{c_3}{\rho_{00}^{1/2}c_0^2}\left[g(k_x^2c_0^2 - \gamma\omega^2/2) - \omega^2c_0^2\sqrt{-\kappa_0^2}\right]\exp\left[\left(\sqrt{-\kappa_0^2} - \frac{\gamma g}{2c_0^2}\right)z\right]. \quad (1.83)$$

Thus in an isothermal, non-magnetic atmosphere, motions are either propagatory or evanescent throughout the region $z < 0$, the demarcation point being the values of ω and k_x such that

$$\frac{\omega^2}{c_0^2} - \frac{\gamma^2g^2}{4c_0^4} - k_x^2 + (\gamma - 1)\frac{g^2k_x^2}{\omega^2c_0^2} = 0. \quad (1.84)$$

The formation of trapped modes requires that wave motions are in some way evanescent above a certain height in the atmosphere, allowing a bounded cavity to form. Thus we would not expect oscillations representing p-modes to be formed above the frequency for which equation (1.84) holds. For the range of frequencies and horizontal wavenumbers we are likely to encounter, the first two terms in equation (1.84) are far larger than the third and fourth terms. Thus the approximate condition on formation of modes in a system comprising a linear polytrope topped by an isothermal non-magnetic chromosphere is that $\omega < \omega_c$, where

$$\omega_c^2 = \frac{\gamma^2g^2}{4c_0^2} = \frac{c_0^2}{4H^2}. \quad (1.85)$$

We identify ω_c as the cut-off frequency for the atmosphere (Lamb, 1932). If the temperature throughout the chromosphere is taken as the temperature minimum value, T_0=4170K, we find that the cut-off frequency $\omega_c/2\pi$ takes the value 5.43mHz. This subject is discussed further in Chapter 2.

In the range of frequencies below ω_c, we may now use the interface conditions described in section 1.5.1 to match the solution for the wave motion in the linear polytrope to the evanescent solution in our chromospheric model. Using equation (1.69) for v_z in $z > 0$ and equation (1.83) for v_z in $z < 0$, the condition that v_z is continuous across the boundary $z = 0$ gives

$$\exp(k_xz_0)\frac{c_3}{\rho_{00}^{1/2}c_0^2}\left[g(k_x^2c_0^2 - \gamma\omega^2/2) - \omega^2c_0^2\sqrt{-\kappa_0^2}\right] =$$

$$c_2\Big\{\left[k_xc_{0L}^2(\omega^2 + gk_x) - \gamma g\omega^2\right]\mathrm{U}(-a, m+2, 2k_xz_0)$$

$$- 2a\omega^2c_{0L}^2k_x\mathrm{U}(1-a, m+3, 2k_xz_0)\Big\}. \quad (1.86)$$

Since we are considering a non-magnetic atmosphere, continuity of p_0 implies that

$$\rho_{0L}c_{0L}^2 = \rho_{00}c_0^2.$$

Thus the condition (1.73) of continuity of p_{Lt} simply reduces to continuity of $\nabla.\boldsymbol{v}$:

$$c_2 \exp(-k_x z_0)\mathrm{U}(-a, m+2, 2k_x z_0) = \frac{c_3}{\rho_{00}^{1/2} c_0^2}. \tag{1.87}$$

The constants c_2 and c_3 can be eliminated from equations (1.86) and (1.87) to give

$$\left[k_x c_{0L}^2(\omega^2 + gk_x) - g(k_x^2 c_0^2 + \gamma\omega^2/2) + \omega^2 c_0^2\sqrt{-\kappa_0^2}\right]\mathrm{U}(a, m+2, 2k_x z_0)$$

$$- 2a\omega^2 c_{0L}^2 k_x \mathrm{U}(1-a, m+3, 2k_x z_0) = 0. \tag{1.88}$$

The equation (1.88) is the dispersion relation for modes formed in a linear polytrope surmounted by an isothermal non-magnetic chromospheric model. An equivalent result to equation (1.88) is given in Campbell and Roberts (1989) There will be a finite number of solutions to equation (1.88) below the cut-off frequency, which is given by equation (1.84). We identify these frequencies as the natural modes of oscillation of the system as modelled, and are thus the frequencies at which, if our model is accurate, p-modes of the given degree l will exist. This dispersion relation, like most others we will encounter, is transcendental, and as such requires a numerical scheme for its solution.

Having found the mode frequencies from equation (1.88), we may then alter the atmospheric conditions, for example by changing the chromospheric temperature, and observe the change in frequency induced. Such procedures form the subject matter of much of the rest of the thesis.

1.5.3 Isothermal model with uniform horizontal magnetic field

We now consider an atmosphere which again is isothermal but now has a magnetic field present, the field being taken to be horizontal and uniform. Consideration of equation (1.7) tells us that the density and gas pressure variations will be as given in section 1.5.2. We must also here consider the Alfvén speed, v_A, which for this model is given by

$$v_A^2 = v_0^2 \exp(-z/H),$$

where v_0 is the Alfvén speed at $z = 0^-$, and H is the scale height (as given in section 1.5.2). Note that the Alfvén speed increases exponentially with height.

For this model, equation (1.21) takes the form (Evans and Roberts, 1990)

$$\left[A_1 + A_2 \exp(-z/H)\right]\frac{d^2 v_z}{dz^2} + \frac{A_1}{H}\frac{dv_z}{dz} + \left[A_4 - k_x^2 A_2 \exp(-z/H)\right] v_z = 0, \tag{1.89}$$

where A_1, A_2 and A_4 are given by

$$\begin{aligned} A_1 &= \omega^2 c_0^2, \\ A_2 &= v_0^2(\omega^2 - k_x^2 c_0^2), \\ A_4 &= (\gamma - 1)g^2 k_x^2 + \omega^2(\omega^2 - k_x^2 c_0^2). \end{aligned}$$

The transformations (Adam, 1975; Nye and Thomas, 1976)

$$s = -\frac{A_1}{A_2}\exp(z/H), \tag{1.90}$$

and

$$v_z = (-s)^{k_x H} W \tag{1.91}$$

then give the equation

$$s(1-s)\frac{d^2 W}{ds^2} + [(1 + 2k_x H) - 2(1 + k_x H)s]\frac{dW}{ds} - \left[k_x H(k_x H + 1) + \frac{A_4 H^2}{A_1}\right] W = 0. \tag{1.92}$$

This is in the form of the hypergeometric equation (Abramovitz and Stegun, 1967: 15.5.1), for which the general solution is

$$W = c_3 \mathrm{F}(p, q; r; s) + c_4 \mathrm{F}(p - r + 1, q - r + 1, 2 - r, s), \tag{1.93}$$

where c_3 and c_4 are arbitrary constants, F is the hypergeometric function, and p, q and r are given by the following set of equations:

$$\begin{aligned} p + q &= 1 + 2k_x H; \\ pq &= k_x H(k_x H + 1) + \frac{A_4 H^2}{A_1}; \\ r &= 1 + 2k_x H. \end{aligned} \tag{1.94}$$

It can be shown (Evans and Roberts, 1990) that for the magnetic energy density to vanish in the limit $z \to -\infty$, we must set $c_4 = 0$. Thus our expression for the vertical velocity is as follows:

$$v_z = c_5 \exp(k_x z)\mathrm{F}(p, q; r; s). \tag{1.95}$$

The coefficients p and q will be complex if and only if

$$\frac{\omega^2}{c_0^2} - \frac{\gamma^2 g^2}{4c_0^2} - k_x^2 + (\gamma - 1)\frac{g^2 k_x^2}{\omega^2 c_0^2} > 0, \tag{1.96}$$

which is the same condition which appears in section 1.5.2. However, it is not obvious that the frequency given by this condition acts as a simple cut-off frequency. The nature of the cut-off frequency in this model is discussed at length in Chapter 2.

We may again form a dispersion relation by matching the solutions on either side of the interface. The dispersion relation is given by (Evans and Roberts, 1990)

$$gk_x^2 + k_x\omega^2 - \frac{\gamma g\omega^2}{c_{0L}^2} - 2ak_x\omega^2\frac{\mathrm{U}(1-a, m+3, 2k_x z_0)}{\mathrm{U}(-a, m+2, 2k_x z_0)}$$
$$= \left(\frac{\rho_{00}}{\rho_{0L}}\right)(\omega^2 - k_x^2 c_0^2)(\omega^4 - g^2 k_x^2)\Big/\mathcal{F}, \tag{1.97}$$

where

$$\mathcal{F} = gk_x^2 c_0^2 + (c_0^2 + v_0^2)(\omega^2 - k_x^2 c_{T0}^2)\left[k_x - \frac{pq}{r}\frac{A_1 A_4}{A_2}\frac{\mathrm{F}(p+1, q+1, r+1, -A_1/A_2)}{\mathrm{F}(p, q, r, -A_1/A_2)}\right].$$

This is the dispersion relation for modes formed in a linear polytrope overlain by an isothermal atmosphere with a uniform horizontal magnetic field. Results gained from this dispersion relation are discussed at length in Chapter 3.

1.6 Thesis outline

In this chapter, we have briefly described some relevant features of the Sun and introduced our area of interest, that is the type of global solar oscillation known as p-modes. We have given the classical explanation of their formation by successive reflection and refraction of sound waves within a cavity resident in the solar interior, and described some of their properties, particularly the observed variation in p-mode frequencies over the solar cycle. We have derived the basic equations governing the general motion of a plasma element in a plane-parallel stratified atmosphere. We have described a polytropic model for the solar interior, and demonstrated from the equations of motion that a cavity can exist, and thus normal modes form, in this model. Under certain conditions, these modes can be considered a mathematical replication of p-modes. We have described two simple models for the solar chromosphere, and derived dispersion relations which incorporate the effect of the chromospheric model on mode frequencies.

In Chapter 2, we examine in detail the nature of the cut-off frequency in the case of an isothermal chromosphere with a uniform horizontal magnetic field. We introduce the concept of the critical frequency, and describe its relevance to the form of plasma motions in the model. This study has implications for the range of frequencies at which we might expect p-modes to form, and the physical processes governing their formation. We then consider the problem of propagation of fast waves at right-angles to a uniform magnetic field, which may be considered as a special case of the earlier investigation, and discuss the critical and cut-off frequencies in this case.

In Chapters 3 and 4 we consider the classical range of p-mode frequencies, that is 1–5mHz, and investigate the observed effect of turnover in p-mode frequency shifts. In Chapter 3 we use an artificial system of equations to diagnose possible causes of the turnover effect. In Chapter 4 we develop an approximate formulation for the calculation of mode frequencies in the presence of a chromosphere, based on the familiar Bohr-Sommerfeld condition. We then use this method to investigate the effect of temperature gradients in the chromosphere on the form of the turnover curve. We conclude with a physical discussion of chromospheric effects on p-mode frequencies, from the viewpoint of a modified Bohr-Sommerfeld condition.

In Chapter 5 we leave the classical range of p-mode frequencies and investigate the formation of modes above the acoustic cut-off frequency. In doing so we exploit the results of Chapter 2, which describe the formation of such high-frequency modes, and the modified Bohr-Sommerfeld condition of Chapter 4, which allows us to calculate mode frequencies. We also extend the 'turnover' curve into a new frequency range, and find many new features of its behaviour.

In Chapter 6 we look at another special case, that of modes of degree zero. We develop a model and dispersion relation for this singular problem, and find mode frequencies which agree well with the observed frequencies of zero-degree p-modes. We also consider changes in the frequencies of such modes caused by certain changes in a simple chromospheric model.

In Chapter 7 we summarise the main results of the thesis, and give a brief description of some possibilities for further research suggested by this work.

Chapter 2

Critical and cut-off frequencies in a uniform magnetic field

2.1 Introduction

In chapter 1 we introduced the concept of the cut-off frequency. This quantity was seen to describe the upper limit of the range of frequencies at which normal modes could be formed for a given physical situation. The existence of such a limit was brought about by the requirement that, for normal modes to form, a bounded cavity must exist in which waves can propagate, surrounded by a region in which waves cannot propagate. The dimensions and characteristics of the cavity then determine the frequencies of the modes formed.

For example, in section (1.4.3) we considered the case of our linear polytrope model, and demanded that a mode cavity, here defined as a range of z bounded by two zeros of $\kappa^2(z)$, be formed entirely within the domain of that model. This implied the existence of an upper limit on frequencies given by $\kappa^2(0^+) = 0$; this upper limit, corresponding to the acoustic cut-off frequency for this problem, is given in equation (1.61).

For the more complete problem of a linear polytrope surmounted by a chromospheric model, a variety of situations arise. In the case of an isothermal non-magnetic model, we see that waves of frequency less than ω_c, as given in equation (1.85), cannot propagate at all in the chromosphere. Thus we can presume that waves below this frequency are trapped in a cavity that is resident in the solar interior model, bounded above by $z = 0$, and that

normal modes may form in this cavity. This feature of the model is taken to represent the reflection of sound waves at the solar surface which allows the formation of a p-mode cavity in the Sun. Waves of frequency greater than ω_c can, however, propagate straight through the interface $z = 0$ and on to indefinitely large heights in the chromosphere. Thus no bounded cavity will form for waves at this frequency, and so we would not expect modes to form at such a frequency. Thus ω_c is described as the cut-off frequency for this problem; it will henceforth be generally termed the *non-magnetic cut-off frequency.*

Where the chromospheric model contains a uniform horizontal magnetic field, however, the situation is less clear. We find a solution for the plasma motions in this model in terms of hypergeometric functions, rather than the sinusoidal or exponential functions found in the non-magnetic model. It is not obvious whether these hypergeometric function solutions represent propagating or non-propagating motions in the chromosphere, and so it is not clear what value the cut-off frequency will take in this case. The nature of the cut-off frequency in this situation will thus form the subject matter of much of this chapter.

A point should be made here about two definitions which will be used here. The *cut-off frequency* will be defined as the frequency above which modes would not be expected to form for a given model. This quantity will in general depend on the global characteristics of the model, including the values of variables such as the temperature and the magnetic field strength. However, it will have one definite value for any one set of model parameters, and will not be a function of height (or depth), z. The *critical frequency*, on the other hand, will be defined as the frequency at which certain local behaviour of the plasma motions will be observed. In general, the critical frequency *will* be a function of z, and may take up different forms depending on the particular facet of wave behaviour being considered.

For example, in section 1.4.3, we expressed the general form of the acoustic cut-off frequency for our linear polytrope as in equation (1.60); in the stricter terms we now employ, this is properly considered as the acoustic critical frequency. For a given z, this equation will determine the frequency such that $\kappa^2(z)$ is zero at that depth. In this situation, the cut-off frequency is defined by the upper limit of frequencies such that $\kappa^2(z)$ will have a zero near $z = 0$; thus its value will be set by the maximum value of the critical frequency in $z \geq 0$. Since this occurs at $z = 0$, we find the expression for the acoustic cut-off frequency given in equation (1.61).

Thus the task we set ourselves in this chapter is to investigate the effect upon both the critical and cut-off frequencies of a uniform horizontal magnetic field in our chromo-

spheric model. To do this, we will consider analytical solutions to the wave equations in various limits, and also consider the qualitative behaviour of certain alternative forms of the wave equation.

We conclude this chapter with an investigation of the propagation of fast magneto-acoustic waves at right-angles to a uniform magnetic field. This problem has been widely considered, for example by Thomas (1982), Musielak, An, Moore and Suess (1989) and Stark and Musielak (1993), and the nature of the critical and cut-off frequencies in this situation has proved controversial. We attempt to bring some of the knowledge gained in sections 2.2 and 2.3 to bear on this problem.

2.2 The cut-off frequency

Our model for this problem is as described in sections 1.4.1 and 1.5.3. We use a linear polytrope for the solar interior, topped by an isothermal chromosphere containing a uniform horizontal magnetic field. In our chromosphere, the wave equation for the vertical component of motion, v_z, is given by equation (1.89), and displayed here for convenience:

$$\left[A_1 + A_2 \exp(-z/H)\right] \frac{d^2 v_z}{dz^2} + \frac{A_1}{H} \frac{dv_z}{dz} + \left[A_4 - k_x^2 A_2 \exp(-z/H)\right] v_z = 0, \qquad (2.1)$$

where A_1, A_2 and A_4 are given by

$$\begin{aligned} A_1 &= \omega^2 c_0^2, \\ A_2 &= v_0^2(\omega^2 - k_x^2 c_0^2), \\ A_4 &= (\gamma - 1) g^2 k_x^2 + \omega^2(\omega^2 - k_x^2 c_0^2). \end{aligned}$$

The exact solution to this equation is

$$v_z = c_5 \exp(k_x z) \mathrm{F}(p, q; r; s), \qquad (2.2)$$

where F is the hypergeometric function, the variable s is defined by

$$s = -\frac{A_1}{A_2} \exp(z/H) \qquad (2.3)$$

and the parameters p, q and r are given by

$$p + q = 1 + 2k_x H;$$

$$pq = k_x H(k_x H + 1) + \frac{A_4 H^2}{A_1};$$

$$r = 1 + 2k_x H; \tag{2.4}$$

p and q will be complex if and only if the frequency ω is above the non-magnetic cut-off frequency.

We have stated that our condition on the formation of a normal mode is that plasma motions must die out above a certain height, ensuring that a bounded cavity is formed. It is not immediately clear at which frequencies this will occur for the hypergeometric function solution, so it is helpful to examine the behaviour of this solution in various asymptotic limits.

It is a general property of Bessel and hypergeometric functions that (Abramovitz and Stegun, 1967: 9.1.70)

$$\mathrm{J}_\eta(t_1) = \frac{(\frac{1}{2}t_1)^\eta}{\Gamma(\eta+1)} \lim \mathrm{F}\left(\lambda, \mu; \eta+1; -\frac{t_1^2}{4\lambda\mu}\right) \tag{2.5}$$

as λ and μ tend to infinity through real or complex values, with t_1 and η being fixed. If we introduce

$$t_2 = -\frac{t_1^2}{4\lambda\mu} \tag{2.6}$$

so that

$$t_1 = (4\lambda\mu)^{1/2}(-t_2)^{1/2}, \tag{2.7}$$

we can rewrite equation (2.5) as follows. As λ and μ tend to infinity through real or complex values and as t_2 tends to zero such that $t_1 = (4\lambda\mu)^{1/2}(-t_2)^{1/2}$ remains fixed,

$$\lim \mathrm{F}(\lambda, \mu; \eta+1; t_2) = \frac{\Gamma(\eta+1)}{(\lambda\mu)^{\eta/2}(-t_2)^{\eta/2}} \mathrm{J}_\eta\left[(4\lambda\mu)^{1/2}(-t_2)^{1/2}\right]. \tag{2.8}$$

We can apply this result to our hypergeometric function solution for v_z. If we consider the limit of high frequency, $\omega^2 \to \infty$ and thus the ratio A_4/A_1 will tend to infinity. Since we can write p and q in the form

$$p, q = \frac{1 + 2k_x H}{2} \pm \frac{1}{2}\left\{1 - \frac{4\left[k_x H(k_x H + 1) + A_4 H^2/A_1\right]}{(1 + 2k_x H)^2}\right\}^{1/2}, \tag{2.9}$$

we see that as A_4/A_1 tends to infinity, p and q tend towards $\pm i\infty$. Also, if we consider the limit of large height, so that $s \to 0$, then we can satisfy the condition that p and q

tend to infinity while $(4pq)^{1/2}(-s)^{1/2}$ remains fixed. Thus, we can use equation (2.8) with $\eta = 2k_xH$ to write the asymptotic form of equation (2.2) as

$$\begin{aligned} v_z &\sim c_5(-s)^{-k_xH}\frac{\Gamma(1+2k_xH)}{(pq)^{k_xH}}\frac{\mathrm{J}_\eta\left[(4pq)^{1/2}(-s)^{1/2}\right]}{(-s)^{-k_xH}} \\ &= c_6\mathrm{J}_\eta\left[(4pq)^{1/2}(-s)^{1/2}\right]. \end{aligned} \tag{2.10}$$

Hence, at high frequencies and large heights, the asymptotic limit of the hypergeometric function solution (2.2) is the Bessel function solution (2.10).

Furthermore, it is a property of Bessel functions that, as t_3 tends to zero for fixed η (Abramovitz and Stegun, 1967: 9.1.7),

$$\mathrm{J}_\eta(t_3) \sim \frac{(\frac{1}{2}t_3)^\eta}{\Gamma(\eta+1)}. \tag{2.11}$$

Thus if we take our Bessel function solution (2.10) in the limit of large height, so that

$$(4pq)^{1/2}(-s)^{1/2} \to 0,$$

then

$$\begin{aligned} v_z &\sim c_6\frac{(pq)^{\eta/2}}{\Gamma(\eta+1)}(-s)^{\eta/2} \\ &= c_8\exp(k_xz). \end{aligned} \tag{2.12}$$

Thus in the limit of large height, the asymptotic limit of our Bessel function solution is the exponential function solution (2.12).

The reduction of the hypergeometric function solution through these asymptotic limits thus demonstrates that at *all* frequencies there exists a sufficiently large height above which plasma motions will die out exponentially with height.

These asymptotic solutions can also be found by considering the differential equation from which we find the hypergeometric function solution. If we apply *only* the transformation (1.90) to equation (2.1), we obtain the differential equation

$$s(1-s)\frac{d^2v_z}{ds^2} + (1-2s)\frac{dv_z}{ds} - \left[\frac{A_4H^2}{A_1} + \frac{k_x^2H^2}{s}\right]v_z = 0. \tag{2.13}$$

Now in the limit of large and negative z, s will tend to zero. Thus terms such as $(1-s)$ and $(1-2s)$ will tend to unity. We also consider the limit of large frequency, so that the

A_4H^2/A_1 term is of comparable size to the $k_x^2H^2/s$ term in the coefficient of v_z. Then, in these limits, we may write equation (2.13) as

$$s\frac{d^2v_z}{ds^2} + \frac{dv_z}{ds} - \left[\frac{A_4H^2}{A_1} + \frac{k_x^2H^2}{s}\right]v_z = 0. \tag{2.14}$$

The transformation

$$u = \left(\frac{4A_4H^2}{A_1}\right)^{1/2}(-s)^{1/2} \tag{2.15}$$

then yields the differential equation

$$u^2\frac{d^2v_z}{du^2} + u\frac{dv_z}{du} + (u^2 - 4k_x^2H^2)v_z = 0. \tag{2.16}$$

This is the standard form of the Bessel differential equation (Abramovitz and Stegun, 1967: 9.1.1), to which solutions are the Bessel function of the first kind, J_η and the second kind Y_η, where in this case $\eta \equiv 2k_xH$. As $u \to 0$, the function $\mathrm{Y}_\eta(u)$ is unbounded for all $\eta > 0$, so our physically realistic solution to equation (2.16) is

$$v_z = c_8\mathrm{J}_\eta(u). \tag{2.17}$$

In the high frequency limit,

$$4pq \to \frac{4A_4H^2}{A_1},$$

and we can see that the argument of the Bessel function solution (2.10) and our variable u are asymptotically equal. Thus the solution (2.17) found from the asymptotic form of the differential equation (2.1) is identical to that found by taking the asymptotic limit of the full solution to equation (2.1). This is not surprising, but serves to confirm the validity of our Bessel function solution. Furthermore, it illustrates the significance of taking both the high frequency and large height limits simultaneously, to ensure that the two terms in the coefficient of v_z in equation (2.13) are of similar order.

We can also consider equation (1.89) and allow z to tend to negative infinity, keeping all other quantities finite. We then find the asymptotic form

$$\frac{d^2v_z}{dz^2} - k_x^2v_z = 0. \tag{2.18}$$

The physically realistic solution to this equation is

$$v_z = c_9\exp(k_xz), \tag{2.19}$$

in agreement with the asymptotic limit of the Bessel function solution (2.10).

What, then, is the conclusion of these various results? We have shown that at sufficiently large heights, the vertical velocity v_z will always die out exponentially with height. Thus we have a region in which waves may propagate; this region is bounded for waves of all frequencies. Thus a cavity with the potential to select normal modes is created. Hence for a linear polytrope surmounted by an isothermal chromosphere with a uniform horizontal magnetic field, we may state that the cut-off frequency is *infinite*. The implication for the solar problem is that if this model reliably represents the Sun, p-modes may be formed at all frequencies.

We have considered some high frequency and large height limits to deduce the value of the cut-off frequency. We now turn to the more general issue of the nature of plasma motions throughout the chromosphere, the study of which requires investigation of the critical frequency.

2.3 The critical frequency

2.3.1 Definition

In section (1.2.1), we gave the classical description of the formation of a p-mode cavity by refraction and reflection of waves, the process of reflection at the solar surface providing the outer shell to the cavity as well as introducing the effect of cut-off. We have modelled this by a non-magnetic chromosphere, for which it is found that trapping will occur at $z = 0$, which represents the solar surface, but only for waves with frequencies less than the cut-off frequency, ω_c. This model thus agrees well with our picture of actual p-mode behaviour, with the trapping of waves at $z = 0$ corresponding to the reflection of waves at the solar surface.

Can we find a similar physical picture for the case where a uniform horizontal magnetic field is present? We have seen that in this situation, a bounded cavity will form for all frequencies, because all waves must be evanescent at sufficiently large heights. However, we know nothing about the form of plasma motions in the chromosphere in general, and we do not have a grasp of the physical processes to which this trapping can be ascribed. To provide this, it is helpful to now consider the critical frequency.

In section 2.1 we gave a general definition of the critical frequency, as the frequency

at which certain local behaviour of the plasma motions will be observed. We now form a more specific definition of the critical frequency by considering again the intuitive picture of plasma motions given in section 1.3.3. There we considered the canonical form of the wave equation for the variable $\nabla.v$, which involved the related variable Q. We associated regions of positive or negative $\kappa^2(z)$ with regions in which oscillatory-type or exponential-type solutions, respectively, would be found for Q. Points at which $\kappa^2(z)$ was zero would then correspond to heights where the nature of plasma motions changed from oscillatory to exponential.

Thus in general, we will define the critical frequency associated with a given plasma motion variable as the frequency such that $\kappa^2(z)$, or its equivalent variable, is zero at a given height, $-z$, in the absence of any refractive process. For example, in section 1.4.3, κ^2 could have two zeros in $z > 0$: one associated with reflection near $z = 0$, when $\omega \approx \omega_a$, and one associated with refraction at large z, when $\omega \approx k_x c_s$. The critical frequency $\omega_a(z)$ is a property solely of the stratified plasma, and is unaffected by the value of k_x; we wish this to be generally true for *any* form of the critical frequency; this ensures that the critical frequency will only contain information about the reflection of waves by the stratification of the plasma, rather than the refraction of waves by a variation in sound speed or fast speed. Thus for the variable Q, the critical frequency ω_q will be the function of z defined by

$$\kappa^2(z, \omega_q)\Big|_{k_x=0} = 0. \tag{2.20}$$

Thus at a given height $-z$ where refractive processes are not significant, the plasma motion variable Q will alter in form from oscillatory-type to exponential-type for waves of frequency $\omega_q(z)$.

We might equally consider the canonical form of the differential equation (1.21) in v_z; this equation will not be identical to that for $\nabla.v$. We can write such a canonical equation in the general form

$$\frac{d^2X}{dz^2} + \psi^2(z)X = 0, \tag{2.21}$$

where X, which is to v_z, and ψ^2, a function of the atmospheric parameters, the frequency ω and the horizontal wavenumber k_x, are to be determined. We can again associate an oscillatory-type form of X with a region of positive ψ^2, and an exponential-type form of X with a region of negative ψ^2. The critical frequency for this variable, which we shall call ω_x, will then be defined by

$$\psi^2(z, \omega_x)\Big|_{k_x=0} = 0. \tag{2.22}$$

Again we can state that at a given height $-z$ where refractive processes are not significant, the variable X will alter in form from oscillatory-type to exponential-type for waves of frequency $\omega_x(z)$.

2.3.2 Canonical equation in v_z

Let us now evaluate the precise form of equation (2.21). Starting from equation (1.21), the transformation

$$v_z = P^{-1/2}X \tag{2.23}$$

yields the form of equation (2.21). The variable $\psi^2(z)$, for profiles of ρ_0, c_s^2 and v_A^2 given by our isothermal model with a uniform magnetic field, takes the form

$$\begin{aligned}\psi^2(z) = {} & \frac{\omega^2}{c_0^2+v_A^2}\left(\frac{\omega^2}{\omega^2-k_x^2c_T^2}\right) \\ & -\frac{1}{2H^2}\left(\frac{c_0^2}{c_0^2+v_A^2}\right)\left(\frac{\omega^2}{\omega^2-k_x^2c_T^2}\right)+\frac{1}{4H^2}\left(\frac{c_0^2}{c_0^2+v_A^2}\right)^2\left(\frac{\omega^2}{\omega^2-k_x^2c_T^2}\right)^2 \\ & -k_x^2+(\gamma-1)\frac{g^2k_x^2}{\omega^2}\left(\frac{1}{c_0^2+v_A^2}\right)\left(\frac{\omega^2}{\omega^2-k_x^2c_T^2}\right) \quad .\end{aligned} \tag{2.24}$$

Thus our definition of the critical frequency in this case, equation (2.22), yields a critical frequency ω_x of the form

$$\omega_x^2(z) = \frac{c_0^2}{4H^2}\left(\frac{c_0^2+2v_A^2}{c_0^2+v_A^2}\right). \tag{2.25}$$

We call this frequency the critical frequency for the wave variable X (for this chromospheric model). Figure 2.1 shows the variation of the critical frequency ω_x (in mHz) with z (in km); remember that height in the chromosphere is given by $-z$. For this Figure, and for Figures 2.2–2.7, we take a chromospheric temperature of 4170K and a magnetic field strength of 30G. We see that ω_x increases with height, tending asymptotically to the value $(c_0^2/2H^2)^{1/2}$.

The significance of this form of the critical frequency may be made clearer by considering the following simplifications. In most of the solar applications we shall consider, the quantity $k_x^2c_0^2/\omega^2$ is very small. For example, for a typical mode of degree 50, we find that $k_x^2 \approx 5.3\times10^{-15}\mathrm{m}^{-2}$; for a mode of frequency 4.5mHz, that $\omega^2 \approx 8.0\times10^{-4}\mathrm{s}^{-2}$; and that for a chromospheric temperature of 4170K, $c_0^2 \approx 4.5\times10^{7}\mathrm{m}^2\mathrm{s}^{-2}$. Thus the value of

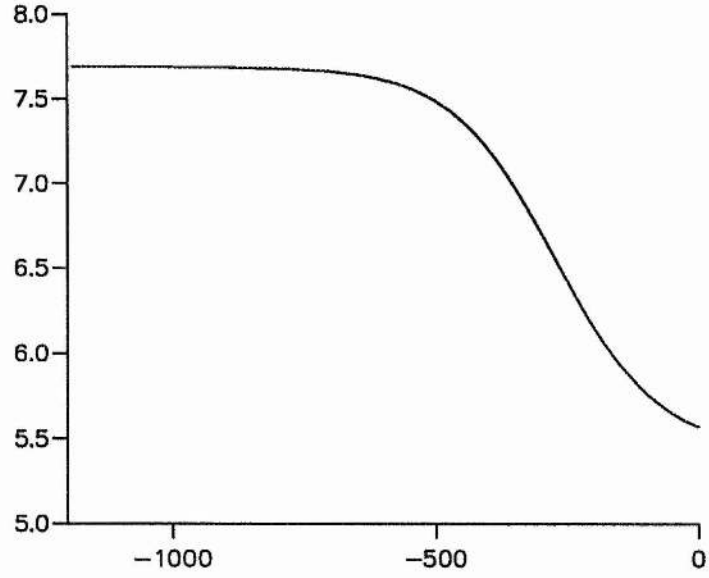

Figure 2.1: The critical frequency ω_x (in mHz) vs. z (in km), for an isothermal chromosphere at a temperature of 4170K with a uniform horizontal magnetic field of strength 30G.

$k_x^2 c_0^2/\omega^2$ is around 3×10^{-4}. Also, the speed c_T is smaller than c_0, so $k_x^2 c_T^2/\omega^2$ must be small also. Under this approximation, the factor $\omega^2/(\omega^2 - k_x^2 c_T^2)$ can be written as

$$\begin{aligned} \frac{\omega^2}{\omega^2 - k_x^2 c_T^2} &= \left(1 - \frac{k_x^2 c_T^2}{\omega^2}\right)^{-1} \\ &\approx 1; \end{aligned} \tag{2.26}$$

thus under this approximation, equation (2.24) can be written as

$$\psi^2 \approx \frac{\omega^2}{c_0^2 + v_A^2} - \frac{c_0^2}{4H^2} \frac{c_0^2 + 2v_A^2}{(c_0^2 + v_A^2)^2} - k_x^2 + (\gamma - 1) \frac{g^2 k_x^2}{\omega^2} \frac{1}{c_0^2 + v_A^2}, \tag{2.27}$$

and the transformation (2.23) can be written as

$$X = \rho_0^{1/2} (c_0^2 + v_A^2)^{1/2} v_z. \tag{2.28}$$

Furthermore, we shall in general be considering high order modes; since

$$\omega^2 \approx g k_x \left(1 + \frac{2n}{m}\right),$$

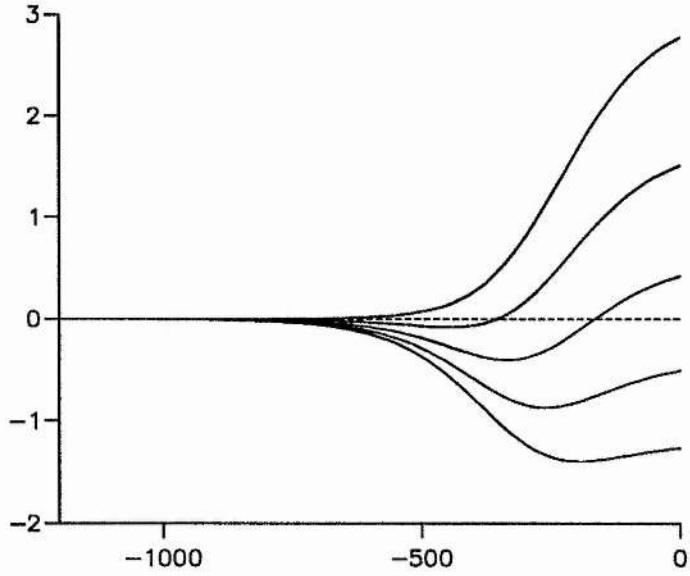

Figure 2.2: ψ^2 (in non-dimensionalised units) vs. z (in km). The solid curves are for frequencies of (from top to bottom) 4, 5, 6, 7 and 8mHz; chromospheric parameters are as for Figure 2.1.

we can be sure that for large n,

$$\frac{g^2 k_x^2}{\omega^4} \ll 1. \tag{2.29}$$

Thus the last term in equation (2.27) must be small in comparison with the first term. Thus we have the following approximate form for $\psi^2(z)$:

$$\psi^2 \approx \frac{\omega^2}{c_0^2 + v_A^2} - \frac{c_0^2}{4H^2} \frac{c_0^2 + 2v_A^2}{(c_0^2 + v_A^2)^2} - k_x^2, \tag{2.30}$$

that is

$$\psi^2 \approx \frac{\omega^2 - \omega_x^2}{c_0^2 + v_A^2} - k_x^2. \tag{2.31}$$

This expression provides a good approximation for $\psi^2(z)$ in our model, and features the critical frequency ω_x. What does it tell us about plasma motions in the model?

Figure 2.2 shows the variation of $\psi^2(z)$ (in non-dimensionalised units) with z (in km) for motions of frequencies 4, 5, 6, 7 and 8mHz; the highest values of ψ^2 are for the highest frequencies. In general, ψ^2 tends to $-k_x^2$ at large heights, implying exponential-type solutions. This corresponds to our deduction in section 2.2 that motions at all frequencies

will be evanescent above some height in the model, and thus that modes may form across an infinite range of frequencies. In the lower part of the model, the form of ψ^2 depends on the frequency of the mode formed. We can classify these as follows.

1. For modes below a certain frequency, which we can deduce is given by the value of the critical frequency ω_x at $z = 0^-$, ψ^2 is negative throughout $z < 0$. We may assume that for modes which form in this frequency range, plasma motions throughout $z < 0$ will be in the form of evanescent standing waves.

2. For modes at frequencies lying between the minimum and maximum of ω_x in $z < 0$, motions may be of oscillatory-type in the lowest part of the chromospheric model. The height at which motions change from oscillatory-type to exponential-type will be approximately given by $\omega = \omega_x$.

3. For modes at frequencies greater than the maximum value attained by ω_x in $z < 0$, motions may again be of oscillatory-type in the lowest part of the model. The height at which motions change from oscillatory-type to exponential-type will be approximately given by $\omega = k_x(c_0^2 + v_A^2)^{1/2}$.

Thus the trapping of wave motions couched in terms of the variable X occurs through two distinct physical effects. One, *reflection*, is associated with the critical frequency ω_x, and is most important for modes of frequency up to 7.5mHz. For modes above this frequency, reflection is unable to completely trap the waves, and the process of *refraction* operates to contain the wave at a greater height in the model.

This conjunction of processes is evident in Figure 2.3. Here the solid line represents the height (in km) at which the turning point $\psi^2 = 0$ occurs, as a function of frequency (in mHz). The dashed line represents the curve $\omega = \omega_x$, that is the height at which a turning point would occur if reflection only were present. The dotted line represents the curve $\omega = k_x(c_0^2 + v_A^2)^{1/2}$, that is the height at which a turning point would occur if refraction only were present. We see that for modes up to around 7.5mHz, the 'reflection-only' approximation is a good one, but above the maximum value attained in the model by ω_x, the behaviour asymptotes towards the 'refraction-only' curve.

We can also illustrate the form of X in $z < 0$ for a mode in each of the above frequency ranges. Figure 2.4 shows the numerically calculated form of X for modes of frequency 4, 6, 8 and 10mHz, each normalised to the same exponentially decaying solution

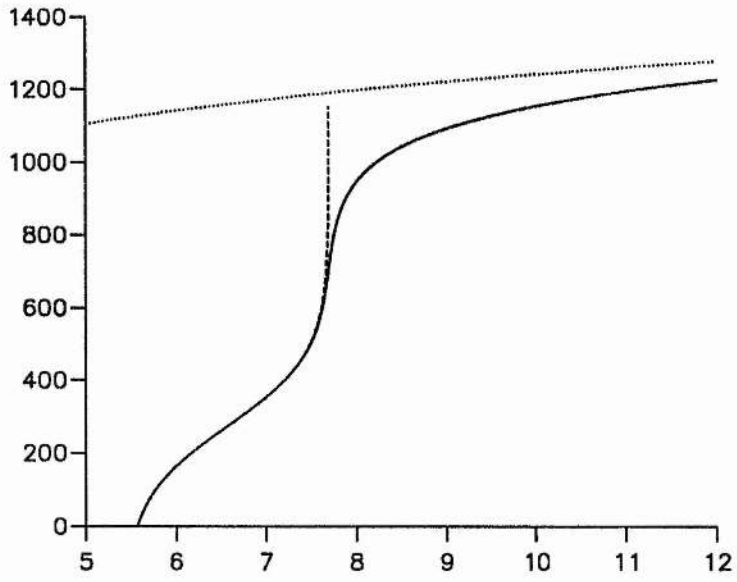

Figure 2.3: Variation of the height of the turning point $\psi^2 = 0$ with frequency (in mHz). The dashed line gives the 'reflection-only' curve, the dotted line 'refraction-only'; chromospheric parameters are as for Figure 2.1.

at large height. In each case the form of X should be compared with the form of ψ^2 displayed in Figure 2.2. We see that for the 4mHz mode, the top curve in Figure 2.4, X is exponentially decaying with height throughout $z < 0$. For the 6mHz mode, X is exponentially decaying throughout most of $z < 0$, but shows signs of the beginning of oscillatory behaviour near $z = 0$; the turning point for this frequency occurs at a height of around 200km. For the 8mHz and 10mHz modes, X is plainly oscillatory in the lowest part of the model; the turning points at these frequencies occur at a height of around 1000km.

In summary, when we are considering the wave variable X, we find that the behaviour of plasma motions in our magnetic chromospheric model depends on the frequency of the motion, and that all waves can be trapped by a combination of reflection, associated with the critical frequency ω_x, and refraction.

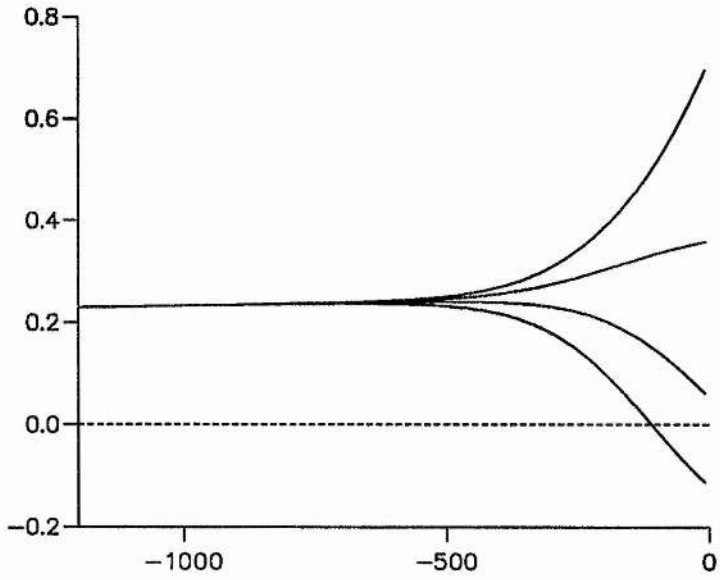

Figure 2.4: The plasma motion variable X (in non-dimensionalised units) vs. z (in km), for frequencies of, from top to bottom, 4, 6, 8 and 10mHz; chromospheric parameters are as for Figure 2.1.

2.3.3 Canonical equation in $\nabla.\boldsymbol{v}$

Let us now look again at the canonical form of the differential equation in $\nabla.\boldsymbol{v}$, equation (1.24), with κ^2 given by equation (1.25). In our model, these equations reduce to

$$\frac{d^2Q}{dz^2} + \kappa^2(z)Q = 0, \tag{2.32}$$

where

$$\kappa^2 = \frac{\omega^2}{c_0^2 + v_A^2}\left(\frac{\omega^2}{\omega^2 - k_x^2 c_T^2}\right) + \frac{1}{2H^2}\left(\frac{\omega^2}{\omega^2 - k_x^2 v_A^2}\right)$$
$$-\frac{3}{4H^2}\frac{\omega^4}{(\omega^2 - k_x^2 v_A^2)^2} - k_x^2$$
$$+\frac{k_x^2}{\omega^2}\frac{g}{H}\left(\frac{\omega^2}{\omega^2 - k_x^2 v_A^2}\right) - \frac{k_x^2}{\omega^2}\left(\frac{g^2}{c_0^2 + v_A^2}\right)\left(\frac{\omega^2}{\omega^2 - k_x^2 c_T^2}\right). \tag{2.33}$$

We can immediately find the critical frequency for this variable, ω_q, as defined in

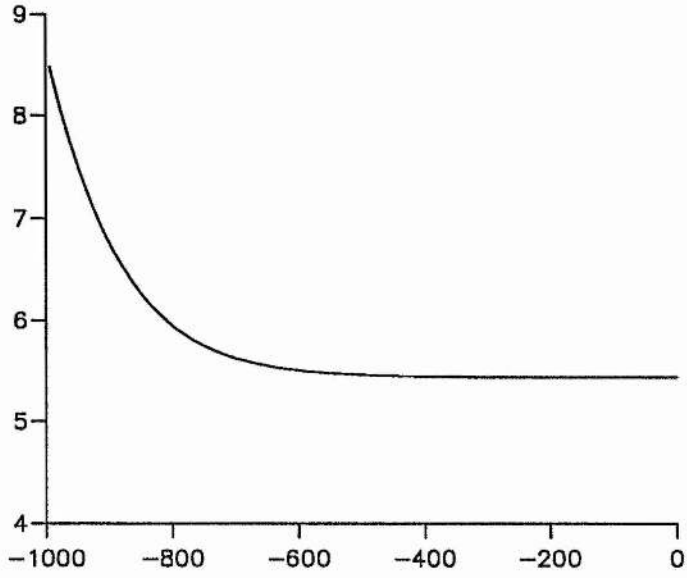

Figure 2.5: The critical frequency ω_q (in mHz) vs. z (in km). Chromospheric parameters are as for Figure 2.1.

equation (2.20); it is given by

$$\omega_q^2(z) = \frac{c_0^2 + v_A^2}{4H^2}. \tag{2.34}$$

Figure 2.5 shows the variation of ω_q (in mHz) with z (in km) for the same chromospheric parameters as Figure 2.1. We see that the critical frequency increases indefinitely with height.

We can also consider the form of κ^2 in $z < 0$. The solid line in Figure 2.6 shows the variation of κ^2 (in non-dimensionalised units) with z (in km) for motions of frequency 6mHz. The main features of this curve are as follows: again, κ^2 tends to $-k_x^2$ at large heights; there is a singularity associated with $\omega^2 - k_x^2 v_A^2 = 0$, at which $\kappa^2 \to -\infty$; and there is a region near $z = 0$ in which $\kappa^2 > 0$. The potential singularity associated with $\omega^2 - k_x^2 c_T^2 = 0$ is unimportant since we have seen that for the modes we shall consider, $\omega^2 - k_x^2 c_T^2 \gg 0$. The dotted line depicts the variation of an approximate form of κ^2 given by

$$\kappa^2 \approx \frac{\omega^2 - \omega_q^2}{c_0^2 + v_A^2}$$

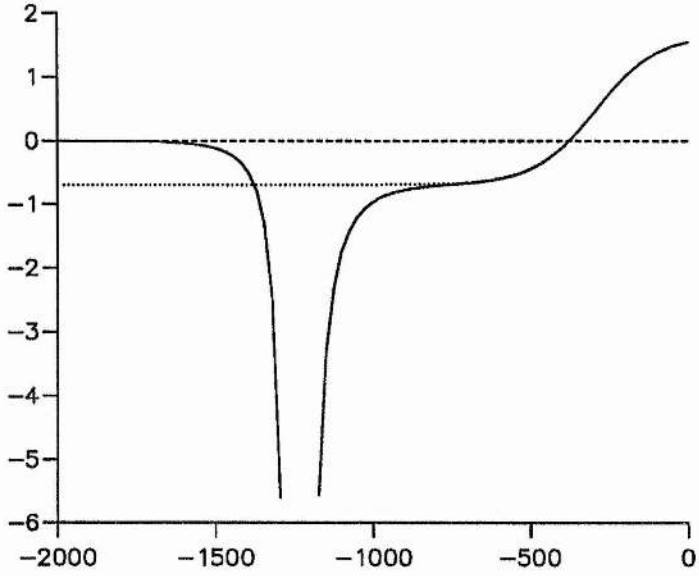

Figure 2.6: κ^2 (in non-dimensionalised units) vs. z (in km) for motions of frequency 6mHz. The solid curve depicts the full form of κ^2, the dotted line the approximate form; chromospheric parameters are as for Figure 2.1.

$$= \frac{\omega^2}{c_0^2 + v_A^2} - \frac{1}{4H^2}, \tag{2.35}$$

obtained by neglecting refractive effects entirely. At heights of less than around 700km, the solid and dotted lines coincide, implying that the position of the turning point $\kappa^2 = 0$ is given accurately by the approximate form for κ^2.

It can be shown that the approximate form of κ^2 will always accurately predict the position of the turning point for modes within a certain range of k_x. Firstly let us assume that in the lowest part of the model, we can consider the asymptotic limit $k_x^2 v_A^2/\omega^2 \ll 1$. This, along with the approximation that $g^2 k_x^2/\omega^4 \ll 1$ which we have already encountered, reduces κ^2 to the form given in equation (2.35). The zero of this approximate form of κ^2 will occur where

$$v_A^2 = 4\omega^2 H^2 - c_0^2; \tag{2.36}$$

the value of $k_x^2 v_A^2/\omega^2$ at this height will thus be given by

$$\frac{k_x^2 v_A^2}{\omega^2} = 4k_x^2 H^2 - \frac{k_x^2 c_0^2}{\omega^2}. \tag{2.37}$$

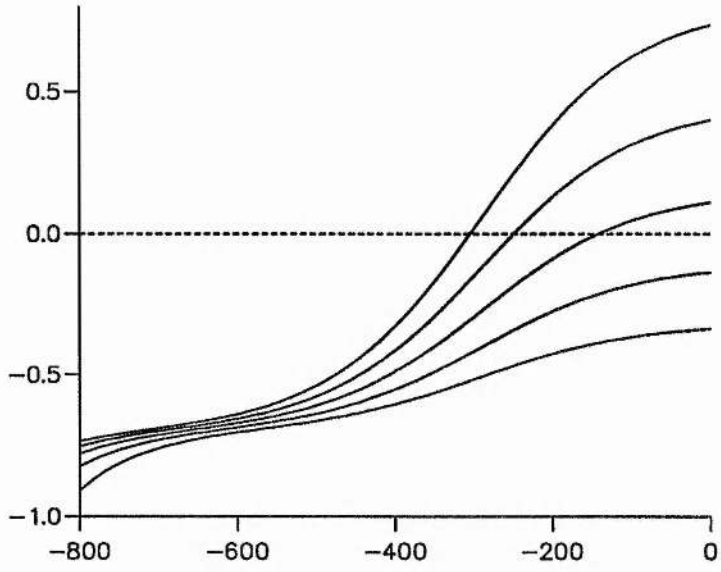

Figure 2.7: κ^2 (in non-dimensionalised units) vs. z (in km) near z=0, for modes of frequency (from bottom to top) 4, 5, 6, 7 and 8mHz. Chromospheric parameters are as for Figure 2.1.

The quantity $4k_x^2H^2$ will be small in our problem as long as $k_x^2 \ll g^2/c_0^4$; this will be satisfied for modes such that $l \ll 4270$. Thus for the range of l we will consider in this thesis, the approximation $k_x^2 v_A^2/\omega^2 \ll 1$ is valid at least up to the height of the turning point given by equation (2.35).

Thus the position of the turning point $\kappa^2 = 0$ for this problem is accurately given by the approximate form of κ^2 given in equation (2.35). The conclusion of this is that reflection of waves by the stratification of the plasma is solely responsible for the trapping of waves expressed in terms of the variable Q. The critical frequency associated with this reflection is ω_q, as given in equation (2.34). Furthermore, under these approximations, we can write that

$$Q \approx \rho_0^{1/2}(c_0^2 + v_A^2)\nabla.\boldsymbol{v}. \tag{2.38}$$

We can consider the form of κ^2 near its zero for modes at a range of frequencies. Figure 2.7 shows the variation of the full form of κ^2 (in non-dimensionalised units) with z (in km) for modes of frequencies 4, 5, 6, 7 and 8mHz. We see that κ^2 is obviously greater for higher ω, as is the height of the turning point. We also see a 'bunching together' of the

κ^2 curves, caused by the fact that at all frequencies, κ^2 tends to the value $-1/4H^2$ before the singularity has its effect.

In the region where $k_x^2 v_A^2/\omega^2 \ll 1$, we can find a more general approximation for κ^2, without requiring that $g^2 k_x^2/\omega^4 \ll 1$. Under the approximation $k_x^2 v_A^2/\omega^2 \ll 1$, terms such as $\omega^2/(\omega^2 - k_x^2 v_A^2)$ can be written as

$$\begin{aligned} \frac{\omega^2}{\omega^2 - k_x^2 v_A^2} &= \left(1 - \frac{k_x^2 v_A^2}{\omega^2}\right) \\ &\approx 1, \end{aligned}$$

allowing us to write the form of κ^2 as

$$\kappa^2 \approx \frac{\omega^2}{c_0^2 + v_A^2} - \frac{1}{4H^2} - k_x^2 + \frac{k_x^2}{\omega^2}\left[\frac{g}{H} - \frac{g^2}{c_0^2 + v_A^2}\right] \tag{2.39}$$

or

$$\kappa^2 = \frac{\omega^2 - \omega_q^2}{c_0^2 + v_A^2} + \frac{k_x^2}{\omega^2}(\omega_{gm}^2 - \omega^2), \tag{2.40}$$

where

$$\omega_{gm}^2 = \frac{g}{H} - \frac{g^2}{c_0^2 + v_A^2}. \tag{2.41}$$

The result (2.39) can be compared with a previously published form of κ^2 obtained under the same approximation. Roberts and Campbell (1986) give a form of κ^2 which, for our model, reads as follows:

$$\kappa^2 = \frac{\omega^2}{c_0^2 + v_A^2} + \frac{k_x^2 c_0^2 v_A^2}{(c_0^2 + v_A^2)^2} - \frac{1}{4H^2} - k_x^2 + \frac{k_x^2 \omega_g^2}{\omega^2}\left(\frac{c_0^2}{c_0^2 + v_A^2}\right) + A, \tag{2.42}$$

where ω_g is the buoyancy frequency and A is described as being of the order $k_x^2 v_A^2/\omega^2 H^2$, and generally negligible. Our form of κ^2 differs from equation (2.42) in two respects.

1. The second term on the right-hand side of equation (2.42) does not appear in equation (2.39). This term is produced by the expansion of the first term on the right-hand side of equation (2.33), that is

$$\begin{aligned} \frac{\omega^2}{c_0^2 + v_A^2}\left(1 - \frac{k_x^2 c_T^2}{\omega^2}\right)^{-1} &\approx \frac{\omega^2}{c_0^2 + v_A^2}\left(1 + \frac{k_x^2 c_T^2}{\omega^2}\right) \\ &= \frac{\omega^2}{c_0^2 + v_A^2} + \frac{k_x^2 c_0^2 v_A^2}{(c_0^2 + v_A^2)^2}. \end{aligned}$$

Thus the term in question is of order $k_x^2 c_T^2/\omega^2$ compared to the term $\omega^2/(c_0^2+v_A^2)$ and may thus be neglected, even though the expanded term does not explicitly involve the small quantity $k_x^2 v_A^2/\omega^2$.

2. We can write the last but one term of equation (2.42) in the form

$$\frac{k_x^2}{\omega^2}\left[\frac{g}{H}\frac{c_0^2}{c_0^2+v_A^2} - \frac{g^2}{c_0^2+v_A^2}\right].$$

Thus the discrepancy between this term and the final term of equation (2.39) is the appearance of the factor $c_0^2/(c_0^2+v_A^2)$ in the first terms inside the square bracket. In other words, the difference between the two expressions is the term

$$\frac{k_x^2}{\omega^2}\frac{g}{H}\frac{v_A^2}{c_0^2+v_A^2}. \tag{2.43}$$

This is apparently a term involving $k_x^2 v_A^2/\omega^2$, and as such may have been neglected in the derivation of equation (2.42). However, unlike the term in 1. above, there is no term elsewhere in the equation compared to which the term (2.43) is definitely small; the only other term involving g/H is

$$\frac{k_x^2}{\omega^2}\frac{g}{H}\frac{c_0^2}{c_0^2+v_A^2},$$

and to neglect the term (2.43) relative to this term would be in effect to state that $v_A^2 \ll c_0^2$, which we do not in general wish to impose.

In any case, the terms in which the discrepancies arise do not affect our description of the significant aspects of the behaviour of κ^2 given above.

In summary, when we are considering the wave variable Q, we find that the behaviour of plasma motions in our magnetic chromospheric model is similar for all frequencies above the non-magnetic cut-off frequency. Waves can be trapped by reflection alone, associated with the critical frequency ω_q.

2.3.4 Discussion

We have found two different critical frequencies, ω_x and ω_q, by considering canonical differential equations in two different variables, X and Q. The forms of the functions ψ^2 and κ^2 tell us about the form of the variables X and Q respectively. But why are there two different critical frequencies, and two functions with apparently different behaviour?

To answer this question, it is helpful to reconsider the linearised basic equations, equations (1.10) to (1.17). We have shown that the behaviour of the variable Q, which is related to the divergence of the velocity, $\nabla.\boldsymbol{v}$, does not depend on the value of k_x. Let us thus look at the case $k_x \equiv 0$. For this case, we see from equation (1.17) that

$$\nabla.\boldsymbol{v} = \frac{dv_z}{dz}, \tag{2.44}$$

while for a uniform magnetic field, equation (1.10) tells us that

$$i\omega B_{1x} = -B_0 \frac{dv_z}{dz}, \tag{2.45}$$

implying that

$$\nabla.\boldsymbol{v} = -\frac{i\omega}{B_0} B_{1x}. \tag{2.46}$$

Thus, in considering the variable $\nabla.\boldsymbol{v}$, we are really considering the variable B_{1x}, the horizontal perturbation of the magnetic field.

It is not surprising that different variables have different forms of behaviour in the model. A fast magneto-acoustic wave propagating upwards will perturb the equilibrium pressure and density, disturb the shape of the magnetic field and induce horizontal and vertical motions into the plasma. Each variable can have a different nature in a particular region, since a combination of gas pressure, magnetic pressure and magnetic tension forces govern the various types of perturbation established. The horizontal component of magnetic field perturbation may well be dying out with height, while the vertical velocity may oscillate with height. The critical frequency we will find is thus completely dependent on the perturbation variable under consideration.

We have found two forms for the critical frequency, and found that the behaviour of motions in the chromospheric model is often similar to that found in the absence of horizontal propagation (that is with $k_x \equiv 0$.) This leads us to the problem of vertical propagation of fast magneto-acoustic waves in a uniform horizontal magnetic field. It is to this problem we now turn.

2.4 Vertical propagation

We proceed with this investigation by reviewing some previous work on the subject, and find a number of contradictions in the literature. We attempt to resolve these by examining in turn the cut-off frequency and critical frequency in this situation.

2.4.1 Review

The general differential equation for wave motions in our model is given in equation (1.89) of section 1.5.3; the transformations (1.90) and (1.91) yield equation (1.92), which can be solved in terms of hypergeometric functions. When motions are purely vertical, corresponding to $k_x \equiv 0$, equation (1.89) reduces to

$$\frac{d^2 v_z}{dz^2} + \frac{c_0^2}{H}\frac{1}{c_0^2 + v_A^2}\frac{dv_z}{dz} + \frac{\omega^2}{c_0^2 + v_A^2} v_z = 0. \tag{2.47}$$

In this limit, the transformation (1.91) is obviously redundant; thus we have the single transformation

$$s = -\frac{c_0^2}{v_A^2} = -\frac{c_0^2}{v_0^2}\exp(z/H), \tag{2.48}$$

and, since v_z is identical to W in this limit, the transformed equation (1.92) can now be written as

$$s(1-s)\frac{d^2 v_z}{ds^2} + (1-2s)\frac{dv_z}{dz} - \frac{\omega^2 H^2}{c_0^2} v_z = 0. \tag{2.49}$$

We can solve this differential equation in terms of hypergeometric functions, as for the non-zero k_x case (section 1.5.3):

$$v_z = c_4 \mathrm{F}(a, b; 1; s), \tag{2.50}$$

where

$$ab = \frac{\omega^2 H^2}{c_0^2}$$

and

$$a + b = 1.$$

Following Thomas (1982), we can also find solutions to the differential equation (2.49) in terms of Legendre functions. Under the transformation

$$\xi = 1 - 2s, \tag{2.51}$$

equation (2.49) becomes

$$(1-\xi^2)\frac{d^2 v_z}{d\xi^2} - 2\xi\frac{dv_z}{d\xi} - \frac{\omega^2 H^2}{c_0^2} v_z = 0; \tag{2.52}$$

this equation is in the form of Legendre's differential equation (Abramovitz and Stegun, 1967: 8.1.1), that is

$$(1-\xi^2)\frac{d^2 u}{d\xi^2} - 2\xi\frac{du}{d\xi} + \left[\eta(\eta+1) - \frac{\mu^2}{1-\xi^2}\right] u = 0, \tag{2.53}$$

with $\mu = 0$ and $\eta(\eta+1) = -\omega^2 H^2/c_0^2$. Solutions to this equation can thus be written in terms of the Legendre functions of order μ and degree η (Abramovitz and Stegun, 1967: 8.1.1).

Thomas (1982) states that in order that the time-dependent solution

$$v_z(z,t) = \mathrm{P}_\eta(\xi)e^{i\omega t} \tag{2.54}$$

represent a wave propagating vertically, it is necessary and sufficient that η have a non-zero imaginary part, that is that

$$\omega^2 > \frac{c_0^2}{4H^2}. \tag{2.55}$$

Thomas concludes that waves above this frequency will propagate to indefinitely large heights, and thus that the cut-off frequency is in this case given by equation (2.55), and is thus identical to that for the non-magnetic problem. From our point of view, the implication is that the magnetic field does not alter the cut-off frequency for p-mode formation from its non-magnetic value.

Another investigation into this problem was carried out by Musielak et al. (1989). They consider a isothermal uniform magnetic field model which extends indefinitely in the $\pm\boldsymbol{g}$ direction. They place a "forcing plane" at some point in their model, and consider the behaviour on either side of the forcing plane separately. On the upper side of the forcing plane, the Alfvén speed increases indefinitely with height, so Musielak et al. consider the cold plasma limit ($\beta \to 0$) of the differential equations. The transformation (2.48) tells us that this limit corresponds to the limit of $s \to 0$ from below. Thus we can write equation (2.49) as

$$s\frac{d^2 v_z}{ds^2} + \frac{dv_z}{ds} - \frac{\omega^2 H^2}{c_0^2} v_z = 0, \tag{2.56}$$

which under the transformation

$$u = \frac{2\omega H}{c_0}(-s)^{1/2} = \frac{2\omega H}{v_A} \tag{2.57}$$

becomes

$$u^2\frac{d^2 v_z}{du^2} + u\frac{dv_z}{du} + u^2 v_z = 0. \tag{2.58}$$

This is equivalent to equation (7) of Musielak et al. (1989). Solutions to this equation occur in the form of the Bessel functions of order zero, $\mathrm{J}_0(u)$ and $\mathrm{Y}_0(u)$ (Abramovitz and Stegun, 1967: 9.1.1); a general solution to equation (2.58) is thus

$$v_z = c_3\mathrm{J}_0(u) + c_4\mathrm{Y}_0(u). \tag{2.59}$$

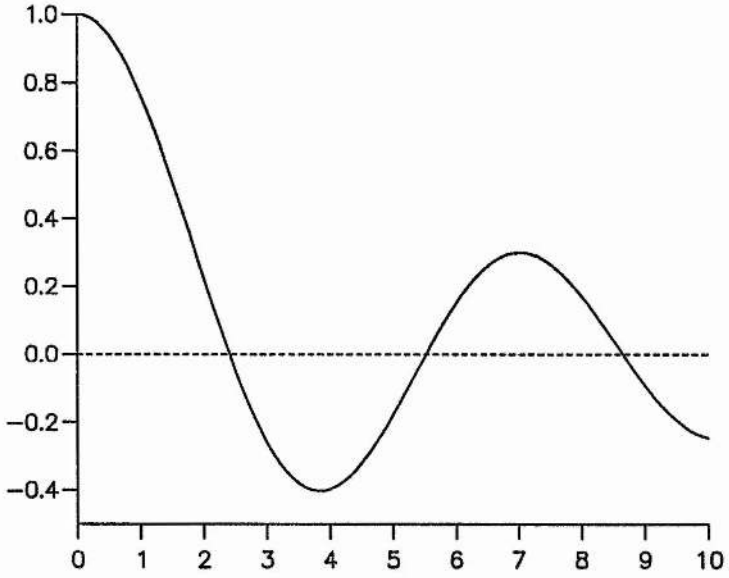

Figure 2.8: The Bessel function $J_0(u)$ vs. u

The important factor is now the behaviour of this expression as $u \to 0$, since equations (2.48) and (2.57) tell us that as $z \to -\infty$, $s \to 0$ and thus $u \to 0$. As $u \to 0^+$, the function $Y_0(u)$ becomes infinitely large (Abramovitz and Stegun, 1967: 9.1.1), so a condition of finite energy density at infinity rules out this solution. Thus we are left with

$$v_z = c_3 J_0(u). \tag{2.60}$$

The behaviour of $J_0(u)$ as $u \to 0^+$ is depicted in Figure 2.8. For u less than around 2, there are no zeros of $J_0(u)$; this implies that there are no nodes of v_z above a certain height in the atmosphere. As $u \to 0$, $J_0(u) \to 1$; thus v_z tends to a constant value at infinite heights. Neither of these features correspond to our idea of oscillatory behaviour.

Furthermore, Musielak et al. (1989) consider the travel time of a fast wave propagating upwards in such a model. In the cold plasma limit, this is given by

$$\tau = -\int_0^{-\infty} \frac{dz}{v_A(z)}, \tag{2.61}$$

which yields a finite travel time of $\tau = 2H/v_0$. They conclude from this that the wave motion *must* form a standing wave above the forcing plane.

Finally, Musielak et al. (1989) consider the analogy of Alfvén waves propagating in a uniform *vertical* magnetic field. The differential equations for this problem are identical to those which hold in the cold plasma limit of our problem. The Alfvén wave problem has been studied by (amongst others) An, Musielak, Moore and Suess (1989), who conclude from a numerical study that partial reflection takes place throughout the atmosphere, allowing standing waves to form. By the time the Alfvén waves reach infinity, reflection has become total.

The conclusion which Musielak et al. (1989) reach from these various perspectives is that upwardly propagating waves at all frequencies are trapped by the magnetic field, implying an infinite cut-off frequency. This is obviously in contradiction to the conclusion of Thomas (1982), which is that in the presence of a uniform magnetic field, the cut-off frequency still takes its non-magnetic value of $c_0/2H$. Musielak et al. (1989) attempt to resolve the situation by considering a wave propagating *downward* from their forcing plane, and, by considering now the high-β limit, demonstrate that the non-magnetic cut-off frequency is appropriate to this situation. Their conclusion is that, in his analysis, Thomas (1982) has picked up the downward-propagating wave, and formed the wrong conclusion about the cut-off frequency as a result.

Musielak, Fontenla and Moore (1992) look again at the parallel problem of Alfvén waves in a vertical magnetic field, and attempt to derive a mathematical form for the critical frequency for this problem. They state that in previous work on this problem, including the numerical study of An et al. (1989), the frequency

$$\omega_a = \frac{v_A(z)}{2H} \tag{2.62}$$

is found to be significant. At a given height $-z$, waves below this frequency will suffer significant reflection. Alternatively, equation (2.62) will give the height at which waves of a given frequency ω will undergo the most significant reflection. This is physically understandable in the following terms. We can form a local vertical wavenumber for the Alfvèn wave, k_z, defined by $k_z = \omega/v_A$. This allows us to calculate a local vertical wavelength, λ_z, given by

$$\lambda_z = \frac{2\pi v_A}{\omega}. \tag{2.63}$$

Where this wavelength is much smaller than the Alfvén speed scale length, $2H$, we would expect the wave to be largely unaffected by the variation in v_A; this will occur when the

condition $v_A/\omega \ll 2H$, and thus the condition $\omega \gg \omega_a$ hold. The wave will start to be affected by the variation in v_A when the wavelength is similar to the Alfvén speed scale height; this will occur around the point where $\omega = \omega_a$. Where $\omega \ll \omega_a$, the local wavelength will be much longer than the Alfvén speed scale height, and so the atmosphere will appear sharply discontinuous to the wave, and severe reflection will occur. Musielak et al. (1992) attempt to derive a form of the critical frequency consistent with this physical observation.

They do this by considering not only the wave equation in terms of velocity perturbations, as we have done up to now, but also the differential equation describing the magnetic field perturbations. They couch these equations in what is known as Klein-Gordon form, which for our purposes may be generally written as

$$\frac{d^2\epsilon}{d\tau^2} + \left(\omega^2 - \omega_{cr}^2(\tau)\right)\epsilon = 0, \tag{2.64}$$

where ϵ is either wave variable, τ is the travel time of the wave relative to some point and ω_{cr} is some frequency, the form of which will depend on the wave variable being considered. In cases where ω_{cr} is a constant, it is found that ω_{cr} represents the cut-off frequency for the problem: waves of frequency greater than ω_{cr} propagate, those below evanesce. Musielak et al. (1992) state that they will demonstrate that, where ω_{cr} is not constant, it can be identified as the local critical frequency for reflection.

The form of the critical frequency featuring in equation (2.64) depends on whether the wave variable considered is the velocity or magnetic field perturbation. Thus the authors attempt to identify the "correct" critical frequency by comparison with the existing knowledge of the problem. The two possible forms of the critical frequency featuring in the two Klein-Gordon equations are given by

$$\omega_c^2 = \frac{v_A^2}{16H^2} \pm \frac{v_A^2}{8H^2}; \tag{2.65}$$

the '+' case is derived from the magnetic field perturbation equation, the '−' case from the velocity perturbation equation. Bearing in mind that the critical frequency would be expected to be similar to that given in equation (2.62), the authors identify

$$\omega_c = \frac{\sqrt{3}}{2}\frac{v_A}{2H} \tag{2.66}$$

as the critical frequency for reflection of Alfvén waves in a vertical field.

Musielak et al. (1992) thus justify the use of their Klein-Gordon equation by demonstrating that the frequency produced is similar to that previously observed. However,

this correspondence is hardly surprising, since they specifically picked that frequency, rather than that given by the velocity perturbation equation, precisely because it is similar to the expected answer. Thus Musielak et al. (1992) have found a self-consistent approach to the problem, but their result does not prove that the Klein-Gordon equation gives a correct, unique critical frequency.

The Klein-Gordon equation is also used by Stark and Musielak (1993) to study the problem of fast waves in a horizontal magnetic field. They construct first the differential equations in v_z and B_{1x}, the magnetic field perturbation. The equation in v_z is as given in equation (2.47); the equation in B_{1x} is given by

$$\frac{d^2B_{1x}}{dz^2} + \frac{c_0^2 - v_A^2}{H}\frac{1}{c_0^2 + v_A^2}\frac{dB_{1x}}{dz} + \frac{\omega^2}{c_0^2 + v_A^2}B_{1x} = 0. \tag{2.67}$$

Stark and Musielak then transform equation (2.67) into Klein-Gordon form as follows. They first transform into the travel time variable τ, here defined by $d\tau = dz/c_f$. They then carry out the transformation $\xi_b = \Phi_b B_{1x}$ to eliminate the first derivative term. The result of these transformations can be written as

$$\frac{d^2\xi_b}{d\tau^2} + \left(\omega^2 - \omega_b^2\right)\xi_b = 0, \tag{2.68}$$

where

$$\omega_b^2 = \frac{1}{\Phi_b}\frac{d^2\Phi_b}{d\tau^2} \tag{2.69}$$

and

$$\frac{1}{\Phi_b}\frac{d\Phi_b}{d\tau} + \frac{2c_0^2 - v_A^2}{4H(c_0^2 + v_A^2)^{1/2}} = 0. \tag{2.70}$$

Calculation of the explicit form of ω_b, which requires the inverse transformation $dz = c_f d\tau$, yields the result

$$\omega_b^2 = \frac{c_0^2}{4H^2} + \frac{3v_A^4}{16H^2(c_0^2 + v_A^2)}. \tag{2.71}$$

We see that in the cold plasma limit ($c_0 = 0$), this is consistent with the result derived by Musielak et al. (1992).

Stark and Musielak (1993) then state that if the critical frequency ω_b is the correct one, it should be possible to derive it from the velocity perturbation equation also. Thus they transform equation (2.47) into Klein-Gordon form. Here they define τ such that $dz = -dz/c_f$, stating that in this case the minus sign corresponds to upward propagating waves; under the further transformation $\xi_u = \Phi_u v_z$, equation (2.47) becomes

$$\frac{d^2\xi_u}{d\tau^2} + \left(\omega^2 - \omega_u^2\right)\xi_u = 0, \tag{2.72}$$

where

$$\omega_u^2 = \frac{1}{\Phi_u}\frac{d^2\Phi_u}{d\tau^2} \tag{2.73}$$

and

$$\frac{1}{\Phi_u}\frac{d\Phi_u}{d\tau} - \frac{2c_0^2 + v_A^2}{4H(c_0^2 + v_A^2)^{1/2}} = 0. \tag{2.74}$$

They state that the critical frequency obtained from equations (2.73) and (2.74) is then identical to that given by equation (2.71). Thus they conclude that $\omega_u = \omega_b$ is the unique fast wave critical frequency for upward propagating waves.

However, this result also appears puzzling. In Musielak et al. (1992), it was clearly demonstrated that the two wave equations produced entirely different critical frequencies. It is physically understandable that this should be the case. Yet Stark and Musielak (1993) find the same critical frequency from different differential equations. What is the reason for this apparent contradiction?

In the remainder of this section we will discuss the two contradictions present in the literature reviewed above. We can summarise the two problems as follows:

1. Thomas (1982) states that, because of the complex nature of the degree of the Legendre function solutions, waves above the non-magnetic cut-off frequency will also propagate in the non-magnetic case; thus the magnetic cut-off frequency is identical to the non-magnetic one. Musielak et al. (1989) state that, from various considerations, waves of all frequencies are trapped by the magnetic field, and so the magnetic cut-off frequency is infinite;

2. Musielak et al. (1992) state that, in the problem of Alfvén waves in a vertical field, different critical frequencies are found from the differential equations in v_z and B_{1x}; physical examination is necessary to pick the "correct" frequency. Stark and Musielak (1993), considering the similar problem of fast waves in a horizontal field, apparently find one unique critical frequency whichever wave variable is considered.

We will consider a range of exact solutions and the qualitative behaviour of certain differential equations in an attempt to resolve these contradictions, firstly in the case of the cut-off frequency and secondly in that of the critical frequency.

2.4.2 The cut-off frequency

Thomas (1982) finds his exact solution in terms of Legendre functions from the

full differential equation in v_z; this solution is equivalent to the hypergeometric function solution given in equation (2.50). He concludes from the behaviour of the Legendre functions that waves propagate at frequencies above the magnetic cut-off. Musielak et al. (1989) find a solution in terms of Bessel functions in the cold plasma limit of the same differential equation, and conclude from this that waves are evanescent sufficiently high in the model. But since these two approaches start from the same differential equation, there must be some relationship between the two apparently contradictory solutions. Consideration of any such relationship should help resolve the argument.

We have seen that it is a general property of Bessel and hypergeometric functions that (Abramovitz and Stegun, 1967: 9.1.70)

$$\mathrm{J}_\eta(t_1) = \frac{\left(\frac{1}{2}t_1\right)^\eta}{\Gamma(\eta+1)} \lim \mathrm{F}\left(\lambda, \mu; \eta+1; \frac{-t_1^2}{4\lambda\mu}\right) \tag{2.75}$$

as λ and μ tend to infinity through real or complex values, with t_1 and η being fixed. In the case of $\eta = 0$, this gives us that as λ and μ tend to infinity through real or complex values for t_1 fixed,

$$\mathrm{J}_0(t_1) = \lim \mathrm{F}\left(\lambda, \mu; 1; \frac{t_1^2}{4\lambda\mu}\right). \tag{2.76}$$

If we now introduce

$$t_2 = \frac{-t_1^2}{4\lambda\mu} \tag{2.77}$$

so that

$$t_1 = (4\lambda\mu)^{1/2}(-t_2)^{1/2},$$

our rule reads as follows: as λ and μ tend to infinity through real or complex values and t_2 tends to zero such that $t_1 = (4\lambda\mu)^{1/2}(-t_2)^{1/2}$ remains fixed,

$$\lim \mathrm{F}(\lambda, \mu; 1; t_2) = \mathrm{J}_0\left[(4\lambda\mu)^{1/2}(-t_2)^{1/2}\right]. \tag{2.78}$$

Let us now look again at the hypergeometric function solution to the differential equation in v_z, as given by equation (2.50), in the case of large ω and large height. Thomas (1982) states that waves above the non-magnetic cut-off frequency will propagate at all heights, while Musielak et al. (1989) state that waves at all frequencies will be evanescent at large heights, so this case is most suitable for divining any discrepancies between the two results. If we let $\omega^2 \to \infty$ and $z \to -\infty$ such that the quantity $\omega^2 \exp(z/H)$ is fixed, then both a and b will tend to infinity, and the quantity $(4ab)^{1/2}(-s)^{1/2}$ will remain fixed. Under

these conditions we can apply the limit given in equation (2.78), allowing us to write the limiting form of the solution (2.50) as

$$\begin{aligned} v_z &\sim c_4 \mathrm{J}_0 \left[(4ab)^{1/2} (-s)^{1/2} \right] \\ &= c_4 \mathrm{J}_0 \left[\frac{2\omega H}{v_0} \exp(z/2H) \right]. \end{aligned} \tag{2.79}$$

Recalling that the variable u is as defined by the transformation (2.57), we see that the solution (2.79) can be written as

$$v_z = c_4 \mathrm{J}_0(u). \tag{2.80}$$

Thus, in the limit of large height and high frequency, the hypergeometric function solution of Thomas (1982) and the Bessel function solution of Musielak et al. (1989) are identical. The propagatory behaviour Thomas (1982) observes in the Legendre functions (equivalent to the hypergeometric function solution) must thus in some way be consistent with the 'evanescent' behaviour deduced by Musielak et al. (1989). The contradiction *must* be introduced in the deductions that either Thomas (1982) or Musielak et al. (1989) make from their solutions.

Thomas (1982) makes the deduction that, because waves can propagate throughout the model at frequencies greater than the non-magnetic cut-off, waves must propagate to infinity. However, this does not mean that some reflection of the waves cannot take place. Musielak et al. (1989) state that above a certain height in the atmosphere, there are no nodes of velocity perturbation, and deduce that wave motions must be evanescent above that point. They also state that the travel time of a wave propagating to infinity is finite, and conclude that a standing wave must be formed. However, both these physical arguments are suspect, since we are dealing with an unphysical situation: the Alfvén speed becomes indefinitely large with height, so it is not necessarily true that a wave would take an infinite time to travel an infinite distance. Also, the form of $\mathrm{J}_0(u)$ shown in Figure 2.8 is 'stretched' by the infinite Alfvén speed, so it is not clear that the absence of nodes above a certain height necessarily implies evanescent behaviour. Indeed, the form of $\mathrm{J}_0(u)$ displayed in Figure 2.8 more resembles oscillatory behaviour.

A more accurate description of the situation might go as follows. We can see that for all frequencies above the non-magnetic cut-off, there is some form of propagating behaviour at any given height in the model. However, as is shown numerically by An et al. (1989), partial reflection will take place, particularly above the height where the local vertical wavelength becomes longer than the density scale height. An et al. (1989) also state

that by infinity, partial reflection will have become total reflection; it can be inferred from this that at any given *finite* height, there will still be some propagatory behaviour. Thus a peculiar situation arises, which we might call 'evanescent propagation'. Waves are propagating, but the increasing Alfvén speed is stretching the velocity nodes of the wave apart; as the Alfvén speed goes to infinity, the form of the wave is also stretched out to infinity. Since reflection is taking place for all frequencies, however, we can conclude that modes may form at all frequencies, and that the cut-off frequency may be taken as infinite.

What we are seeing here, then, is a highly singular problem; were the wave not attempting to propagate at precisely right-angles to the magnetic field, the behaviour would be very different, as we have already seen. There is also an unphysical element introduced into the problem by the effect of indefinitely increasing Alfvén speed. Thus the application of this knowledge to the solar problem is limited.

Our conclusion on the debate between Thomas (1982) and Musielak et al. (1989) is that neither is telling the whole story; waves are in a sense both propagatory and evanescent in such a situation. Since reflection occurs at all frequencies, however, there is the possibility for normal modes to form at all frequencies, and so the cut-off frequency must be considered to be infinite.

2.4.3 The critical frequency

We have described how Musielak et al. (1992) find two forms of the Klein-Gordon equation describing vertical Alfvén wave propagation in a vertical magnetic field, one in terms of the velocity perturbation v_z and one in terms of the magnetic field perturbation B_{1x}. The two critical frequencies implied by the two equations are different. Stark and Musielak (1993), considering the related problem of vertical propagation of fast magneto-acoustic waves in a horizontal field, find the same form of the critical frequency from the equations in the two different wave variables. Their critical frequency derived from the B_{1x} differential equation is given in equation (2.71); in the cold plasma limit, this reduces to the critical frequency found by Musielak et al. (1992) from the corresponding B_{1x} equation, as we would expect. However, the critical frequency found by Stark and Musielak (1993) from the v_z equation does not reduce to that found by Musielak et al. (1992) from the corresponding equation. Why is this?

In the derivation of equations (2.68), (2.69) and (2.70), Stark and Musielak (1993)

used the transformation $d\tau = dz/c_f$, whereas in the derivation of equations (2.72), (2.73) and (2.74) they used the transformation $d\tau = -dz/c_f$, stating that this transformation corresponds to the case of an upward propagating wave. There appears to be no basis for this difference in transformation, since no first derivatives in τ appear. We confirm this by carrying out the general transformation $d\tau = \pm dz/c_f$, firstly in the case of the B_{1x} differential equation. We find that equations (2.68) and (2.69) are unchanged, but that equation (2.70) is replaced by

$$\frac{1}{\Phi_b}\frac{d\Phi_b}{d\tau} \pm \frac{2c_0^2 - v_A^2}{4H(c_0^2 + v_A^2)^{1/2}} = 0. \tag{2.81}$$

The evaluation of ω_b then demands taking the first derivative with respect to τ of each term in equation (2.81); then the inverse transformation $dz = \pm c_f d\tau$ is invoked, since c_0^2 and v_A^2 are expressed as functions of z. The effect of this is to square the '$\pm$' factor. Thus the critical frequency found from equation (2.81) does not depend on whether the '+' or '−' sign is taken in the transformation.

Thus there appears to be no need to specify that $d\tau = -dz/c_f$ when considering the v_z differential equation. Indeed, we can carry out the general process described above for the v_z differential equation also. We naturally find the same Klein-Gordon form as in equation (2.72), but with the critical frequency ω_u now given by

$$\omega_u^2 = \frac{c_0^2}{4H^2} - \frac{v_A^4}{16H^2(c_0^2 + v_A^2)}. \tag{2.82}$$

The cold plasma limit of this result, that is

$$\omega_u^2 = -\frac{v_A^2}{16H^2}, \tag{2.83}$$

is consistent with the result of Musielak et al. (1992) for this variable.

If, however, we specify the initial transformation $d\tau = -dz/c_f$, as Stark and Musielak (1993) have done, and then use the incorrect inverse transformation $dz = +c_f d\tau$, we find the answer given by Stark and Musielak (1993) for this variable, namely $\omega_u = \omega_b$. Our conclusion is that Stark and Musielak (1993) have made a mistake in their derivation of ω_u. This leads them to conclude that they have found a unique critical frequency ω_c; our conclusion, on the other hand, agrees with the previous work of Musielak et al. (1992) in that the wave equations themselves produce two distinct candidates for the critical frequency.

Where we differ from Musielak et al. (1992) is in their process of selection of one unique critical frequency from the two candidates. They choose the frequency appearing in

the magnetic field perturbation equation as the critical frequency, and apparently discard the frequency appearing in the velocity perturbation equation. However, this frequency must have a significance for the form of the v_z solution, and, as we have seen, it is physically understandable that different wave variables should be governed by different critical frequencies. Thus it is neither necessary or possible to choose one unique critical frequency for the problem.

This concludes our investigation into the problem of vertical propagation. We now summarise the main findings of this chapter.

2.5 Summary

We have considered the case of an isothermal plasma containing a uniform horizontal magnetic field. We can employ this as a chromospheric model in our discussion of the solar problem.

For this model, wave motions are always evanescent above a certain height in the chromospheric model; thus the magnetic field has the capacity to provide a 'roof' to our mode cavity, even for modes of frequency above the non-magnetic cut-off frequency. Our conclusion is thus that the cut-off frequency is infinite in this situation.

We have demonstrated that both reflection and refraction play a role in the trapping of waves, and that propagating waves arise in the lowest part of the chromospheric model for modes with frequencies above the magnetic cut-off. The nature of the wave motion that an observer would be likely to detect will depend on the particular variable (pressure, velocity etc.) under consideration.

In the problem of purely vertical propagation, we have examined the apparent contradiction between Thomas (1982) and Musielak et al. (1989) and, through an asymptotic comparison of their results, demonstrated that there is no actual contradiction, except in the inferences drawn from their results. We have also considered the examination of critical frequency conducted by Musielak et al. (1992) and Stark and Musielak (1993), and found an apparent error in the latter paper. In any case, we conclude that it is neither necessary nor possible to find a unique critical frequency valid for all wave variables, as has been attempted in both these papers.

Chapter 3

An initial investigation of frequency shift turnover

3.1 Introduction

Our aim in this Chapter is to investigate some possible causes of the observed shifts in p-mode frequencies over the solar cycle. This phenomenon, reported in the observational work of Libbrecht and Woodard (1990, 1991) and Elsworth et al. (1990), was described in section 1.2.3. In particular we are interested in the apparent "turnover" in frequency shift at around 4mHz, as reported by Libbrecht and Woodard (1991). What processes could have a role to play in creating this effect?

We discussed in section 1.1.2 that the solar cycle is considered to be fundamentally a magnetic effect. The strength of field, or the amount of magnetic flux, resident in the various magnetic field sites, both within and on the surface of the Sun, would be expected to vary over the solar cycle. There may be additional indirect effects. For example, the solar magnetic field can alter the temperature of large regions of plasma, either by inhibiting energy flows (as in the case of sunspots), or by heating (as, for example, through the dissipation of Alfvén waves.) Thus it is likely that the temperature of magnetic regions such as the chromosphere would also change over the solar cycle.

We may identify a number of potential effects which could influence p-mode frequencies. Firstly, the magnetic field generation site at the base of the convection zone could in principle influence such factors as the wave travel time within the cavity, and thus the

frequency selected for an individual p-mode (Roberts and Campbell, 1986; Campbell and Roberts, 1988). It has been noted that the frequency shift of modes of given order, n, increases linearly with degree, l, while the very highest degree modes are not thought to penetrate sufficiently deeply into the solar interior to be affected by such a field. Magnetic fields at the base of the convection zone could, however, play a significant part in the observed frequency shifts of low-degree modes, as discussed in Chapter 6.

It is also possible that the strong magnetic fields in sunspots could influence p-mode frequencies. The oscillations of vertical photospheric fields and their possible influence on global solar oscillations have been widely considered (Bogdan and Zweibel, 1985; Zweibel and Bogdan, 1986; Bogdan, 1987, 1989; Bogdan and Cattaneo, 1989; Zweibel and Däppen, 1989).

Another magnetic field site which has been considered is that of the chromospheric magnetic field, which exists in the form of a magnetic canopy (described in section 1.1.2). We would expect this region to be particularly sensitive to solar cycle changes, as the chromosphere is a low-β plasma, and so dominated by the magnetic field. It is reasonable to assume that the strength of the magnetic field in the chromosphere varies during the solar cycle; it is conceivable also that the temperature of the plasma in the chromosphere would vary. Variations in p-mode frequencies caused by the chromosphere would be expected to show a larger magnitude of shift for higher degree modes, and this is observed. Thus, in our task of explaining the existence and nature of p-mode frequency shifts, it is the influence of the chromosphere upon mode frequencies which we shall investigate further.

Various investigations into chromospheric effects on p-mode frequencies (Campbell, 1989; Campbell and Roberts, 1989; Evans and Roberts, 1990, 1991, 1992; Evans, 1991; Jain, 1992; Jain and Roberts, 1993) have employed the form of model introduced in sections 1.4 and 1.5. For the solar interior, a plane-parallel, linear polytrope model is chosen, with the temperature scale height selected so as to ensure marginal stratification. The chromosphere is modelled by a plane-parallel atmosphere, within which is embedded a horizontal magnetic field.

Campbell and Roberts (1989) looked at an isothermal chromosphere with a magnetic field structured such that the Alfvén speed remained constant throughout the chromosphere. This implied a magnetic field strength which decayed exponentially with height. This model is particularly amenable to analytical investigation, since the governing equation leads to a constant-coefficient differential equation for the vertical velocity v_z, as for

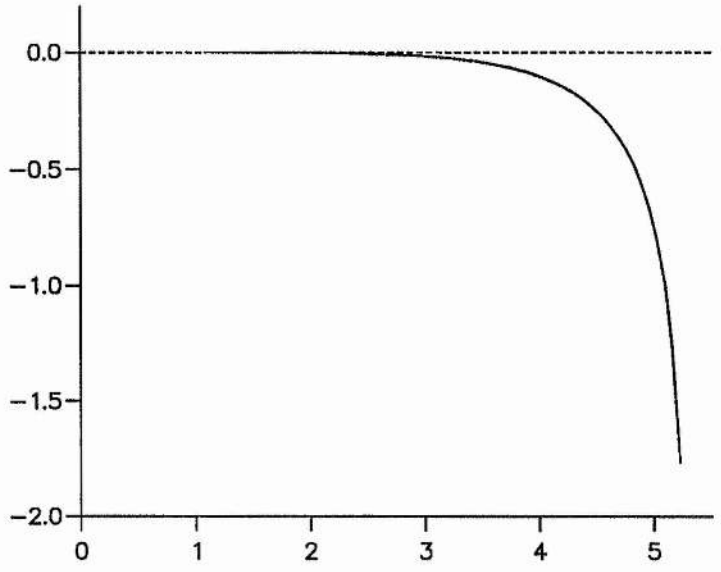

Figure 3.1: Frequency shift (in μHz) vs. original frequency (in mHz), for an increase in chromospheric temperature from 4170K to 4400K in the isothermal non-magnetic model (after Campbell and Roberts, 1989). Modes considered are of degree 50 and of order varying from 1 to 40.

the non-magnetic case described in section 1.5.2. Campbell and Roberts then expressed the dispersion relation gained as a correction to equation (1.67), the dispersion relation for a p-mode in the absence of a chromosphere. Their expression was also valid in the limit of zero field; it then described the change in frequency induced by the introduction of an isothermal non-magnetic chromosphere. This situation is also described by Evans and Roberts (1990).

It is also possible to calculate from these relationships the change in frequency induced by a change in either the chromospheric temperature or the chromospheric magnetic field strength. We do this by calculating the frequencies of a certain set of modes for one set of chromospheric parameters, repeating the calculation for a different set of chromospheric parameters, and then comparing the frequencies of corresponding modes to calculate frequency shifts. Figure 3.1 shows the frequency shifts induced by increasing the chromospheric temperature from 4170K to 4400K in the isothermal non-magnetic model. In this Figure, and in Figures 3.2 and 3.3, we consider modes of degree 50 and allow the order to vary from 1 to 40. Parameters in the linear polytrope are as given in Tables 1.1

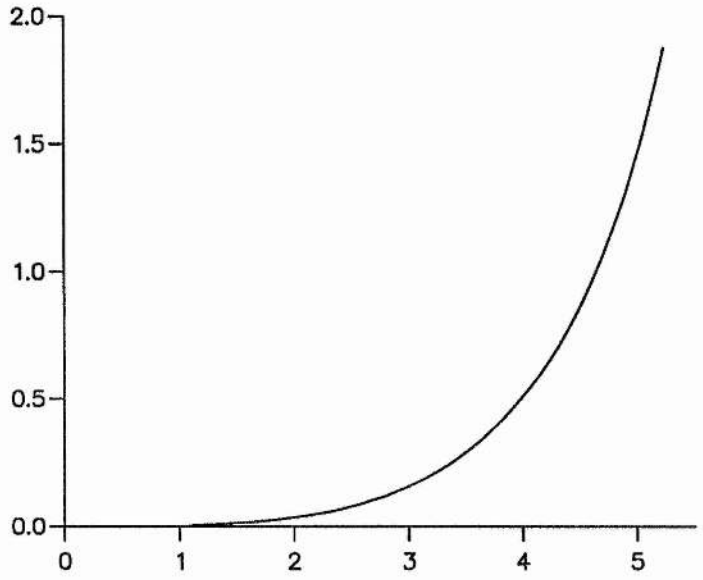

Figure 3.2: Frequency shift (in μHz) vs. original frequency (in mHz), for an increase in magnetic field strength from 10G to 30G; the chromospheric temperature is held at 4170K (after Evans and Roberts, 1990)

and 1.2. Mode frequencies are calculated using numerical routines based on the dispersion relations published in Campbell and Roberts (1989) and Evans and Roberts (1990), and kindly passed on by R. Jain. For each mode we plot the frequency shift (in μHz) against the original mode frequency (in mHz). The frequency shift curve shows that the frequency drops as the chromospheric temperature increases; the change is largest at high frequencies.

For the constant Alfvén speed model of Campbell and Roberts (1989), the change in frequency induced by an increase in the magnetic field strength is of a similar form to that displayed in Figure 3.1.

Evans and Roberts (1990) also looked at an isothermal atmosphere with a *uniform* magnetic field, as described in section 1.5.3. They looked at the effect on mode frequencies of altering the magnetic field strength. Figure 3.2 shows the frequency shift curve produced by increasing the magnetic field strength from 10G to 30G, with the chromospheric temperature held at 4170K, for the same modes considered in Figure 3.1. In this case, the mode frequencies *increase* with increasing magnetic field strength.

An alternative way of looking at frequency shifts of this form is to specify the

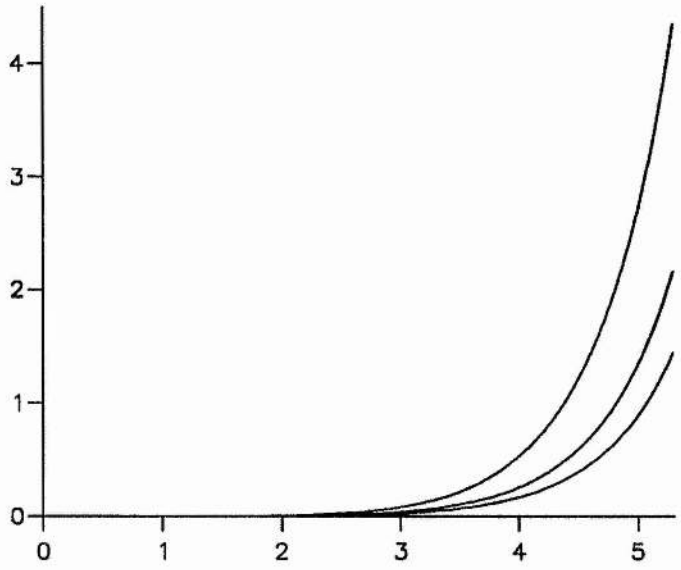

Figure 3.3: Frequency shift (in μHz) vs. original frequency (in mHz) for the same change in chromospheric parameters as Figure 3.2. We here consider modes of orders n =10 (highest curve), 20 and 30, and allow the degree to vary from 1 up to the cut-off.

order and allow the degree to vary up to the cut-off. Figure 3.3 shows the frequency shift curves obtained for orders n=10, 20 and 30 for the same change in magnetic field strength as Figure 3.2. The highest frequency shifts are for n=10, as l is lower at a given frequency for a higher n.

In a subsequent paper, Evans and Roberts (1991) investigated the effect of a two-part chromospheric model, involving a non-magnetic segment in the low chromosphere overlain by a uniform magnetic field. This was an attempt to model the magnetic canopy more accurately. For a given canopy height, the frequency shift curves generated by a change of magnetic field strength are qualitatively similar to those shown in Figure 3.2.

We can compare these theoretical curves with the observations of Libbrecht and Woodard (1991) described in section 1.2.3. Figure 1.5 plots the actual frequency shifts induced by the increase in solar activity between the years 1986 and 1989; Figure 3.2 plots the theoretically predicted frequency shifts induced by an increase in chromospheric magnetic field strength from 10G to 30G. These changes are consistent, and the two sets of frequency shift data are also consistent up to aound 4mHz. It seems that the model

describes well the effect of p-mode frequency shifts, up to a point. We are left to postulate on the possible causes of the turnover effect observed above 4mHz. Evans and Roberts (1991) postulate that, since the uniform magnetic field model produces a positive shift, while the constant Alfvén speed model produces a negative shift, a hybrid of these two models could provide a $\Delta\nu$ curve which would display the effect of turnover. However, progress on this problem proved difficult to achieve (Jain, 1992). Jain and Roberts (1993) provide a frequency shift curve displaying turnover using the model and dispersion relation of Evans and Roberts (1990), based on a similar premise to that deduced by this Chapter; we discuss the results of Jain and Roberts (1993) in section 4.1.

It is evident that the nature of frequency shifts generated by the chromosphere is very sensitive to the specific model chosen. Accordingly, it would be instructive to examine a much wider range of chromospheric profiles, in an attempt to understand how the turnover effect can be generated. Unfortunately, temperature structures in the chromosphere that are more complex than those discussed by Campbell and Roberts (1989) and Evans and Roberts (1990) render the differential equations impossible to solve analytically in the magnetic field case. Thus, either a numerical treatment or some form of approximate solution is be required. Since the ideal end result would be a simple dispersion relation which described the turnover effect, it was decided that it would be preferable to attempt to solve the problem analytically. The bulk of this Chapter thus describes an attempt to diagnose the cause of turnover in the frequency shift curve, using an approximate WKB method.

We start by reviewing some basic WKB theory (Nayfeh, 1983; Bender and Orszag, 1987).

3.2 Review of WKB theory

WKB theory describes the asymptotic behaviour if certain differential equations where one parameter in the equation is large in some way. The involvement of G. Wentzel, H.A. Kramers and L. Brillioun in the development of the theory led to the general name of 'WKB theory'; the contribution of H. Jeffreys is reflected in the fact that the name 'WKBJ theory' is also occasionally used. We consider first the form of asymptotic solution named for R.E. Langer.

3.2.1 The Langer solution

We consider first the differential equation

$$\frac{d^2Q}{dz^2} + \left[\lambda^2 f(z) + g(z)\right] Q = 0, \tag{3.1}$$

where λ is a large parameter and where $f(z)$ is a function such that at a location $z = z_0$ $f(z_0) = 0$, with $f(z) > 0$ for $z < z_0$ and $f(z) < 0$ for $z > z_0$; a point such as z_0 is known as a *turning point.* Using the Langer transformation (Nayfeh, 1983), we can find an asymptotic solution to equation (3.1) in the limit of large λ. This solution, which we refer to as the Langer solution, is given by (Langer, 1934; Nayfeh, 1983)

$$Q(z) \sim \left[-\frac{t(z)}{f(z)}\right]^{1/4} \{c_3 \mathrm{Ai}(t) + c_4 \mathrm{Bi}(t)\}, \tag{3.2}$$

where Ai and Bi are the Airy functions (Abramovitz and Stegun, 1967), c_3 and c_4 are arbitrary constants and the function $t(z)$ is given by

$$\frac{2}{3}[t(z)]^{3/2} = \lambda \int_{z_0}^{z} [-f(s)]^{1/2}\, ds. \tag{3.3}$$

Note that the transformed variable t will be of opposite sign to $f(z)$ for all z, and will be zero at z_0. The Langer solution has the distinction of being valid throughout z for this $f(z)$ profile, as opposed to standard WKB solutions which have specific regions of validity. However, the Langer solution will not be valid close to another turning point.

If the $f(z)$ profile is reversed, that is if $f(z)$ is positive for $z > z_0$ and negative for $z < z_0$, then the solution (3.2) still applies, but with $t(z)$ now given by

$$\frac{2}{3}[t(z)]^{3/2} = \lambda \int_{z}^{z_0} [-f(s)]^{1/2}\, ds. \tag{3.4}$$

Let us look briefly at the behaviour of the Airy functions, Ai and Bi, which comprise the Langer solution. Figure 3.4 shows the function $\mathrm{Ai}(t)$, while Figure 3.5 shows $\mathrm{Bi}(t)$. We see that when t is negative, both Airy functions have an oscillatory form. When t is positive, both Airy functions have an exponential form, with $\mathrm{Ai}(t)$ exponentially decaying and $\mathrm{Bi}(t)$ exponentially growing with increasing $t > 0$.

The dotted lines in each graph are obtained from the asymptotic expansions of the Airy functions (Nayfeh, 1983). As $t \to -\infty$,

$$\begin{aligned} \mathrm{Ai}(t) &\sim \frac{1}{\sqrt{\pi}} \frac{1}{(-t)^{1/4}} \sin\left[\frac{2}{3}(-t)^{3/2} + \frac{\pi}{4}\right] \\ \mathrm{Bi}(t) &\sim \frac{1}{\sqrt{\pi}} \frac{1}{(-t)^{1/4}} \cos\left[\frac{2}{3}(-t)^{3/2} + \frac{\pi}{4}\right], \end{aligned} \tag{3.5}$$

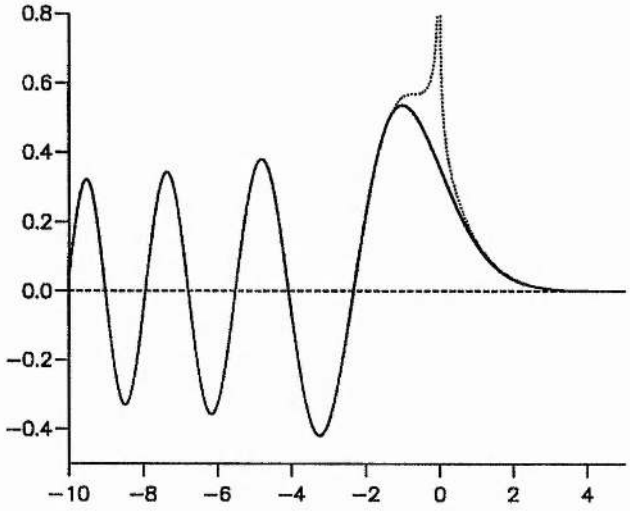

Figure 3.4: The Airy function $\mathrm{Ai}(t)$ (shown as a solid curve) and its asymptotic expansions (shown dotted).

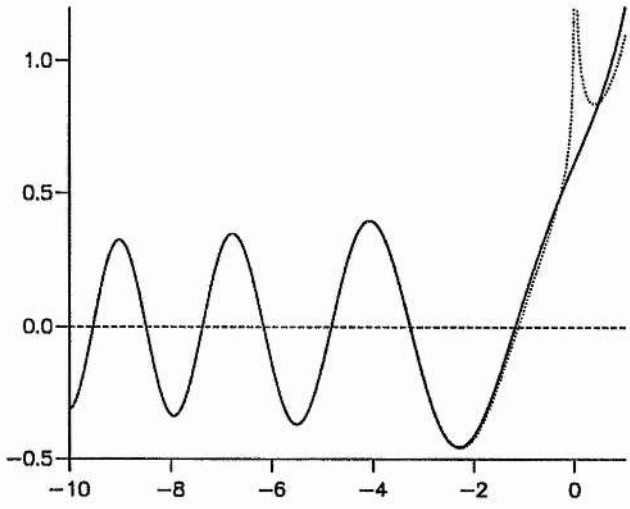

Figure 3.5: The Airy function $\mathrm{Bi}(t)$ (shown as a solid curve) and its asymptotic expansions (shown dotted).

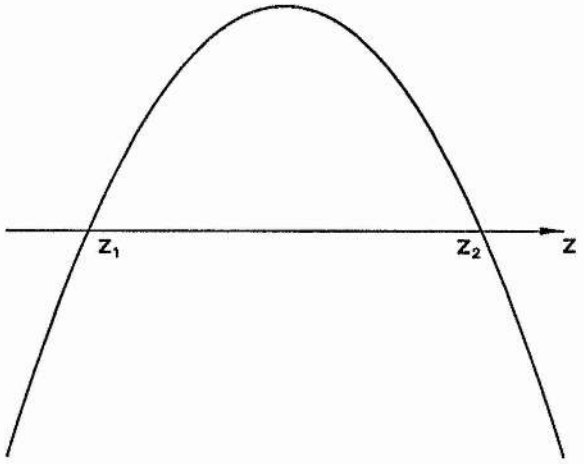

Figure 3.6: $f(z)$ profile for Bohr-Sommerfeld condition

and as $t \to \infty$,

$$\begin{aligned} \mathrm{Ai}(t) &\sim \frac{1}{2\sqrt{\pi}} \frac{1}{t^{1/4}} \exp[-\frac{2}{3}t^{3/2}] \\ \mathrm{Bi}(t) &\sim \frac{1}{\sqrt{\pi}} \frac{1}{t^{1/4}} \exp[\frac{2}{3}t^{3/2}]. \end{aligned} \tag{3.6}$$

We see that, sufficiently far away from the turning point, the Airy functions are well described by their asymptotic expansions. The Langer solution expressed in terms of one of these expansions gives the standard WKB solution for that region.

3.2.2 Derivation of Bohr-Sommerfeld condition

For the situation depicted in Figure 3.6, that is where two turning points are present, we may derive an eigenvalue which incorporates certain boundary conditions. This useful result is known as the *Bohr-Sommerfeld condition.* We form two separate Langer solutions, Q_1 and Q_2, round the turning points z_1 and z_2 respectively. We require the solutions to be evanescent at $\pm\infty$, and so we discard the $\mathrm{Bi}(t)$ solutions for each. Each solution will not be valid around the other's turning point, but there will be some region in (z_1, z_2) where both will be valid. The matching of the asymptotic expansions of each solution in this region gives us our eigenvalue condition.

Thus we have

$$Q_1(z) \sim c_1 \left[-\frac{t_1(z)}{f(z)}\right]^{1/4} \mathrm{Ai}(t_1), \tag{3.7}$$

where

$$\frac{2}{3}[-t_1(z)]^{3/2} = \lambda \int_{z_1}^{z} f^{1/2}(s)\, ds,$$

and

$$Q_2 \sim c_3 \left[-\frac{t_2(z)}{f(z)}\right]^{1/4} \mathrm{Ai}(t_2), \tag{3.8}$$

where

$$\frac{2}{3}[-t_2(z)]^{3/2} = \lambda \int_{z}^{z_2} f^{1/2}(s)\, ds.$$

From the asymptotic expansions (3.5), we have for $z_1 \ll z \ll z_2$,

$$\begin{aligned} Q_1 &\sim \frac{c_1}{\sqrt{\pi}} \left[\frac{1}{f(z)}\right]^{1/4} \sin\left[\frac{2}{3}(-t_1)^{3/2} + \frac{\pi}{4}\right] \\ &= \frac{c_1}{\sqrt{\pi}} \left[\frac{1}{f(z)}\right]^{1/4} \sin\left[\lambda \int_{z_1}^{z} f^{1/2}(s)\, ds + \frac{\pi}{4}\right], \end{aligned} \tag{3.9}$$

and

$$\begin{aligned} Q_2 &\sim \frac{c_3}{\sqrt{\pi}} \left[\frac{1}{f(z)}\right]^{1/4} \sin\left[\frac{2}{3}(-t_2)^{3/2} + \frac{\pi}{4}\right] \\ &= \frac{c_3}{\sqrt{\pi}} \left[\frac{1}{f(z)}\right]^{1/4} \sin\left[\lambda \int_{z}^{z_2} f^{1/2}(s)\, ds + \frac{\pi}{4}\right]. \end{aligned} \tag{3.10}$$

Now

$$\lambda \int_{z_1}^{z} f^{1/2}(s)\, ds + \frac{\pi}{4} = \int_{z_1}^{z_2} f^{1/2}(s)\, ds + \frac{\pi}{2} - \left[\lambda \int_{z}^{z_2} f^{1/2}(s)\, ds + \frac{\pi}{4}\right],$$

so for Q_1 and Q_2 to be asymptotically equal we require that

$$c_1 \sin\left\{\int_{z_1}^{z_2} f^{1/2}(s)\, ds + \frac{\pi}{2} - \left[\lambda \int_{z}^{z_2} f^{1/2}(s)\, ds + \frac{\pi}{4}\right]\right\} = c_3 \sin\left[\lambda \int_{z}^{z_2} f^{1/2}(s)\, ds + \frac{\pi}{4}\right]. \tag{3.11}$$

This will be satisfied if

$$\lambda \int_{z_1}^{z_2} f^{1/2}(s)\, ds + \frac{\pi}{2} = n\pi,$$

and

$$(-1)^n c_1 = c_3.$$

Thus our eigenvalue condition is

$$\lambda \int_{z_1}^{z_2} f^{1/2}(s)\, ds = (n - \frac{1}{2})\pi. \tag{3.12}$$

This is the standard Bohr-Sommerfeld condition (Nayfeh, 1983; Bender and Orszag, 1987).

If we are not dealing with precisely the situation described above, of two well-separated turning points z_1 and z_2 in a continuous medium, it is convenient to generalise this result by invoking a phase constant α, replacing equation (3.12) by

$$\lambda \int_{z_1}^{z_2} f^{1/2}(s)\, ds = (n + \alpha)\pi. \tag{3.13}$$

Note also that the Bohr-Sommerfeld condition can only include information contained within the turning points of the problem; changes in the model *outside* the cavity cannot affect results gained from this method.

3.3 Description of method

In section 1.4.4 we described a simple application of the Bohr-Sommerfeld condition, and found a dispersion relation for modes completely contained within the solar interior. How do we extend this method to incorporate chromospheric effects? It has been noted above that, using the Bohr-Sommerfeld condition, we can only consider effects which occur in the region between the two turning points, that is within the cavity. However, we have also seen that, for the range of frequencies we would like to consider, the acoustic cut-off term prevents the interior cavity from reaching the chromosphere. Our way round this problem is to construct an artificial system whereby the effect of the cut-off term is ignored.

Our model consists of a marginally stratified linear polytrope for the solar interior, separated by an interface at $z = 0$ from an as yet undefined chromospheric model. We consider the canonical form of the wave equation, equation (1.24), and use an approximate form of κ^2:

$$\kappa^2 = \frac{\omega^2}{c_s^2 + v_A^2} - k_x^2. \tag{3.14}$$

In using this form of κ^2, we are ignoring the cut-off term in both the solar interior and the chromosphere, and also neglecting the buoyancy frequency in the chromosphere; the buoyancy frequency is already set to zero in the interior by choice of the temperature gradient there. The effect of this is that we are forcing a wave to propagate upwards into the chromosphere, so that any changes in the state of the model can directly influence wave motions. We still require an upper turning point to exist in order to close the cavity; thus

we may only consider profiles of chromospheric temperature and magnetic field such that κ^2 drops below zero at some height. Thus we require that the fast speed, c_f, defined by $c_f^2 = c_s^2 + v_A^2$, increases with height in the chromosphere. Any wave propagating upwards with non-zero k_x would then be refracted by the increasing fast speed, just as a sound wave propagating into the solar interior is refracted by the increasing sound speed. Indeed, a non-magnetic chromospheric model with temperature increasing with height would be a suitable candidate for this approach.

The advantage of our approach is that we are free to consider any profile of chromospheric temperature and magnetic field strength which gives an integrable form of κ in the Bohr-Sommerfeld condition. In the following sections, we shall consider a variety of chromospheric profiles. For each we will use the Bohr-Sommerfeld condition to derive a dispersion relation, and then investigate the effect of changes in the model upon the mode frequencies calculated. Our principal motivation is to look for a clue to the possible causes of frequency shift turnover.

It must be stressed that this is a completely artificial approach, which cannot be defended as a realistic treatment of the problem of chromospheric effects on p-mode frequencies. Any conclusion reached would have to be confirmed with separate, more rigorous treatments of the problem. However, since the intention of this work is simply to point out possible processes by which turnover could occur, it is reasonable to consider a simpler physical problem which could in some way diagnose the effects at work on the Sun itself. Once this is done, we can return to models which are more representative of the Sun, and hopefully explain the existence of turnover.

3.4 Isothermal model with a uniform magnetic field

As a first investigation, we look at the case of an isothermal chromosphere in which is embedded a uniform magnetic field. The model is described in section 1.5.3 and is the model considered by, among others, Evans and Roberts (1990) and Jain and Roberts (1993).

The profiles of sound speed and Alfvén speed in this model are given in section 1.5.3. From these we find that the form of κ^2 for $z < 0$ is given by

$$\kappa^2 = \frac{\omega^2}{c_0^2 + v_0^2 \exp(-z/H)} - k_x^2, \tag{3.15}$$

where c_0 is the sound speed in the chromosphere, v_0 is the Alfvén speed at $z = 0^-$ and

H is the scale height. Note that as $z \to -\infty$, $\kappa^2 \to -k_x^2$, which is negative as desired. Also, since we require that $\kappa^2(0^-) > 0$, we are restricted to frequencies sufficiently high that $\omega^2 - k_x^2(c_0^2 + v_0^2) > 0$. For the temperatures, magnetic field strengths and horizontal wavelengths we will be considering, this condition will always be satisfied. For example, for a mode of degree 50, a chromospheric temperature of 4170K and a magnetic field strength of 30G, this condition will be satisfied for all modes of frequency greater than 0.08mHz. Thus κ^2 will be positive at $z = 0^-$ and decreases with height, passing through zero at a point we shall call z_1 (< 0).

In the interior, $z > 0$, κ^2 will have the form

$$\kappa^2 = \frac{\omega^2}{c_{0L}^2(1 + z/z_0)} - k_x^2, \tag{3.16}$$

where c_{0L} is the sound speed at $z = 0^+$. Again, κ^2 will be negative at sufficiently large z, and will be positive at $z = 0^+$ since the condition $\omega^2 - k_x^2 c_{0L}^2 > 0$ is generally satisfied. There will be a zero of κ^2 at the point z_2 (> 0).

We now introduce the Bohr-Sommerfeld condition as follows. We write

$$\begin{aligned} (n + \alpha)\pi &= \int_{z_1}^{z_2} \kappa \, ds \\ &= \mathrm{I}_1 + \mathrm{I}_2, \end{aligned} \tag{3.17}$$

where

$$\mathrm{I}_1 = \int_{z_1}^{0} \kappa \, ds$$

is the integral of κ over that part of the cavity located in the chromosphere ($z < 0$), and

$$\mathrm{I}_2 = \int_{0}^{z_2} \kappa \, ds$$

the integral of κ over the part of the cavity in the solar interior ($z > 0$). The details of the evaluation of these integrals are given in Appendix A. The dispersion relation obtained from equation (3.17) is as follows:

$$\begin{aligned} (n + \alpha)\pi &= m\Omega^2 \left[\frac{\pi}{4} + \frac{1}{2}\sin^{-1}\left(1 - \frac{2k_x z_0}{m\Omega^2}\right)\right] - (k_x z_0)^{1/2}(m\Omega^2 - k_x z_0)^{1/2} \\ &+ \frac{r^{1/2}}{\gamma}(\Omega^2 - r)^{1/2}\log X - \frac{r}{\gamma}\left[\frac{\pi}{2} + \sin^{-1}\left(1 - \frac{2r(1+\sigma)}{\Omega^2}\right)\right], \end{aligned} \tag{3.18}$$

where $r = \gamma k_x H$, $\sigma = v_0^2/c_0^2$ and

$$X = \frac{2}{\sigma\Omega^2}(\Omega^2 - r)^{1/2}[\Omega^2 - r(1+\sigma)]^{1/2}(1+\sigma)^{1/2} + \frac{2}{\sigma\Omega^2}(\Omega^2 - r)(1 + \sigma/2) - \frac{r}{\Omega^2}.$$

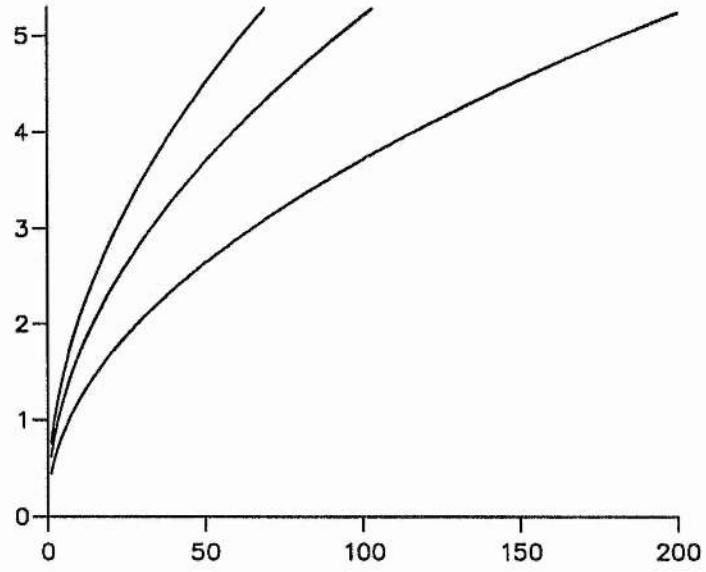

Figure 3.7: Frequency (in mHz) vs. degree l for modes of order 10 (lowest curve), 20 and 30. The chromospheric temperature is 4170K, the magnetic field strength is 10G.

The terms m, Ω^2 and z_0 are as previously defined (section 1.4.1). Equation (3.18) is obviously not a simple dispersion relation. However, we can determine its roots numerically giving the frequencies of the modes of oscillation of this system. Then, by altering parameters such as r and σ, we can induce changes in these frequencies which we can then examine. It is not clear which value should be taken for the parameter α, since we are considering a cavity which is 'split' between two models; variables such as the density are not continuous across $z = 0$. For the sake of this investigation, we set $\alpha = -1/2$.

We can solve the dispersion relation (3.18) to find the mode frequencies. Figure 3.7 shows the frequency (in mHz) versus degree l curves obtained for modes of orders n=10, 20 and 30, the last being the highest of the three curves. The frequencies are calculated for a chromospheric temperature of 4170K and a magnetic field strength of 10G. These curves show the basic parabolic form of p-modes.

We can then alter certain parameters of the chromospheric model and examine the effect on mode frequencies. Figure 3.8 shows the effect of increasing the magnetic field strength from 10G to 20G, for a fixed temperature of 4170K. The three curves are plots of frequency shift (in μHz) versus original frequency (in mHz), for orders 10 (the highest

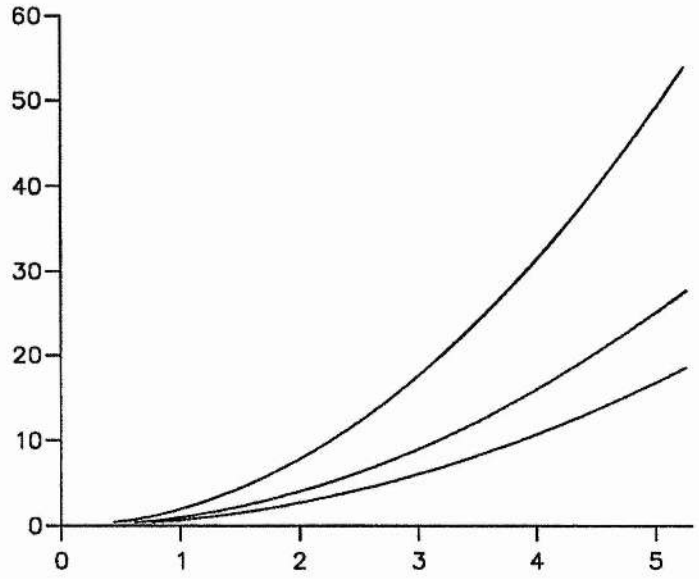

Figure 3.8: Frequency shift (in μHz) vs. original frequency (in mHz) induced by an increase in magnetic field strength from 10G to 30G, with the chromospheric temperature held at 4170K. The curves are for modes of orders 10 (highest curve), 20 and 30.

curve), 20 and 30. We see that this dispersion relation gives an increase in mode frequency with increasing magnetic field, consistent with the exact treatment of the full problem (Evans and Roberts, 1990). The major difference is that the magnitudes of the frequency shifts found here are much larger than those found through the exact analysis. This is not surprising, since the magnetic field now resides within the cavity, and can directly affect the oscillatory wave motions within that region, rather than merely affecting the evanescent 'tail' of the mode. Thus any change in the magnetic field strength has a more significant effect on mode frequencies.

Finally, Figure 3.9 shows the effect of increasing the chromospheric temperature from 4170K to 4400K, for a fixed magnetic field strength of 10G. Again the curves are for orders 10, 20 and 30, and again the general trend of the exact results (Campbell and Roberts, 1989) is recreated by our artificial dispersion relation.

Thus we have seen that our somewhat contrived approach can provide a reasonable simulacrum of the true problem in at least one case. However, if this approach is to provide any useful end result, we must investigate the factors underlying the behaviour displayed

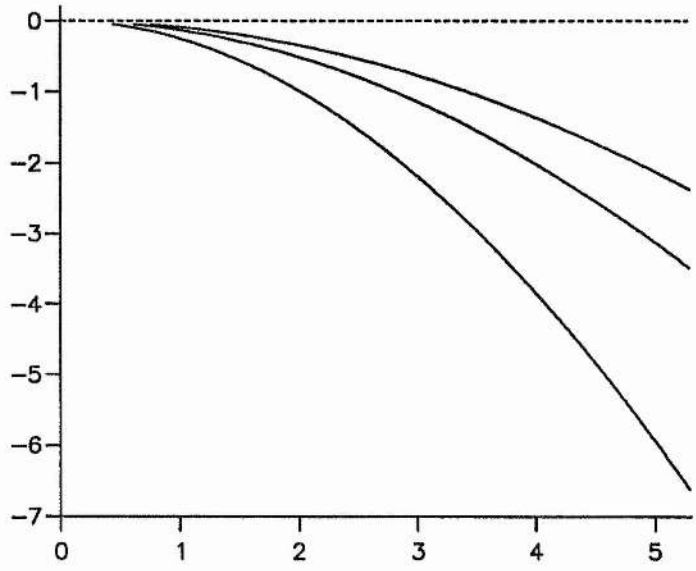

Figure 3.9: Frequency shift (in μHz) vs. original frequency (in mHz) induced by an increase in chromospheric temperature from 4170K to 4400K, with the magnetic field strength held at 10G. Modes considered are the same as for Figure 3.8.

in Figures 3.8 and 3.9. To do this it is helpful to consider the variation of the fast speed, c_f, in the chromospheric model.

Recalling that

$$c_f^2 = c_s^2 + v_A^2,$$

we can write the κ^2 of equation (3.14) in the form

$$\kappa^2 = \frac{\omega^2}{c_f^2} - k_x^2. \tag{3.19}$$

From this it is immediately apparent that the turning point of κ^2, which we identify as the 'top' of the mode cavity, resides at the point where

$$c_f^2 = \frac{\omega^2}{k_x^2}. \tag{3.20}$$

Thus, for a given frequency and wavelength, the cavity will extend to the point where the exponentially rising Alfvén speed lifts the fast speed to the value ω/k_x. For example, a mode of frequency 4mHz and degree 100 gives a value of ω^2/k_x^2 of around $3\text{x}10^4\text{km}^2\text{s}^{-2}$.

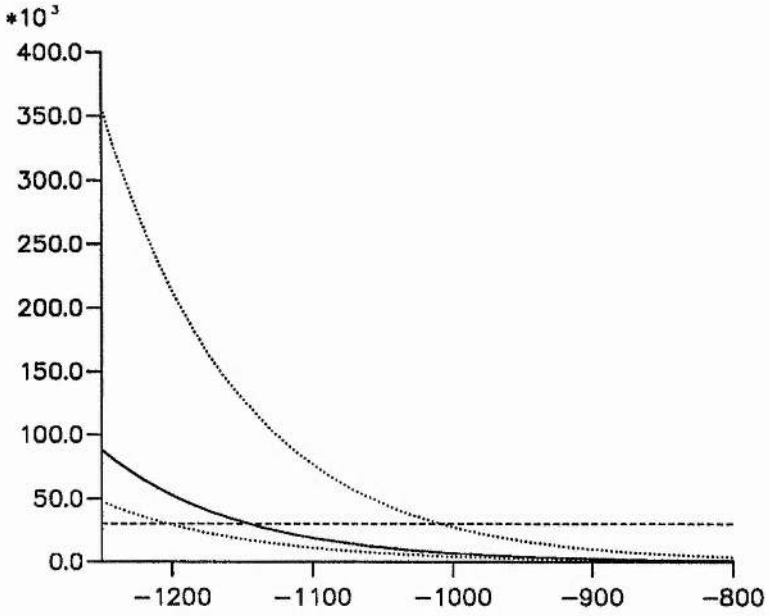

Figure 3.10: Profiles of c_f^2 (in $\mathrm{km^2 s^{-2}}$) vs. z (in km) in the magnetic chromosphere. The solid line is the profile of c_f^2 for a chromospheric temperature of 4170K and magnetic field strength of 10G. The upper dotted line is for a temperature of 4170K and a field strength of 20G; the lower dotted line is for a temperature of 4400K and a field strength of 10G. The dashed line plots the (constant) value of ω^2/k_x^2 for a typical mode.

For a chromospheric temperature of 4170K and a magnetic field strength of 10G, the fast speed squared at $z = 0^-$ is $47\mathrm{km^2 s^{-2}}$. As the Alfvén speed increases with height, the fast speed squared increases to $3\mathrm{x}10^4\mathrm{km^2 s^{-2}}$ at a height of around 1150km. This information is displayed in Figure 3.10. The solid line represents the run of c_f^2 in the chromosphere for a temperature of 4170K and a magnetic field strength of 10G. The dashed line represents the value of c_f^2 required to produce a turning point for a mode of frequency 4mHz and degree 100. The point of intersection of the curve and the dashed line gives the position of the turning point.

Altering the chromospheric parameters alters the form of the c_f^2 profile. The upper dotted line in Figure 3.10 shows the c_f^2 profile for the same temperature as the solid line, but with the field strength increased to 20G. The fast speed is increased by this change, lowering the top of the cavity and increasing the speed of propagation within the cavity. We would expect both these effects to contribute towards an increase in mode frequency, and indeed

this is what is demonstrated in Figure 3.8. In terms of equation (3.17), what has happened is that I_1, the integral of κ over that part of the cavity resident in the chromospheric model, has decreased because of the increase in fast speed, and so I_2 must increase to satisfy the Bohr-Sommerfeld condition. Since I_2 is approximately proportional to Ω^2, an increase in I_2 results in an increase in frequency.

The lower dotted line in Figure 3.9 shows the c_f^2 profile for a magnetic field of 10G, as for the solid line, but at an increased temperature of 4400K. Here we see that the fast speed has actually *decreased*, despite the increase in sound speed. The reason for this is that the scale height in the chromosphere H, given by

$$H = \frac{c_0^2}{\gamma g},$$

is proportional to the sound speed squared. Thus in a hotter chromosphere, the Alfvén speed *increases more slowly with height*; thus the effect of higher temperatures is to lower the fast speed. The consequence of this is to raise the top of the cavity and to lower the propagation speed within the cavity. Figure 3.9 shows the drop in frequency we would expect in such a situation.

Let us now turn to other fast speed profiles and examine their effects on mode frequencies. At each stage we will be looking for possible causes of frequency shift turnover.

3.5 Algebraic fast speed profile

We look now at a fast speed profile formed from a simple algebraic expression, chosen so as to prevent the fast speed from increasing indefinitely with height. The form of c_f^2 we consider is as follows:

$$c_f^2 = c_{f\infty}^2 \left(1 - \frac{A^2}{1 - z/B^2}\right), \tag{3.21}$$

where $c_{f\infty}$ is the value of the fast speed at infinite height and A^2 and B^2 are shape parameters. If we specify the value of c_f^2 at $z = 0^-$ as c_{f0}^2, and the scale height of c_f^2 at $z = 0^-$ as being given by

$$\left.\frac{c_f^2}{(c_f^2)'}\right|_{z=0^-} = H_0, \tag{3.22}$$

where the dash ($'$) denotes the derivative with respect to z, then

$$A^2 = 1 - \frac{c_{f0}^2}{c_{f\infty}^2} \tag{3.23}$$

and

$$B^2 = \left(\frac{c_{f\infty}^2}{c_{f0}^2} - 1 \right) H_0. \tag{3.24}$$

Since the fast speed does not become infinite, the cut-off effect will reappear for this profile. For a turning point in the chromosphere to exist we require that

$$\omega^2 - k_x^2 c_{f0}^2 > 0 \tag{3.25}$$

and that

$$\omega^2 - k_x^2 c_{f\infty}^2 < 0. \tag{3.26}$$

Thus we may only consider values of the frequency such that

$$k_x^2 c_{f0}^2 < \omega^2 < k_x^2 c_{f\infty}^2. \tag{3.27}$$

For frequencies at which these conditions are satisfied, we can carry out a similar calculation to that given in section 3.4, details of which are given in Appendix A. The resulting dispersion relation is as follows:

$$\begin{aligned} (n+\alpha)\pi &= m\Omega^2 \left[\frac{\pi}{4} + \frac{1}{2} \sin^{-1} \left(1 - \frac{2k_x z_0}{m\Omega^2} \right) \right] - (k_x z_0)^{1/2} (m\Omega^2 - k_x z_0)^{1/2} \\ &- k_x B^2 (1-A^2)^{1/2} (A^2 + D^2 - 1)^{1/2} \\ &+ \frac{k_x A^2 B^2 D^2}{2(1-D^2)^{1/2}} \left[\frac{\pi}{2} + \sin^{-1} \left(1 - \frac{2(1-A^2)(1-D^2)}{A^2 D^2} \right) \right], \end{aligned} \tag{3.28}$$

where

$$D^2 = \frac{\omega^2}{k_x^2 c_{f\infty}^2}. \tag{3.29}$$

Figure 3.11 shows the modes found from this dispersion relation. The three solid curves are for modes of orders 5, 10 and 20 and the dashed lines are the limits on frequency set by conditions (3.25) and (3.26). Since the dispersion relations (3.18) and (3.28) are both dominated by their first terms, which are identical, it is not surprising that the familiar p-mode parabolae are again recovered here. The curves are stopped at $l = 200$ and $\nu = 5.3$mHz to enable comparison with Figure 3.7; in practice they could be extended indefinitely. The modes are calculated for a fast speed profile with the characteristics listed in column 'a' of Table 3.1. This profile is plotted in Figure 3.12.

Figure 3.13 shows the effect on mode frequencies of changing from profile 'a' in Figure 3.12 to profile 'b', for modes of order 10. We do this by decreasing H_0, the fast speed

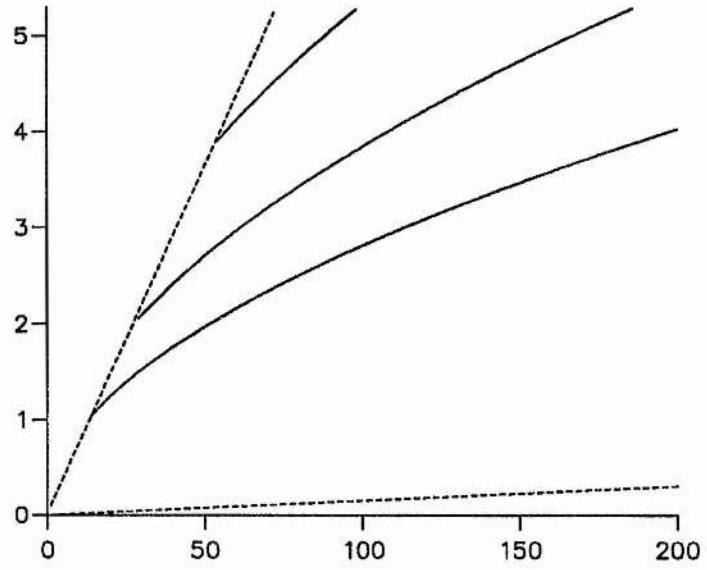

Figure 3.11: Mode frequency (in mHz) vs. degree l for modes of order n=5 (lowest curve), 10 and 20, for profile 'a' of Table 3.1. Dashed lines show the limits on frequency set by the profile parameters.

scale height at $z = 0^-$, from 10m to 1m; the effect is to raise c_f^2 throughout $z < 0$. We see that mode frequencies increase by a small amount as a result of this process. This is understandable in the same terms as the frequency shifts of Figure 3.9. Increasing the fast speed lowers the roof of the cavity and increases the propagation speed within the cavity, so frequencies will increase.

Figure 3.13 shows an interesting additional effect, however, with frequency shifts being particularly large at the very lowest frequencies. The reasoning behind this is as follows. The position of the roof of the cavity depends on the value of ω^2/k_x^2, and since ω^2 is approximately proportional to k_x for given n, the height of the roof of the cavity will scale as $1/k_x$. So lower degree modes have higher roofs. Since n is fixed along our $\Delta\nu$ curves, this implies that it is the lower frequency modes whose cavities extend highest into the chromospheric model. Thus, what we are seeing in the 2–3mHz range of Figure 3.13 is the effect of the levelling-off of c_f^2 at large heights. Consider the two dashed lines in Figure 3.12. The upper line displays the value of c_f^2 required to provide a roof for a mode of around 2.2mHz, the lower for a mode of around 4.5mHz. We see that the change from

Profile	a	b
c_{f0}^2 (km^2s^{-2})	46.6	46.6
$c_{f\infty}^2$ (km^2s^{-2})	100000.0	100000.0
H_0 (m)	10.0	1.0

Table 3.1: Parameters for algebraic fast speed profile

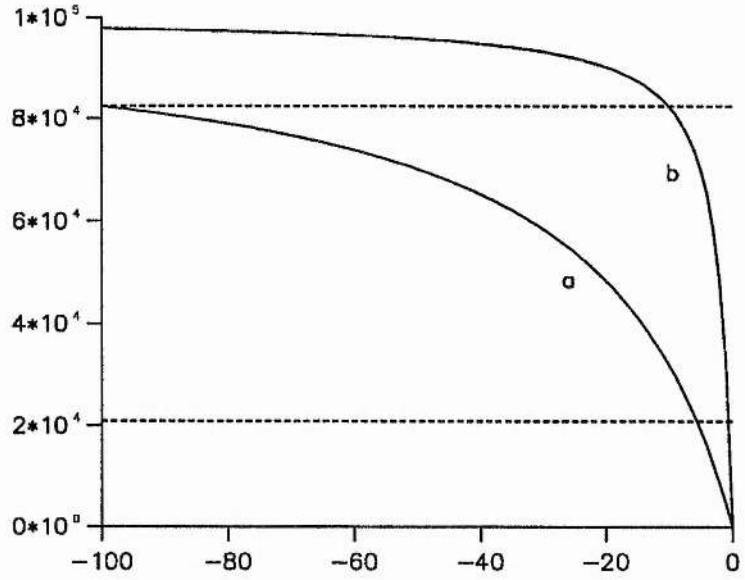

Figure 3.12: Fast speed squared (in km^2s^{-2}) vs. z (in km) for the algebraic profiles given in Table 3.1.

profile 'a' to profile 'b' induces a far larger change in the cavity roof height for the 2.2mHz mode than for the 4.5mHz mode. Thus the changes in I_1, and therefore the frequency shifts generated, are larger for the lowest frequency modes.

This effect points out a second flaw in our artificial method. In the solar p-mode problem, with a cut-off term, we would expect *higher* frequency modes to be more sensitive to effects occurring at large heights, since low-frequency modes will be cut-off well below the site of any such effects. This inversion of the 'correct' behaviour must be borne in mind in our attempts to use the artificial problem to explore the causes of turnover.

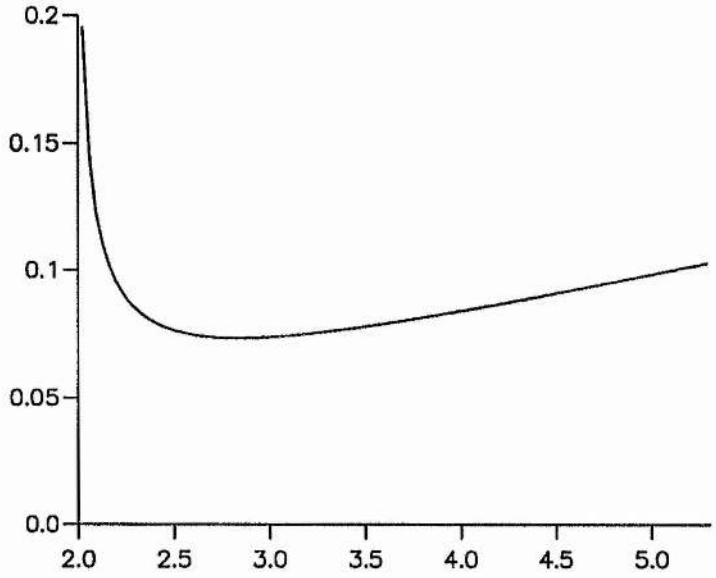

Figure 3.13: Frequency shift (in μHz) vs. original frequency (in mHz) induced by the change in the algebraic fast speed profile given in Table 3.1.

3.6 Hyperbolic tangent fast speed profile

We look now at a fast speed profile involving the tanh function, allowing us to combine the exponentially growing behaviour of the isothermal uniform magnetic field model (section 3.4) with the levelling-off of fast speed given by the algebraic profile (section 3.5). The form of c_f^2 we dictate is as follows:

$$c_f^2 = c_{fi}^2 + A^2 \tanh(-z/B^2 - D^2),$$

where c_{fi} is the fast speed at the point of inflexion of the c_f^2 curve; we again state that c_{f0} is the fast speed at $z = 0^-$ and $c_{f\infty}$ is the fast speed at infinity. We also define H_i, the scale height of c_f^2 at the point of inflexion, by

$$\left.\frac{c_f^2}{(c_f^2)'}\right|_{z=-B^2D^2}. \tag{3.30}$$

The terms A, B and D are then given by

$$A^2 = c_{f\infty}^2 - c_{fi}^2, \qquad B^2 = \left(\frac{c_{f\infty}^2}{c_{fi}^2} - 1\right) H_i, \qquad \tanh D^2 = \frac{c_{fi}^2 - c_{f0}^2}{c_{f\infty}^2 - c_{fi}^2}. \tag{3.31}$$

The conditions for the existence of the turning point in the chromosphere are the same as in section 3.5.

We again use the Bohr-Sommerfeld condition (3.17) to derive a dispersion relation for modes in this system. The details of the integration are given in Appendix A. The resulting dispersion relation is as follows:

$$(n+\alpha)\pi = m\Omega^2\left[\frac{\pi}{4}+\frac{1}{2}\sin^{-1}\left(1-\frac{2k_xz_0}{m\Omega^2}\right)\right]-(k_xz_0)^{1/2}(m\Omega^2-k_xz_0)^{1/2}$$
$$+k_xF^2H_i\left\{\frac{(F^2+E^2-1)^{1/2}}{(F^2-1)^{1/2}}\left[\frac{\pi}{4}-\frac{1}{2}\sin^{-1}X_1\right]\right.$$
$$\left.-\frac{(F^2-E^2-1)^{1/2}}{(F^2+1)^{1/2}}\left[\frac{\pi}{4}-\frac{1}{2}\sin^{-1}X_2\right]\right\}, \qquad (3.32)$$

where

$$X_1 = 1+\frac{2(F^2-1)}{E^2}-\frac{2(F^2-1)(F^2+E^2-1)}{E^2F^2(1-\tanh D^2)},$$
$$X_2 = 1-\frac{2(F^2-1)}{E^2}+\frac{2(F^2+1)(F^2-E^2+1)}{E^2F^2(1+\tanh D^2)},$$

and E and F are given by

$$E^2=\frac{\omega^2}{k_x^2c_{fi}^2}, \qquad F^2=\frac{c_{f\infty}^2}{c_{fi}^2}-1.$$

The modes calculated from this dispersion relation again show the form of Figure 3.11. We once more alter the form of the profile and examine the resultant changes in frequency. Figure 3.14 shows the form of the two c_f^2 profiles whose parameters are given in Table 3.2. Figure 3.15 then shows the frequency shift induced by changing from profile 'a' to profile 'b', for modes of order 10. Again we see an increase in frequency being associated with an increase in the fast speed.

Profile	a	b
c_{f0}^2 (km^2s^{-2})	46.6	46.6
c_{fi}^2 (km^2s^{-2})	49500.0	49500.0
$c_{f\infty}^2$ (km^2s^{-2})	100000.0	100000.0
H_0 (m)	200.0	50.0

Table 3.2: Parameters for hyperbolic tangent fast speed profile

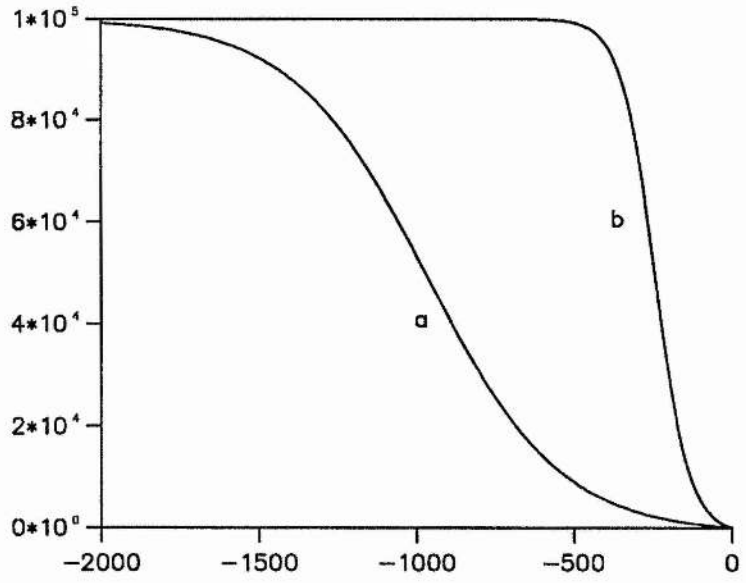

Figure 3.14: Fast speed squared (in km^2s^{-2} vs. z (in km) for the hyperbolic tangent profiles given in Table 3.2.

3.7 Discussion

We have now examined three distinct profiles for the fast speed in our chromospheric model, and calculated the frequency shifts associated with changes in profile parameters. In each case, an *increase* in fast speed in the chromosphere resulted in an *increase* in all mode frequencies. The question is, have we learnt anything about the effect by which some mode frequencies increase in frequency, while others, subject to the same change in profile, show a decrease in frequency?

A clue to answering this question comes from the algebraic profile. We saw there that the lowest frequency modes, those whose cavities extend highest into the chromosphere, suffer a relatively large change in mode frequency, bringing to mind that *modes of different frequencies sample different parts of the chromospheric model.* This raises the question of whether it is possible to construct a change of profile such that some modes encounter an increase in fast speed over their cavity, while others encounter a decrease in fast speed? If this could be achieved, then by our reasoning above, it would be possible for some modes to suffer an increase in frequency while others would suffer a decrease.

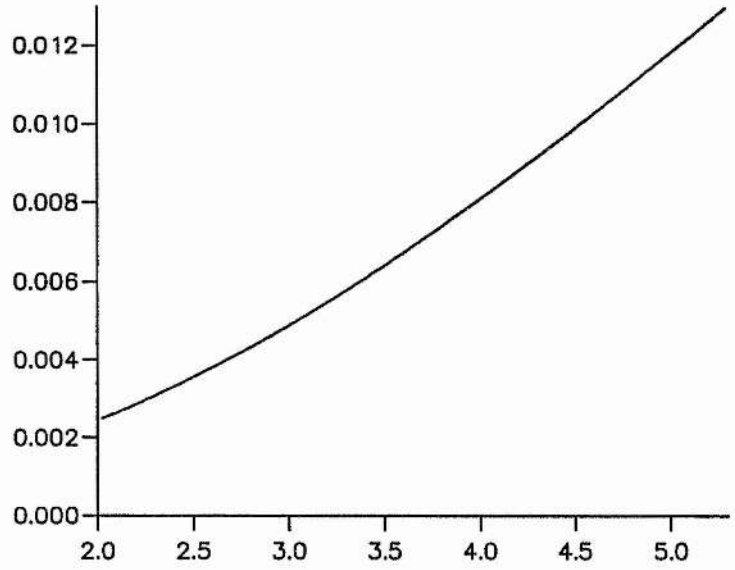

Figure 3.15: Frequency shift (in μHz) vs. original frequency (in mHz) induced by the change in the hyperbolic tangent profile given in Table 3.2.

What we need, then, is a change in profile such that in one region of the model the fast speed increases, while elsewhere the fast speed decreases; in other words, in a plot such as Figure 3.10 showing the 'before' and 'after' profiles of c_f^2, there would need to be some point at which the two profiles *crossed.* The manner in which this situation can arise can, in fact, be deduced from our earlier study of the isothermal magnetic model.

In section 3.4 we stated that, for this model, increasing the magnetic field strength increases the fast speed throughout the model. We also stated that increasing the chromospheric temperature had the paradoxical effect of lowering the fast speed, by decreasing the rate at which the Alfvén speed grows with height. However, if, in moving from our 'before' to 'after' profiles, we increase *both* the field strength and the temperature, the Alfvén speed must be augmented immediately above the interface. At increasing height, the effect of the larger Alfvén speed scale height would begin to be felt, and at some height the two effects cancel each other out. Here the two c_f^2 profiles cross. Above this height, the fast speed will have decreased as a result of the change in profile.

Such a situation is shown in Figure 3.16, whose profiles have been calculated for the parameters given in Table 3.3. We see that below around 600km in height, the effect

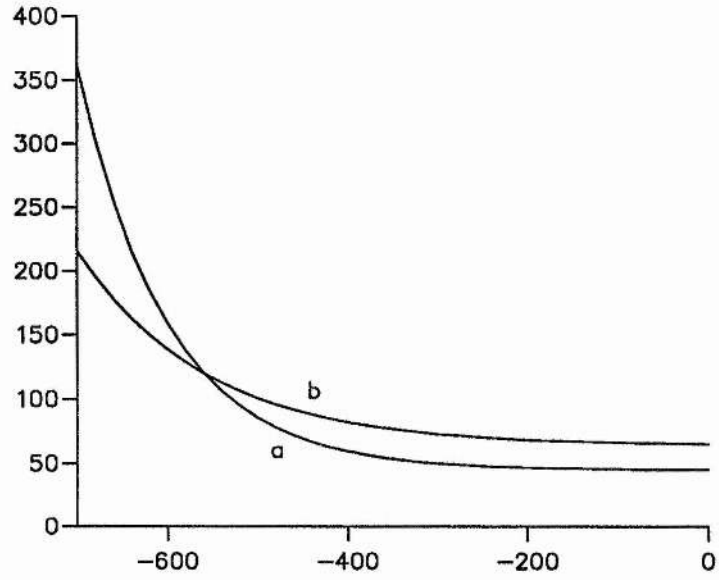

Figure 3.16: Fast speed squared (in km^2s^{-2} vs. z (in km) displaying crossed profiles. We here consider an isothermal chromosphere with a uniform horizontal magnetic field; chromospheric parameters are given in Table 3.3.

of increasing B_0 and T_c together is to increase the fast speed. Above this point, however, the fast speed decreases as a result of this change. Thus high frequency modes, whose cavity roof lies below $\approx$ 600km, would be expected to suffer an increase in frequency. Lower frequency modes, however, would also sample some of the decrease in fast speed, and would start to suffer a negative frequency shift effect. This differentiation of shift behaviour with frequency is the basis for a form of turnover.

Profile	a	b
B_0	10G	20G
T_c	4170K	6000K

Table 3.3: Parameters for crossed profiles

Figure 3.17 shows the frequency shift calculated using our approximate dispersion relation (3.18), for the change in profile from a 10G field in a chromosphere of temperature 4170K to a 20G field in a chromosphere of temperature 6000K. We see that at low frequen-

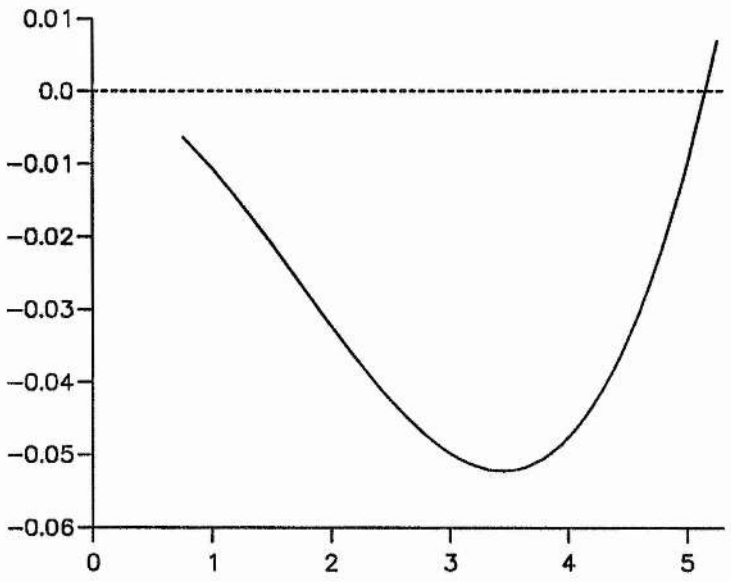

Figure 3.17: Frequency shift (in μHz) vs. original frequency (in mHz) induced by the change in the isothermal, magnetic chromophere given in Table 3.3

cies, there is indeed a drop in frequency. As the frequency increases, the cavity roof height decreases, and the lower regions of the model become dominant. Thus we see the frequency shift curve start to turn around, until the very highest frequency modes suffer an actual increase in frequency.

Figure 3.17 demonstrates a turnover effect. Can we relate this effect to the turnover apparent in the observational data? Our curves have been obtained by increasing the magnetic field strength and chromospheric temperature, changes which we might well expect to occur in the real solar chromosphere as the Sun approaches maximum. We have also seen that the results of Evans and Roberts (1990), gained by increasing the magnetic field strength, matched well with the observed data up to around 4mHz. Our results, while showing a turnover effect, do not agree with the observational data. Why is this?

The underlying reason is the inversion in the correct behaviour brought about by the neglect of the cut-off term (section 3.5). In method, it is the high-frequency modes which suffer an increase in frequency; the prediction is thus that in the actual problem, it will be the low-frequency modes which will increase in frequency. Similarly, our method gives a decrease in frequency for low-frequency modes, so we would expect that in the actual

problem it will be the high-frequency modes which which will decrease in frequency. In other words, taking our deduced inversion of the correct behaviour into account, Figure 3.17 suggests that the full problem will show the observed turnover effect for the change in profile described in Table 3.3.

Let us check this prediction by returning to the exact treatment of the problem (section 1.5.3). We have seen that the dispersion relation (1.97) of Evans and Roberts (1990) can produce the frequency shift curves displayed in Figures 3.2 and 3.3; does it produce a turnover curve for the situation described above?

Figure 3.18 shows the frequency shift induced by changing the chromospheric magnetic field strength from 10G to 30G, while increasing the chromospheric temperature from 4170K to 6000K, calculated from the exact dispersion relation of Evans and Roberts (1990). We see that the turnover effect *does* appear when this particular change of state is imposed upon the chromospheric model.

For a given change in magnetic field strength, there will be a range of temperature changes which yield turnover. Very small temperature increases will not result in turnover within the relevant range of frequency, while very large changes in temperature dominate the positive shift observed at lower frequencies. The magnitudes of frequency shifts so generated will also depend on the precise changes in field strength and temperature (see Jain and Roberts, 1993).

Thus the 'recipe' for turnover deduced from and predicted by our artificial system does indeed introduce the effect of turnover into frequency shift curves produced by the exact dispersion relation. The existence of turnover in these curves is one thing, but how well do the results gained quantitatively match the observed frequency shifts? Also, our deduction of a turnover mechanism was based on a consideration of the fast speed profile within an artificial chromospheric cavity; obviously this cannot be a valid description of the physical causes of frequency shifts in the true problem. Thus we are left with the further question, how can we give a physical description of the processes operating behind the observed variations in p-mode frequencies?

Answering both the above questions requires a more rigorous treatment of the mathematical problem than that given above. We turn to this topic in the following Chapter.

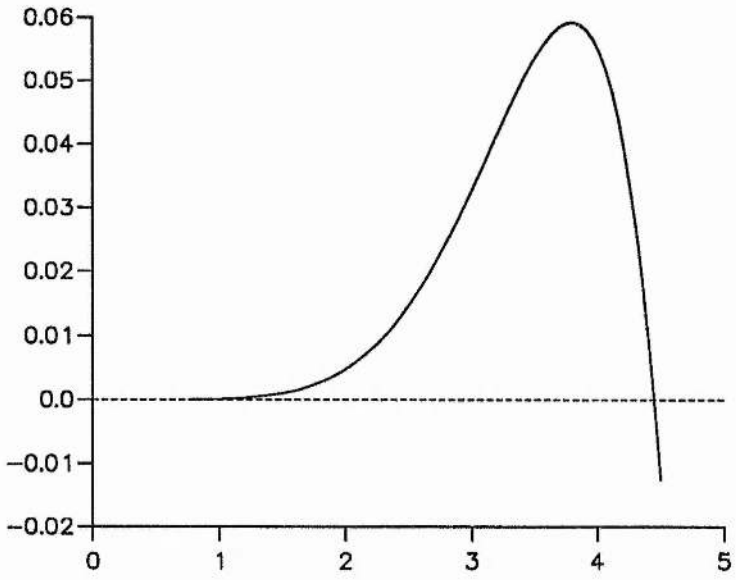

Figure 3.18: Frequency shift (in μHz) vs. original frequency (in mHz) for an increase in magnetic field strength from 10G to 30G and an increase in chromospheric temperature from 4170K to 6000K, for the isothermal chromospheric model with a uniform horizontal magnetic field. Frequency shifts are calculated from the dispersion relation of Evans and Roberts (1990).

Chapter 4

Chromospheric temperature effects

4.1 Introduction

We have seen in Chapter 3 that turnover can be introduced into the theoretical frequency shift curve of Evans and Roberts (1990) by the simple step of increasing the magnetic field strength and chromospheric temperature simultaneously. However, this is not the end of the story. Jain and Roberts (1993) report that, while this procedure can produce frequency shift curves showing turnover, the curves do not agree well with observational data (Libbrecht and Woodard, 1991). The generation of sufficiently large frequency shifts in the 2–3mHz range demands that the magnetic field strengths involved be relatively large, increasing from some 40G to 50G. Given such field strength changes, a large increase in temperature, from 4170K up to around 6000K, is then necessary to induce turnover at around 4mHz. Even in this case, turnover acts as a smooth, gradual effect, rather than the steep plummet in frequency shifts found in the observational data. Jain and Roberts conclude that refinements in their model may be needed to produce better agreement with the observed data.

A prime candidate for further investigation is the temperature profile of the chromosphere, which until now has been taken as isothermal in exact analytical studies. For example, we could look at the effect of a temperature profile which increases with height in a manner that resembles the observed behaviour in the solar chromosphere. It is in-

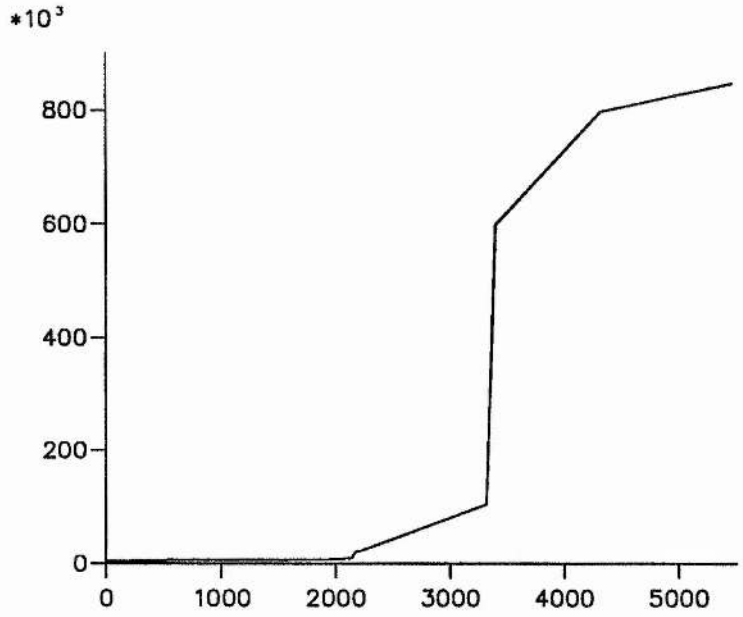

Figure 4.1: Variation of temperature (in K) with height (in km) in the solar atmosphere (after R. Ulrich, personal communication, 1993).

structive to look here at a numerical model constructed by R. Ulrich in an attempt to describe the variations of temperature, density and pressure in the chromosphere (Ulrich, personal communication, 1993). Figure 4.1 shows the variation of temperature with height in the model of Ulrich, while Figure 4.2 shows a detail of the model at lower heights. We see that in this model, the temperature increases gradually up to around 600km, is then roughly constant up to around 2000km, and then rises sharply above that point. Above around 3000km temperatures rise to their coronal values of around 8×10^5K. Note that we customarily place our magnetic interface, $z = 0$, at the temperature minimum, which does not exactly correspond with zero height in Ulrich's model. In any case, the effects of the gradual rise in temperature in the lowest part of the chromosphere and the steep rise in temperature above 2000km are areas of interest.

How can we investigate the influence of such features on frequency shifts? It seems clear that some numerical treatment of the chromosphere is appropriate. Such an approach is used by Wright and Thompson (1992) to study the effect of the chromospheric magnetic field on p-mode frequencies. They solve the wave equation numerically for an isothermal model with a uniform magnetic field, to find the value of a quantity which will be continuous

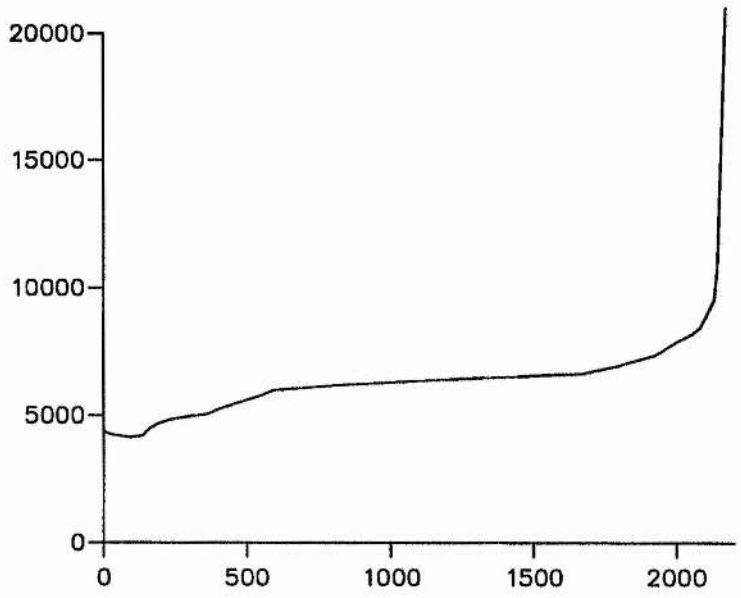

Figure 4.2: Detail of temperature profile

across an interface at the solar surface. They then form a perturbation method describing the effect of a small change in this quantity on the frequency of the global oscillation.

This approach to the chromosphere is appropriate to our demands: we too will use a numerical treatment for the chromosphere. However we would also like to make further use of the Bohr-Sommerfeld condition of Chapter 3, for two reasons. Firstly, we have already obtained analytical forms of the integral for the linear polytrope model, and secondly, the Bohr-Sommerfeld condition is widely used in studies of p-modes and helioseismology generally (e.g. Christensen-Dalsgaard, Duvall, Gough, Harvey and Rhodes, 1985). A form of the Bohr-Sommerfeld condition which included the influence of the chromosphere could prove a valuable tool with more general applications.

The aim of the following sections of this Chapter is to derive a form of the Bohr-Sommerfeld condition which incorporates the effect of the chromosphere in a general way. To do this, we must develop the basic WKB theory given in section 3.2.

4.2 Derivation of the modified Bohr-Sommerfeld condition

4.2.1 Further WKB theory

In section 3.2 we considered the differential equation (3.1), and considered a situation where the function $f(z)$ has a profile as shown in Figure 3.6. We then applied conditions to the Langer solutions around each turning point, stating that the Q_1 solution must be evanescent as $z \to -\infty$, while the Q_2 solution must be evanescent as $z \to \infty$. Let us now remove one of these conditions, and allow the Q_1 solution to remain general. Thus we have that

$$Q_1(z) = \left[-\frac{t_1(z)}{f(z)}\right]^{1/4} \{c_1 \mathrm{Ai}(t_1) + c_2 \mathrm{Bi}(t_1)\}. \tag{4.1}$$

We define an angle ϕ by

$$\tan\phi = \frac{c_2}{c_1}, \tag{4.2}$$

so that equation (4.1) reads

$$Q_1(z) = c_1 \left[-\frac{t_1(z)}{f(z)}\right]^{1/4} \{\mathrm{Ai}(t_1) + \tan\phi\, \mathrm{Bi}(t_1)\}. \tag{4.3}$$

For $z \gg z_1$, the asymptotic relations 3.5 give

$$Q_1 \sim \frac{c_1}{\sqrt{\pi}} \left[\frac{1}{f(z)}\right]^{1/4} \left\{\sin\left[\int_{z_1}^{z} f^{1/2}(s)\, ds + \frac{\pi}{4}\right] + \tan\phi\, \cos\left[\int_{z_1}^{z} f^{1/2}(s)\, ds + \frac{\pi}{4}\right]\right\}. \tag{4.4}$$

Write

$$\theta(z) = \int_{z_1}^{z} f^{1/2}(s)\, ds + \frac{\pi}{4}.$$

Then the $\{\}$ bracket in (4.4) becomes

$$\sin\theta + \tan\phi \cos\theta = \sec\phi \sin(\theta + \phi). \tag{4.5}$$

Recall that the asymptotic expansion of the Q_2 solution for $z \ll z_2$ is

$$Q_2 \sim \frac{c_3}{\sqrt{\pi}} \left[\frac{1}{f(z)}\right]^{1/4} \sin\left[\int_{z}^{z_2} f^{1/2}(s)\, ds + \frac{\pi}{4}\right]. \tag{4.6}$$

Then since

$$\begin{aligned} \theta + \phi &= \int_{z_1}^{z} f^{1/2}(s)\, ds + \frac{\pi}{4} + \phi \\ &= \int_{z_1}^{z_2} f^{1/2}(s)\, ds + \frac{\pi}{2} + \phi - \left[\int_{z}^{z_2} f^{1/2}(s)\, ds + \frac{\pi}{4}\right], \end{aligned}$$

the condition that the asymptotic expansions of Q_1 and Q_2 match is that

$$c_1 \sec\phi \sin\left\{\int_{z_1}^{z_2} f^{1/2}(s)\,ds + \frac{\pi}{2} + \phi - \left[\int_z^{z_2} f^{1/2}(s)\,ds + \frac{\pi}{4}\right]\right\}$$
$$= c_3 \sin\left[\int_z^{z_2} f^{1/2}(s)\,ds + \frac{\pi}{4}\right]. \tag{4.7}$$

This will be satisfied if

$$\int_{z_1}^{z_2} f^{1/2}(s)\,ds + \frac{\pi}{2} + \phi = n\pi,$$

and

$$(-1)^n c_1 \sec\phi = c_3.$$

Thus our modified Bohr-Sommerfeld condition is

$$\int_{z_1}^{z_2} f^{1/2}(s)\,ds = (n - \frac{1}{2})\pi - \phi \tag{4.8}$$

where

$$\tan\phi = \frac{c_2}{c_1}.$$

4.2.2 Application to the linear polytrope model

We can now apply the general modified Bohr-Sommerfeld condition, equation (4.8), to our particular wave equation and our particular model for the solar interior, the linear polytrope model with adiabatic stratification. Unlike our somewhat cavalier use of WKB theory in the previous chapter, here we will attempt to monitor the errors introduced by our approximate method.

Our differential equation is as described in section 1.4.2, that is

$$\frac{d^2Q}{dz^2} + \kappa^2(z)\,Q = 0, \tag{4.9}$$

where

$$Q = \rho_0^{1/2} c_s^2 \nabla.\boldsymbol{v}$$

and

$$\kappa^2 = k_x^2 \left\{\frac{\omega^2}{k_x^2 c_{0L}^2}\frac{1}{1+z/z_0} - \frac{m(m+2)}{4k_x^2 z_0^2}\frac{1}{(1+z/z_0)^2} - 1\right\}. \tag{4.10}$$

We found that κ^2 will have two zeros in $z > 0$ if the condition

$$\omega^2 < \frac{m(m+2)c_{0L}^2}{4z_0^2} \tag{4.11}$$

is met. We will assume for now that this is the case.

Let us look first at the solution around z_2, the turning point which lies deep within the linear polytrope model, at large z. We shall call this solution Q_2. The turning point will exist at the depth at which approximately

$$\frac{\omega^2}{k_x^2 c_{0L}^2} \frac{1}{1+z/z_0} = 1, \tag{4.12}$$

so let us form the transformed variable s_2 defined through

$$\frac{\omega^2}{k_x^2 c_{0L}^2} \frac{1}{1+z/z_0} = \frac{1}{s_2}. \tag{4.13}$$

Near the turning point the variable s_2 will then be of order 1, which will help us to pick out the dominant terms in κ^2. In terms of s_2 the differential equation (4.9) becomes

$$\frac{d^2Q_2}{ds_2^2} + \left[m^2\Omega^4\left(\frac{1}{s_2}-1\right) - \frac{m(m+2)}{4}\frac{1}{s_2^2}\right] Q = 0, \tag{4.14}$$

where $\Omega^2 = \omega^2/gk_x$. We have already seen the approximate result that for a p-mode of order n,

$$\Omega^2 = 1 + \frac{2n}{m}, \tag{4.15}$$

so for modes of large order we can ensure that the quantity $m^2\Omega^4$ is large. The quantity $m(m+2)/4$, on the other hand, will always be of order 1. Thus we have the formal situation described in equation (3.1) involving a 'large parameter' λ, given here by $\lambda^2 = m^2\Omega^4$. As a consequence of this we may neglect the smaller order term in equation (4.14). Transforming back into z then gives the differential equation

$$\frac{d^2Q_2}{dz^2} + \kappa_2^2(z)Q = 0, \tag{4.16}$$

where

$$\kappa_2^2 = k_x^2\left\{\frac{\omega^2}{k_x^2 c_{0L}^2}\frac{1}{1+z/z_0} - 1\right\}.$$

The Langer solution to the differential equation (4.16) is then

$$Q_2(z) \sim \left[-\frac{t_2(z)}{\kappa_2^2(z)}\right]^{1/4} \{c_3\mathrm{Ai}(t_2) + c_4\mathrm{Bi}(t_2)\}, \tag{4.17}$$

where

$$\frac{2}{3}[t_2(z)]^{3/2} = \int_{z_1}^{z} [-\kappa_2^2(w)]^{1/2}\, dw.$$

We now apply our condition that as $z \to \infty$, we require that the Q_2 solution be evanescent. As before, this implies that the coefficient of the Bi solution must be zero, so we set $c_4 = 0$. Thus

$$Q_2(z) \sim c_3 \left[-\frac{t_2(z)}{\kappa_2^2(z)}\right]^{1/4} \mathrm{Ai}(t_2). \tag{4.18}$$

This solution will be an accurate representation of the exact solution for modes such that $m^2\Omega^4$ is large.

Let us now turn to Q_1, the solution around z_1, the turning point nearer $z = 0$. Here we can introduce the variable

$$s_1 = 1 + z/z_0,$$

and s_1 will be of order 1 near the turning point. Our differential equation (4.9) becomes

$$\frac{d^2Q}{ds_1^2} + k_x^2 z_0^2 \left\{ \frac{\omega^2}{k_x^2 c_{0L}^2} \frac{1}{s_1} - \frac{m(m+2)}{4k_x^2 z_0^2} \frac{1}{s_1^2} - 1 \right\} Q = 0. \tag{4.19}$$

Since $\omega^2/k_x^2 c_{0L}^2 \gg 1$ and $k_x^2 z_0^2 \ll 1$ for the ranges of frequency and horizontal wavelength we shall be considering, the first two terms in equation (4.19) will dominate the third term, which we thus neglect. We can then proceed as before, taking the first two terms only as our approximation for κ^2. However, these terms are not large in the same way as the dominant terms in the differential equation around z_2, and thus our Langer solution around z_1 will not be as accurate as that around z_2. This reflects the fact that κ^2 changes much more rapidly near $z = 0$ than it does for large z. We must recognise that this will be the major source of error in this approximation.

Our differential equation around z_1 is thus taken to be

$$\frac{d^2Q_1}{dz^2} + \kappa_1^2(z) Q_1 = 0, \tag{4.20}$$

where

$$\kappa_1^2 = k_x^2 \left\{ \frac{\omega^2}{k_x^2 c_{0L}^2} \frac{1}{1 + z/z_0} - \frac{m(m+2)}{4k_x^2 z_0^2} \frac{1}{(1 + z/z_0)^2} \right\},$$

and our solution is given by

$$Q_1 \sim \left[-\frac{t_1(z)}{\kappa_1^2(z)}\right]^{1/4} \{c_1 \mathrm{Ai}(t_1) + c_2 \mathrm{Bi}(t_1)\}, \tag{4.21}$$

where

$$\frac{2}{3} [t_1(z)]^{3/2} = \int_z^{z_1} [-\kappa_1^2(w)]^{1/2} \, dw. \tag{4.22}$$

We now have our two Langer solutions, Q_1 and Q_2. We proceed to match these two solutions by their asymptotic expansions, precisely as described in section 4.2.1. The only complication is that since we have approximated κ^2 by κ_1^2 and κ_2^2 around z_1 and z_2, respectively, we must ensure that in the region where we match the two solutions, $\kappa_1^2 \sim \kappa_2^2$. This will be true in a region where the first term in κ^2 dominates both the other terms. For such a region to exist, we require that

$$\Omega^2 \gg \frac{1}{2}\sqrt{1+2/m}.$$

This is satisfied for all modes other than those with very low n.

Matching the two solutions then gives the condition that

$$\int_{z_1}^{z_2} \kappa(z)\, dz \sim (n - \frac{1}{2})\pi - \phi, \tag{4.23}$$

where $\tan\phi = c_2/c_1$. This is the modified Bohr-Sommerfeld condition.

The evaluation of the integral in equation (4.23) proceeds as described in section 1.4.4. The resulting dispersion relation is

$$\Omega^2 \sim -\frac{1}{m} + \left(1 + \frac{2}{m}\right)^{1/2} + \frac{2n}{m} - \frac{2\phi}{m\pi}. \tag{4.24}$$

This is very similar to the dispersion relation gained from the standard Bohr-Sommerfeld condition in section 1.4.4, the only difference involving our phase term ϕ. It is through this term that the effect of the chromosphere will express itself, as we shall now see.

4.2.3 Evaluation of ϕ

We have seen that Q_1, the general Langer solution around the turning point z_1, takes the form

$$Q_1 \sim \left[-\frac{t_1(z)}{\kappa_1^2(z)}\right]^{1/4} \{c_1 \mathrm{Ai}(t_1) + c_2 \mathrm{Bi}(t_1)\},$$

where

$$\frac{2}{3}\,[t_1(z)]^{3/2} = \int_z^{z_1} [-\kappa_1^2(w)]^{1/2}\, dw.$$

For $z < z_1$, t_1 will be positive and will increase as we move away from the turning point towards $z = 0$. The functions $\mathrm{Ai}(t_1)$ and $\mathrm{Bi}(t_1)$ will then display the behaviour shown in Figures 3.4 and 3.5: the Ai solution will decay exponentially with t_1, while the Bi solution will grow exponentially. In the derivation of the standard Bohr-Sommerfeld condition,

our condition on Q_1 was that as z becomes large and negative, so that t_1 became large and positive, Q_1 must be evanescent; thus the Bi solution must be excluded, requiring that $c_2 = 0$. In the terms of the modified Bohr-Sommerfeld condition, the condition of evanescence of Q_1 at large t_1 also implies $c_2 = 0$ and thus $\phi = 0$, returning us to the original Bohr-Sommerfeld condition.

However, we now wish to apply a different condition on the Q_1 solution. We place an interface at $z = 0$, and state that above this interface lies an as yet unspecified chromosphere. In principle, we can calculate the value of the quantity v_z/p_{Lt} immediately above the interface for any chosen model. Since v_z, the vertical component of velocity, and p_{Lt}, the partial time derivative of the Lagrangian pressure perturbation, are both continuous across an interface, so too is their ratio. Thus, given a chromospheric solution of any sort, we can find a condition which the Q_1 solution must satisfy. The matching of Q_1 to this condition will demand a particular combination of the Ai and Bi functions which comprise the Q_1 solution. In other words, the interface condition picks the relative values of c_1 and c_2, and thus the value of the phase ϕ.

For example, an interface condition which constrained the Q_1 solution to being very close to evanescent at $z = 0$ would give a small value of c_2 relative to c_1, and thus a small value of ϕ. An interface condition which implied that the Q_1 solution departed significantly from evanescent behaviour at $z = 0$ would give a larger relative value of c_2, and thus a larger value of ϕ.

We carry out this process as follows. Let us introduce the quantity Δ, defined by

$$\Delta = \left.\frac{v_z}{p_{Lt}}\right|_{z=0-} . \tag{4.25}$$

The quantity Δ will be calculated (by whatever means) for whatever chromospheric atmosphere is to be considered. By considerations of continuity across the interface, $z = 0$, we can then say that

$$\left.\frac{v_z}{p_{Lt}}\right|_{z=0+} = \Delta.$$

We now wish to relate the function $Q = \rho^{1/2} c_s^2 \nabla . \boldsymbol{v}$ to the function v_z/p_{Lt}. Recalling (see section 1.5.1) that *in the absence of a magnetic field*, the time derivative of the Lagrangian pressure perturbation is given by

$$p_{Lt} = -\rho_0 c_s^2 \nabla . \boldsymbol{v},$$

we find that Q, v_z and p_{Lt} are related by

$$\frac{Q'(z)}{Q(z)} = \left[-\frac{1}{2}\frac{\rho_0'}{\rho_0} + \frac{gk_x^2}{\omega^2}\right] + \frac{\rho_0}{\omega^2}\left[\omega^4 - g^2k_x^2\right]\frac{v_z(z)}{p_{Lt}(z)}. \tag{4.26}$$

Now $\Delta = v_z/p_{Lt}$ at $z = 0^+$; so evaluation of equation (4.26) at $z = 0^+$ gives

$$\left.\frac{Q'}{Q}\right|_{z=0+} = A + C\Delta, \tag{4.27}$$

where A and C are given by

$$A = -\frac{m}{2z_0} + \frac{gk_x^2}{z_0}$$

and

$$C = \frac{\rho_{0L}}{\omega^2}[\omega^4 - g^2k_x^2].$$

Thus, given the value of Δ, we can calculate the value of the quantity Q'/Q at $z = 0^+$.

Let us now return to the general form of our Langer solution for Q_1, and derive the functional form of Q_1'/Q_1. We will eventually equate the value of this function at $z = 0^+$ with the value of Q'/Q given by equation (4.27). We have

$$Q_1 = c_1\left[-\frac{t_1(z)}{\kappa_1^2(z)}\right]^{1/4}\left[\mathrm{Ai}(t_1) + \tan\phi\,\mathrm{Bi}(t_1)\right], \tag{4.28}$$

from which we find that

$$\frac{Q_1'}{Q_1} = -\frac{1}{4t_1}\left[-\frac{\kappa_1^2}{t_1}\right]^{1/2} - \frac{1}{4}\frac{(\kappa_1^2)'}{\kappa_1^2} - \left[-\frac{\kappa_1^2}{t_1}\right]^{1/2}\frac{\mathrm{Ai}'(t_1) + \tan\phi\,\mathrm{Bi}'(t_1)}{\mathrm{Ai}(t_1) + \tan\phi\,\mathrm{Bi}(t_1)}. \tag{4.29}$$

This then is the functional form of Q_1'/Q_1 from our Langer solution. Evaluating this at $z = 0^+$ then gives the expression

$$\left.\frac{Q_1'}{Q_1}\right|_{z=0+} = -\frac{1}{4t_1(0)}\left[-\frac{\kappa_1^2(0)}{t_1(0)}\right]^{1/2} - \frac{1}{4}\frac{[\kappa_1^2(0)]'}{\kappa_1^2(0)} - \left[-\frac{\kappa_1^2(0)}{t_1(0)}\right]^{1/2}\frac{\mathrm{Ai}'[t_1(0)] + \tan\phi\,\mathrm{Bi}'[t_1(0)]}{\mathrm{Ai}[t_1(0)] + \tan\phi\,\mathrm{Bi}[t_1(0)]}. \tag{4.30}$$

We now match at $z = 0^+$ the value of Q_1'/Q_1 formed from our Langer solution with the value of Q'/Q imposed by the interface condition (4.27):

$$A + C\Delta = -\frac{1}{4t_1(0)}\left[-\frac{\kappa_1^2(0)}{t_1(0)}\right]^{1/2} - \frac{1}{4}\frac{\kappa_1^{2\prime}(0)}{\kappa_1^2(0)} - \left[-\frac{\kappa_1^2(0)}{t_1(0)}\right]^{1/2}\frac{\mathrm{Ai}'[t_1(0)] + \tan\phi\,\mathrm{Bi}'[t_1(0)]}{\mathrm{Ai}[t_1(0)] + \tan\phi\,\mathrm{Bi}[t_1(0)]}. \tag{4.31}$$

Introduce the quantity $X(0)$ by

$$X(0) = A + C\Delta + \frac{1}{4t_1(0)}\left[-\frac{\kappa_1^2(0)}{t_1(0)}\right]^{1/2} + \frac{1}{4}\frac{(\kappa_1^2)'(0)}{\kappa_1^2(0)}. \tag{4.32}$$

Then (4.31) becomes

$$X(0) = -\left[-\frac{\kappa^2(0)}{t_1(0)}\right]^{1/2} \frac{\mathrm{Ai}'[t_1(0)] + \tan\phi\,\mathrm{Bi}'[t_1(0)]}{\mathrm{Ai}[t_1(0)] + \tan\phi\,\mathrm{Bi}[t_1(0)]}, \tag{4.33}$$

which we may rearrange into the form

$$\tan\phi = -\frac{X(0)\mathrm{Ai}[t_1(0)] + \left[-\frac{\kappa_1^2(0)}{t_1(0)}\right]^{1/2} \mathrm{Ai}'[t_1(0)]}{X(0)\mathrm{Bi}[t_1(0)] + \left[-\frac{\kappa_1^2(0)}{t_1(0)}\right]^{1/2} \mathrm{Bi}'[t_1(0)]}. \tag{4.34}$$

This is the desired result for the phase angle ϕ.

Thus, in summary, we have the following formulation for out problem. Given Δ, calculated from a model of the chromosphere, we can use the modified Bohr-Sommerfeld condition, equation (4.23), with the phase ϕ evaluated from equation (4.34). In equation (4.34), the value of $X(0)$ depends on the value of Δ, and the value of $t_1(0)$ can be calculated from the general expression for t_1 given in equation (4.22).

We now look briefly at the possible ways of adapting this approach to deal with the situation where only one turning point exists in $z > 0$.

4.2.4 One turning point problem

The two turning point problem described above will be applicable for modes of sufficiently low frequency that $\kappa^2(0^+) < 0$, as demanded by condition (4.11). However, there may well be modes for which $\kappa^2(0^+)$ is positive, but for which wave motions are still evanescent in the chromosphere. Can we formulate a procedure for dealing with these modes?

Let us first attempt to formulate another modified Bohr-Sommerfeld condition particular to this case. We can do this by considering only the solution around the turning point z_2, and matching this solution to our interface condition. We have

$$Q_2(z) = c_3\left[-\frac{t_2(z)}{\kappa^2(z)}\right]^{1/4} \mathrm{Ai}(t_2). \tag{4.35}$$

Assuming that the interface $z = 0$ lies in the region for which the asymptotic expansion for Ai at large and negative t_2 is valid, we have

$$Q_2 = \frac{c_3}{\sqrt{\pi}}\left[\frac{1}{\kappa^2(z)}\right]^{1/4} \sin\left[\int_z^{z_2} \kappa(w)\,dw + \frac{\pi}{4}\right], \tag{4.36}$$

from which we find that

$$\frac{Q_2'}{Q_2} = -\kappa(z)\cot\left[\int_z^{z_2}\kappa(w)\,dw + \frac{\pi}{4}\right]. \tag{4.37}$$

A similar matching procedure to that carried out above then gives

$$A + C\Delta = -\kappa(0)\cot\left[\int_0^{z_2}\kappa(w)\,dw + \frac{\pi}{4}\right], \tag{4.38}$$

which may be rearranged to give

$$\int_0^{z_2}\kappa(w)\,dw = (n+\frac{3}{4})\pi - \tan^{-1}\left[\frac{\kappa(0)}{A+C\Delta}\right]. \tag{4.39}$$

Thus we can derive a modified Bohr-Sommerfeld condition for this particular situation. However, preliminary numerical investigations cast doubt on the accuracy of this formulation, especially when considering modes for which $\kappa^2(0^+)$ was close to zero. This is because the κ^2 profile is sensitive to the cut-off term near $z = 0$, even if that effect is not sufficient to reduce κ^2 to zero. Also, recall that in the process of deriving the general Langer solution we found that such a solution is not valid near a turning point other than the one for which the solution was obtained (section 3.2). The consequence of this is that near $z = 0$, the Q_2 solution does not give an accurate representation of the exact solution, and so applying the interface condition directly to the Q_2 solution does not yield an accurate evaluation of the modes. The one turning point problem described here could, however, be applicable for very high frequency modes where the effect of the cut-off term is less significant.

It is desirable, then, to form a separate Langer solution near $z = 0$, as done in the two turning point problem. Such a solution would give a more accurate approximation to the exact solution in this region. Then we could match this solution to the interface condition as before, except that in this case $z = 0$ would lie in the region in where t_1 is negative. We can form such a solution by constructing an extension to the linear polytrope model as shown in Figure 4.3.

We extend the linear temperature profile so that $T = T_0(1 + z/z_0)$ for $z \geq -z_0$, so that $T = 0$ at $z = -z_0$. Then for all frequencies for which $\kappa^2(0^+) > 0$, we are guaranteed to find a turning point in $(-z_0, 0)$. We can construct a Langer solution around this turning point, and then match that solution evaluated at $z = 0$ to the interface condition. Now, our application of the interface condition to the Q_1 solution in section 4.2.3 made no assumptions about where the turning point lay, so we can use precisely this formulation, allowing only

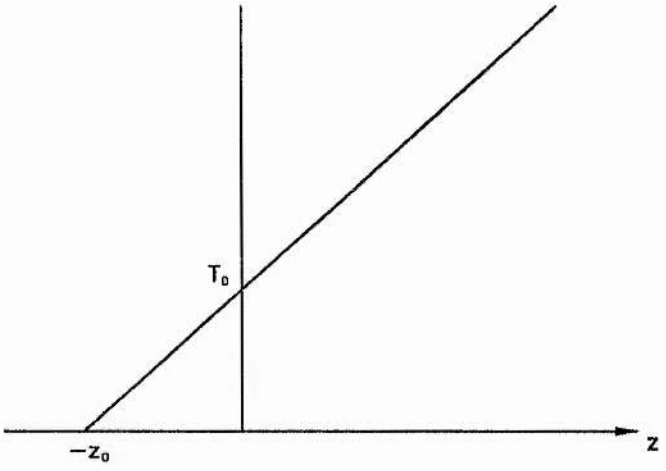

Figure 4.3: Temperature profile for one turning point problem

for the fact that $t_1(0)$ will be negative in this case. It proves convenient to rewrite the definition of $t_1(z)$, given in equation (4.22), in the form

$$\frac{2}{3}\left[-t_1(z)\right]^{3/2} = \int_{z_1}^{z} \kappa_1(w)\, dw.$$

Thus we have extended the approach given in sections 4.2.2 and 4.2.3 to include the one turning point problem described here.

As a final point, we have defined $t_1(z)$ in terms of integrals of κ_1^2, the leading order form of κ^2. However, since we can also analytically integrate the full κ^2 (see Appendix A), it makes sense to use the full κ^2 to avoid any unnecessary approximation.

This completes our description of the derivation of the modified Bohr-Sommerfeld condition and its general application to the problem of p-modes.

4.2.5 Summary of method

The method we have formulated is as follows. Our approximate eigenvalue condition for an oscillation representing a p-mode is

$$\int_{z_1}^{z_2} \kappa(w)\, dw = (n - \frac{1}{2})\pi - \phi, \tag{4.40}$$

where z_1 and z_2 are the zeros of $\kappa^2(z)$, n is the order of the mode and ϕ is a phase shift associated with the effect of the chromospheric interface. We take $\kappa^2(z)$ in the form given

by the linear polytrope model, as shown in equation (4.10), but in general κ^2 may be of any form satisfying the canonical equation (3.1) in the absence of a magnetic field. We evaluate ϕ through the expression

$$\tan\phi = -\frac{X(0)\mathrm{Ai}[t_1(0)] + \left[-\frac{\kappa_1^2(0)}{t_1(0)}\right]^{1/2}\mathrm{Ai}'[t_1(0)]}{X(0)\mathrm{Bi}[t_1(0)] + \left[-\frac{\kappa_1^2(0)}{t_1(0)}\right]^{1/2}\mathrm{Bi}'[t_1(0)]}. \tag{4.41}$$

where Δ, defined by

$$\Delta = \left.\frac{v_z}{p_{Lt}}\right|_{z=0^-}, \tag{4.42}$$

must be calculated for the particular chromospheric model chosen. In general, Δ will be a function of frequency, and so equations (4.40), (4.41) and (4.42) will form an implicit system; thus some form of iteration will be required to find the mode frequency. The quantity $t_1(0)$ is calculated from

$$\frac{2}{3}[t_1(0)]^{3/2} = \int_0^{z_1}[-\kappa_1^2(w)]^{1/2}\,dw, \qquad z_1 > 0, \tag{4.43}$$

$$\frac{2}{3}[-t_1(0)]^{3/2} = \int_{z_1}^{0}\kappa_1(w)\,dw, \qquad z_1 < 0. \tag{4.44}$$

The evaluation of these integrals is described in Appendix A.

4.3 Evaluation of the modified Bohr-Sommerfeld condition

We now look at the application of this method to p-modes for two simple chromospheric models, to evaluate its accuracy by comparison with exact results for the same models.

4.3.1 Isothermal non-magnetic chromospheric model

We look first at the chromospheric model described in section 1.5.2. For this model, v_z and $\nabla.\boldsymbol{v}$ are given by equations (1.83) and (1.82) respectively, so we can calculate that Δ, the value of v_z/p_{Lt} at $z = 0^-$, by

$$\Delta = \frac{\omega^2\left[\sqrt{-\kappa_0^2} + \gamma g/2c_0^2 - gk_x^2/\omega^2\right]}{\rho_{00}(\omega^4 - g^2k_x^2)}, \tag{4.45}$$

for given ω, k_x and c_0^2. The value of ρ_{00}, the equilibrium density at $z = 0^-$, is calculated from the condition of continuity of equilibrium pressure across the interface. We specify

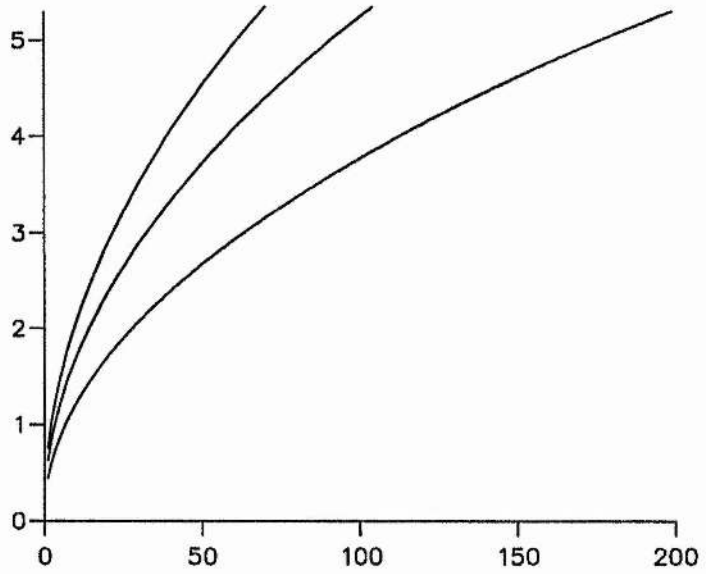

Figure 4.4: Mode frequency (in mHz) vs. degree l, calculated from the modified Bohr-Sommerfeld condition. Modes considered are of order n=10 (lowest curve), 20 and 30; the chromosphere is non-magnetic, and at a temperature of 4170K.

$p_0(0^+)$, the equilibrium gas pressure at $z = 0^+$, which in this non-magnetic case must be equal to the equilibrium gas pressure at $z = 0^-$. We can then find the value of ρ_{00} from the equation

$$c_0^2 = \frac{\gamma p_0(0^-)}{\rho_{00}}.$$

We can then tie equation (4.45) to our modified Bohr-Sommerfeld condition (4.40) through an iterative scheme to calculate the frequency of a mode of given order n. Figure 4.4 shows curves of frequency against degree l for modes of orders 10, 20 and 30; individual modes will of course be distinct points on these curves. Once again we see the distinctive parabolic form of p-modes.

Let us now examine the accuracy of the method as follows. We are using the same model as for the exact solution, so the most we can hope to achieve in our approximation for this case is to accurately reproduce the exact results. Figure 4.5 shows the fractional error in our results, defined by

$$\epsilon = \frac{|\nu_{WKB} - \nu_{exact}|}{\nu_{exact}},$$

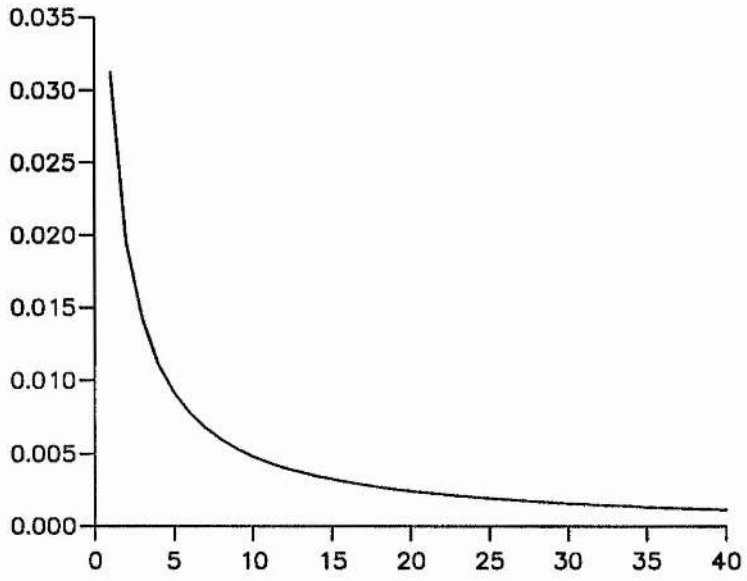

Figure 4.5: Fractional error in mode frequency vs. order n for modes of degree 50.

for modes of degree 50 with varying order n. We see that our approximate method yields frequencies accurate to better than 0.5% for modes of order greater than 10.

The error in frequency at around 5mHz is about 6μHz. This is larger than the frequency shifts in which we are interested, but this does not mean that we are unable to study frequency shifts with this method. A change in chromospheric conditions will result in a change in the error, ϵ, and it is this change in ϵ which will have to be smaller than the frequency shifts we are interested in if the use of our method is to be justifiable. Since for this reason it is impossible to quantify the errors in the frequency shifts, we must evaluate the accuracy of our method for such curves by direct comparison with exact frequency shift curves. We do this for this model by generating frequency shifts through a change in chromospheric temperature, from 4170K to 4400K. Figure 4.6 shows the frequency shifts generated in $l = 50$ modes for the exact dispersion relation (dotted line) and for our approximate method (solid line). We see again that our method gives a good approximation to the exact situation. The trend in the exact results is faithfully recreated, and the actual magnitudes of frequency shift found are reproduced to within 0.1μHz.

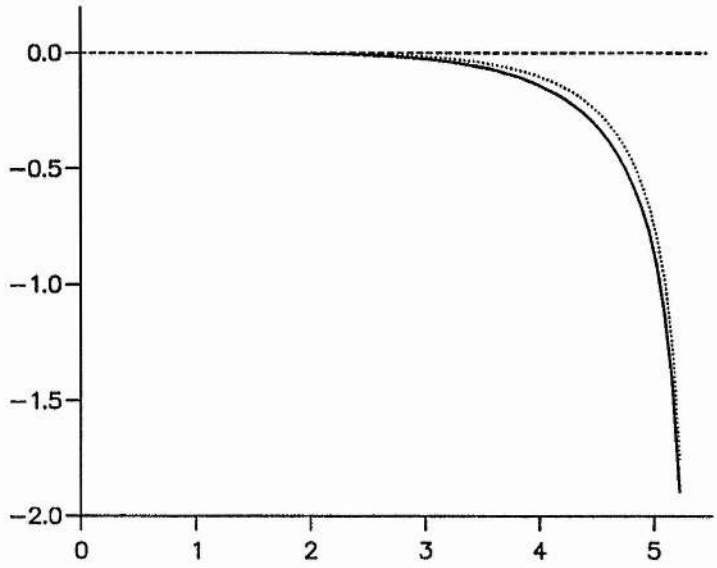

Figure 4.6: Frequency shift (in μHz) vs. original frequency (in mHz) induced by an increase in chromospheric temperature from 4170K to 4400K, for modes of degree 50 and varying order n. The solid curve depicts frequency shifts calculated from the modified Bohr-Sommerfeld condition, the dotted curve those calculated from the exact dispersion relation (Campbell and Roberts, 1989).

4.3.2 Isothermal model with uniform magnetic field

We now look at the isothermal chromospheric model with a uniform magnetic field, as described in section 1.5.3. The exact results for this model (Evans and Roberts, 1990; Jain and Roberts, 1993) are discussed in sections 3.1 and 4.1; this model gives turnover, as discussed in section 3.7.

For this model we turn to a numerical solution in the chromosphere. The starting point is the asymptotic behaviour of the wave equation as $z \to -\infty$. Our wave equation is as given in equation (1.89), so the asymptotic form of this equation as $z \to -\infty$ is

$$\frac{d^2 v_z}{dz^2} - k_x^2 v_z = 0. \tag{4.46}$$

The exponentially decaying asymptotic solution to our wave equation is thus

$$v_z = c_3 \exp(k_x z), \qquad z < 0. \tag{4.47}$$

We first consider a point in the chromospheric model at sufficiently large and negative z that this asymptotic solution is accurate. We then integrate the full equation (1.89) down through the chromospheric model, using a 4th-order Runge-Kutta method (Abramovitz and Stegun, 1967: 25.5.10). We thus find the values of v_z and its derivative at each of the chosen number of grid points, and ultimately at $z = 0^-$. From these values we can also calculate the value of $\nabla.\boldsymbol{v}$ immediately above the interface, and thus the value of Δ. Since the definition of Δ involves the ratio of v_z and $\nabla.\boldsymbol{v}$, the arbitrary constant c_3 will not affect its value. In general, however, Δ will be a function of frequency, and so some iteration will be required between our numerical scheme and the eigenvalue condition (4.40). Note also that there is no upper limit on frequency in this problem, so no cut-off effect will be present.

We again calculate the value of ρ_{00} by considering the continuity of the equilibrium total pressure across $z = 0$. We specify the value of p_0 at $z = 0^+$; this must then be equal to the equilibrium total pressure, $p_0 + B_0^2/2\mu_0$, at $z = 0_-$. For a chosen field strength B_0, we can then calculate $p_0(0^-)$ and thus ρ_{00} and thus v_0, the Alfvén speed at the base of the chromosphere.

Mode frequencies calculated by this method again show the parabolic form of Figure 4.4, and the fractional error curve is virtually identical to that shown in Figure 4.5.

Once again, we can also investigate the accuracy of our method in generating frequency shifts. Figure 4.7 shows the effect of increasing the magnetic field from 10G to 30G; the dotted line again represents the exact results, while the solid line depicts results derived from our approximate method. Again the two curves are in good agreement.

Figure 4.8 shows the effect of increasing the magnetic field from 40G to 50G while also increasing the chromospheric temperature from 4170K to a) 5000K and b) 6000K. We see that the trend in the exact results is again reproduced, and that the magnitudes of the frequency shifts are again close to those found by the exact method. The accuracy appears to be least good in the curves of Figure 4.8, and particularly in the case of curve b). This effect is due to the fact that, in curve b), the largest shifts are not for modes of the highest order. The larger errors at these lower orders are thus stressed by the form of the turnover curve. The magnitudes of these errors are still less than around 50nHz, however.

Thus we can summarise the accuracy of our method as follows. The trend in the exact frequency shift data is reproduced in all cases, although there is a tendency for our method to over-estimate the frequency shifts induced. We believe that this error has been introduced by the less accurate approximation to the solution of the wave equation near

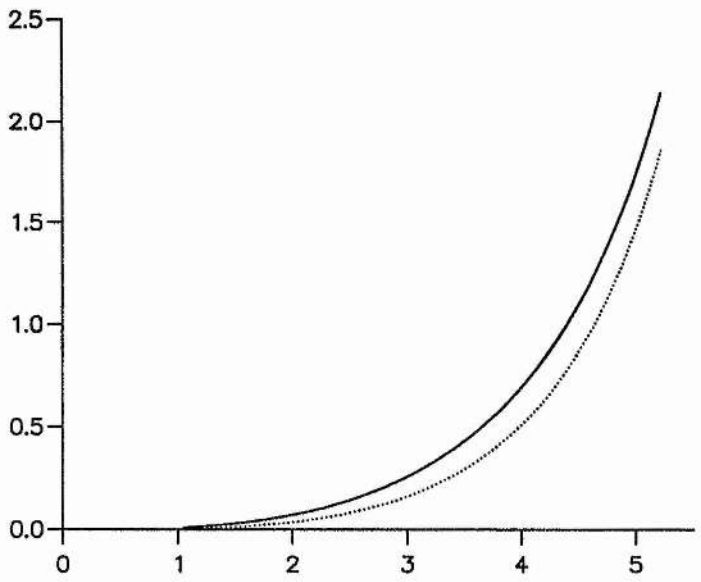

Figure 4.7: Frequency shift (in μHz) vs. original frequency (in mHz) induced by an increase in magnetic field strength from 10G to 30G in an isothermal chromosphere at a temperature of 4170K. The solid curve depicts the approximate results, the dotted curve the exact results (Evans and Roberts, 1991).

$z = 0$. However, we can be reasonably confident that the form of frequency shifts gained from our approximate method for a general chromospheric model will accurately represent the *form* of such a curve gained from an exact treatment of the same problem.

We are now in a position to investigate the effect of some of the features in the chromospheric temperature profile introduced in section 4.1.

4.4 Effect of temperature gradients

4.4.1 Low chromosphere temperature gradients

Let us consider first the gradual rise in temperature present in the lowest region of the chromospheric model of Ulrich (1993). In Ulrich's model, the temperature rises from 4150K at the temperature minimum to 6000K at a height of around 500km. In what follows, we express temperature gradients in the units Kelvin per Megametre (KMm^{-1}); this rise

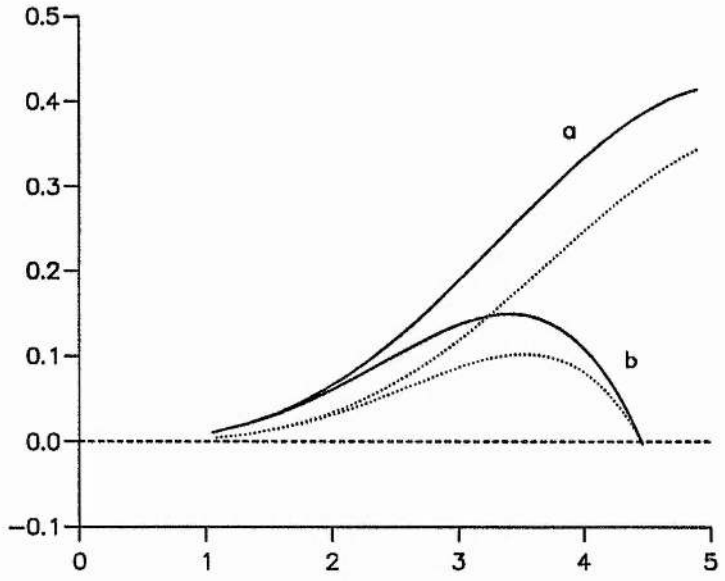

Figure 4.8: Frequency shift (in μHz) vs. original frequency (in mHz) induced by an increase in magnetic field strength from 40G to 50G and an increase in chromospheric temperature from 4170K to a) 5000K and b) 6000K. Solid curves depict approximate results, dotted curves exact results (Evans and Roberts, 1991).

in temperature corresponds to a gradient of 3700KMm^{-1}. How does such a chromospheric temperature profile affect the mode frequencies? How does the presence of a temperature gradient modify the effects of changing the magnetic field strength and base temperature? And, finally, how significant an effect can be caused by a change in such a gradient?

We attempt to answer these questions by setting up the following chromospheric model. We specify the temperature to be given by

$$T = T_c - T'z, \qquad z < 0, \tag{4.48}$$

where T_c is the temperature at the base of the chromospheric model and T' is the temperature gradient. Thus the temperature increases linearly with height in the model. The sound speed in the model is thus given by

$$c_s^2 = c_0^2(1 - z/z_h), \qquad z < 0, \tag{4.49}$$

where c_0, the sound speed at the base of the model, is given by $c_0^2 = \gamma R T_c$, and z_h, the

scale height for this model, is given by

$$z_h = \frac{c_0^2}{\gamma R T'}. \tag{4.50}$$

The magnetic field is again taken to be uniform and horizontal. Our general equilibrium equation (1.7) then gives the density and Alfvén speed variations in the model:

$$\rho_0 = \rho_{00}(1 - z/z_h)^{-(m_c+1)} \tag{4.51}$$

and

$$v_A^2 = v_0^2(1 - z/z_h)^{m_c+1}. \tag{4.52}$$

Here ρ_{00} and v_0 are the values of the equilibrium density and Alfvén speed, respectively, at the base of the model, and the parameter m_c is defined by

$$m_c = \frac{\gamma g z_h}{c_0^2}. \tag{4.53}$$

Note also that since

$$\lim_{y\to\infty}(1 + a/y)^y = e^a, \tag{4.54}$$

in the limit $z_h \to \infty$ the expression (4.51) for the equilibrium density becomes the same as for the isothermal model.

For this profile, the asymptotic form of the wave equation (1.89) will be the same as that given in equation (4.46). Thus our numerical solution in the chromosphere will proceed as described in section 4.3.2. We can then invoke the modified Bohr-Sommerfeld condition, equation (4.40), to calculate mode frequencies for this choice of chromospheric model, and thus the frequency shifts induced by a change in the model. With so many parameters involved, there are obviously a number of degrees of freedom available to generate frequency shifts for this model. We can change T_c, the temperature at the base of the chromospheric model; we can change B_0, the strength of the magnetic field; and we can change T', the gradient of the temperature profile in the model. As the possibility exists for confusion to arise from this multiplicity of factors, we will attempt to deal with them one at a time.

Consider the effect on mode frequencies of **introducing a temperature gradient where previously none was present.** Our initial frequency is calculated for the isothermal limit of this profile, with a magnetic field of 10G and a base temperature of 4170K. We then introduce a temperature gradient, whose magnitude can be varied, keeping the base temperature and magnetic field unchanged, and compare the frequencies obtained

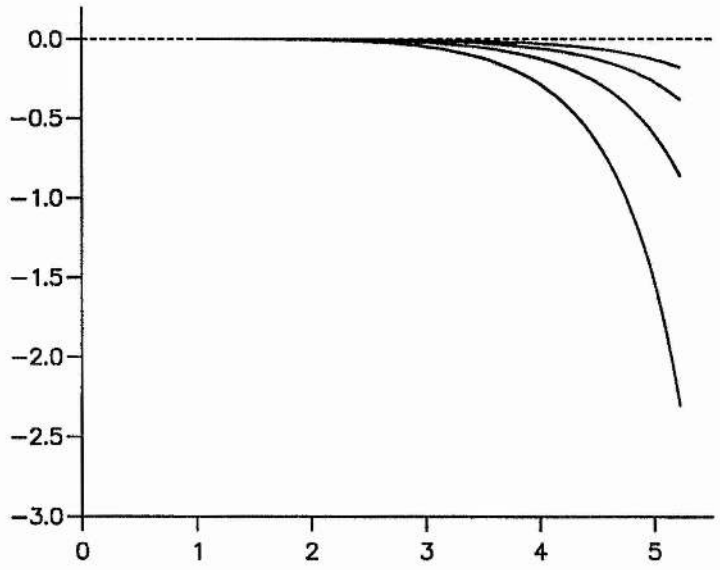

Figure 4.9: Frequency shift (in μHz) vs. original frequency (in mHz) induced by the introduction of a temperature gradient where previously none was present. Curves displayed are for a subsequent temperature gradient of 500 (smallest shifts), 1000, 2000 and 4000 KMm^{-1}. The base temperature is fixed at 4170K, the magnetic field strength at 10G.

with our isothermal results. Figure 4.9 shows the frequency shifts obtained by introducing a progressively steeper temperature gradient of 500, 1000, 2000 and 4000 Kelvin per megametre. We see that the general trend is to lower the mode frequencies, particularly at higher frequencies. Since what we are doing is raising the temperature for all points in the chromosphere, other than $z = 0$, it is not surprising that these results are similar in form to Figure 4.6 above.

As well as looking at the effect of introducing a temperature gradient, we can also examine how the presence of a temperature gradient modifies frequency shifts resulting from a change in base temperature and/or magnetic field. In this pursuit we are basically repeating the calculations of section 4.3.2 above, but with some kind of temperature gradient present.

Let us look at the effect of **increasing the base temperature, keeping the magnetic field and temperature gradient unaltered.** Figure 4.10 shows the result of changing the base temperature from 4170K to 4400K, with a magnetic field of 10G. The

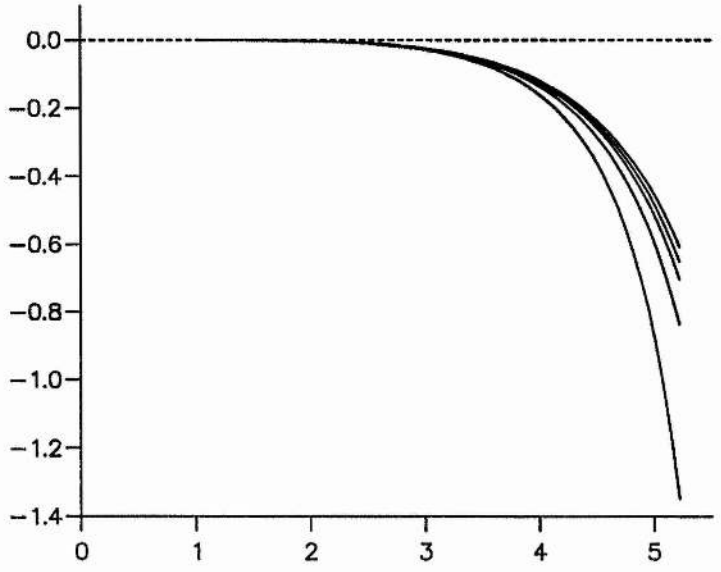

Figure 4.10: Frequency shift (in μHz) vs. original frequency (in mHz) induced by an increase in the base temperature from 4170K to 4400K, for a variety of fixed temperature gradients. Curves displayed are firstly for the isothermal limit (smallest shifts), then for temperature gradients of 500, 1000, 2000 and 4000KMm^{-1}. The magnetic field strength is held at 10G.

curves plotted are firstly for the isothermal limit, and then for temperature gradients of 500, 1000, 2000 and 4000 KMm^{-1}. We see that the higher the temperature gradient, the greater the negative frequency shift; the temperature gradient has the effect of emphasizing the frequency shift due to a change in base temperature.

We now turn to the effect of **increasing the magnetic field strength, keeping the base temperature and temperature gradient fixed**. Figure 4.11 shows the result of changing the magnetic field strength from 10G to 30G, with a base temperature of 4170K. The curves plotted are for the same temperature gradients as Figure 4.10. Again we see that the temperature gradient has the effect of emphasizing the frequency shift due to the change in magnetic field strength.

We can look at the effect of **increasing the magnetic field strength and the base temperature together, keeping the temperature gradient fixed**. Figure 4.12 shows the effect of changing the base temperature from 4170K to 5000K while the magnetic field strength is increased from 40G to 50G. The curves plotted here are for the isothermal

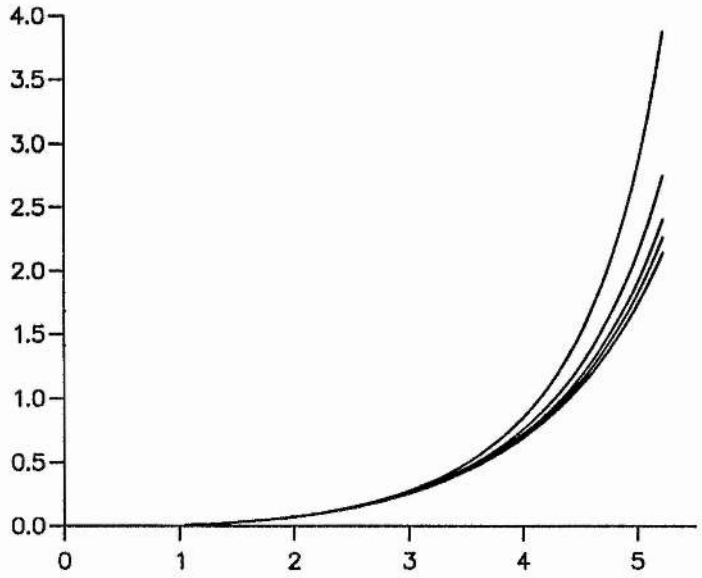

Figure 4.11: Frequency shift (in μHz) vs. original frequency (in mHz) induced by an increase in magnetic field strength from 10G to 30G, for a variety of temperature gradients. Curves diplayed are firstly for the isothermal limit (smallest shifts), then for temperature gradients of 500, 1000, 2000 and 4000KMm^{-1}. The base temperature is fixed at 4170K.

case and for temperature gradients of 1000, 4000, 7000 and 10000 KMm^{-1}. Figure 4.13 is calculated for the same change in magnetic field and the same temperature gradients, but with the base temperature now rising to 6000K. We see in Figure 4.12 that the temperature gradient again increases the magnitude of the frequency shift, although it does not assist the onset of 'turnover' in the $\Delta\nu$ curve. In Figure 4.13, however, the sharpness of the turnover is increased by strong temperature gradients, since the dominant effect at high frequencies is the negative shift associated with the increase in base temperature.

Finally, we can extend this approach further by allowing the temperature gradient to change *at the same time* as the base temperature and/or magnetic field strength change. We then have three degrees of freedom in the problem, and an endless variety of situations could be considered. We will attempt to consider only those which are relevant to our specific problem, that of turnover, and to Ulrich's chromospheric model.

We thus look at the turnover scenario shown in Figure 4.13, and examine the effect of **increasing the temperature gradient at the same time as the magnetic**

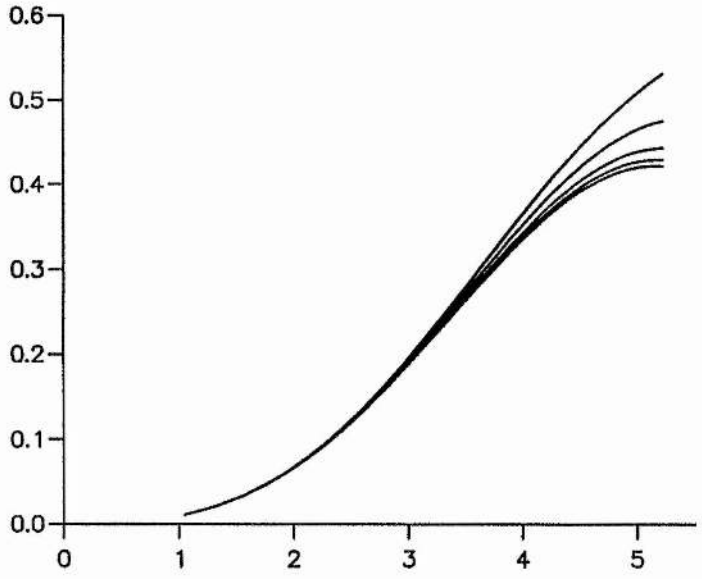

Figure 4.12: Frequency shift (in μHz) vs. original frequency (in mHz) induced by simultaneous increases in base temperature from 4170K to 5000K and in magnetic field strength from 40G to 50G, for a variety of temperature gradients. Curves displayed are for the isothermal limit (smallest shifts), then for temperature gradients of 1000, 4000, 7000 and 10000KMm^{-1}.

field strength and base temperature are being increased. Figure 4.14 shows the effect of increasing the magnetic field strength from 40G to 50G, the base temperature from 4170K to 5500K, and the temperature gradient from zero, the isothermal limit, to a higher value. The curves plotted are firstly for no change in temperature gradient, then for a subsequent temperature gradient of 500, 1000 and 2000KMm^{-1}. We see that the increase in temperature gradient has the effect of assisting the frequency shift turnover, without significantly reducing the peak frequency shift.

What conclusions can we draw from these various numerical experiments? We summarise these as follows.

1. The introduction of temperature gradients, such as those present in Ulrich's model, do have a significant effect on mode frequencies (Figure 4.9); increasing the temperature gradient has an effect that is similar to increasing the base temperature.

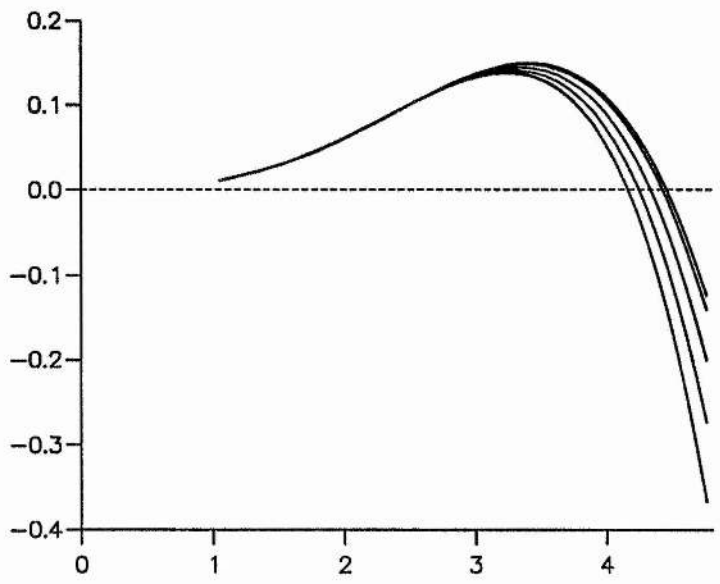

Figure 4.13: Frequency shift (in μHz) vs. original frequency (in mHz) induced by simultaneous increases in base temperature from 4170K to 6000K and in magnetic field strength from 40G to 50G, for a variety of temperature gradients. Curves displayed are for the isothermal limit (topmost curve), then for temperature gradients of 1000, 4000, 7000 and 10000KMm^{-1}.

2. The fundamental behaviour appears to be that a non-isothermal chromosphere has the effect of emphasizing any frequency shifts that are present in an isothermal model (Figures 4.10–4.12).

3. When turnover is present, the presence of a temperature gradient assists this effect (Figure 4.13). An increase in temperature gradient also strengthens the turnover effect (Figure 4.14).

What is the relevance of these conclusions to the solar problem? We have seen that studies of an isothermal chromosphere do not produce the precipitous drop in frequency shifts present in observations. It has been demonstrated here that the presence of temperature gradients has the effect of sharpening the turnover effect to a significant extent. An increase in the magnitude of the temperature gradient can also contribute to this effect.

Many different situations could now be considered in an attempt to match the

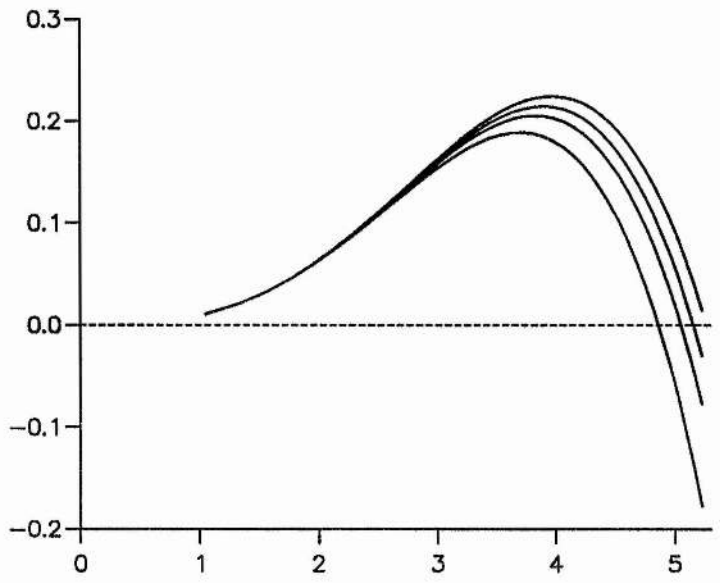

Figure 4.14: Frequency shift (in μHz) vs. original frequency (in mHz) induced by simultaneous increases in chromospheric base temperature from 4170K to 5500K and magnetic field strength from 40G to 50G, firstly for zero temperature gradient (topmost curve), then for an increase in the temperature gradient from zero to one of 500, 1000 and 2000KMm^{-1}.

observational data more exactly. We can consider many different changes of base temperature and magnetic field strength; for the linear temperature model, the behaviour for all such situations is consistent with that shown in Figures 4.10–4.14. A further study has been carried out featuring a model comprised of a linear temperature region topped by an isothermal region; the effects observed for this model turn out to be very similar to those found for the simple linear temperature model.

We now turn to the second temperature feature we wish to investigate, that of the steep rise in temperature in the high chromosphere.

4.4.2 High chromosphere temperature gradients

One of the most notable features of the solar chromosphere is the sharp rise in temperature at its upper boundary, around 2000km above the photosphere, where the chromosphere gives way to the transition region and the corona. This feature is depicted in

the numerical model of Ulrich shown in Figure 4.1. From around 2000km, the temperature rises to around 100 000K by a height of around 3000km, then rising even more steeply to a value of around 1 000 000K by a height of 4000km. The largest temperature gradients in these regions can thus be of the order of 1 000 000KMm^{-1}. These temperature gradients are far larger than those considered in section 4.4.1. The difference here, of course, is that the temperature does not rise at this rate immediately from the photosphere, but from a point some 2000km higher, which will greatly reduce its effect on modes resident in the solar interior.

We model this form of temperature variation as follows. We consider the low chromosphere to be isothermal, with the temperature then increasing linearly above a certain height. This variation is this described by

$$T = \begin{cases} T_c - T'(z+d), & z < -d, \\ T_c, & -d \leq z \leq 0, \end{cases} \tag{4.55}$$

where d is the height in the chromospheric model at which the temperature starts to rise. We again impose a uniform horizontal magnetic field of strength B_0, and calculate the density and Alfvén speed variations from the equilibrium equation (1.7).

To investigate these effects, it proves useful to consider the numerical value calculated for Δ. All that our eigenvalue condition (4.40) knows about the chromosphere is encapsulated in the value of Δ, so any change in the state of the chromosphere will affect mode frequencies through a change in the value of Δ. As a yardstick, for an isothermal chromosphere with a 10G magnetic field, changing the temperature from 4170K to 4400K alters the value of Δ from 3174.9m^{2}s^{2}kg^{-1} to 3119.9m^{2}s^{2}kg^{-1} for a frequency of 4.5mHz; this results in a frequency shift of around 0.3μHz.

Following the model of Ulrich, we first take d, the height at which the temperature starts to rise, as 2000km. We consider a base temperature of 4170K and a magnetic field of 10G. Table 4.1a shows the value of Δ firstly for the isothermal limit, $T' \to 0$, and then for various values of the temperature gradient. We see that even for a temperature gradient of 10^8KMm^{-1} there is no significant change in Δ; thus we would not expect frequencies calculated for such a chromosphere to differ significantly from those calculated for an isothermal chromosphere. Since 2000km corresponds to about 8 density scale heights, it is not surprising that a temperature rise so high in the chromosphere has no significant effect.

T' ($\mathrm{KMm^{-1}}$)	$\Delta(\mathrm{m^2s^2kg^{-1}})$
0	3174.91773
100 000	3174.91774
1 000 000	3174.91776
10 000 000	3174.91829
100 000 000	3174.91894

d (km)	$\Delta(\mathrm{m^2s^2kg^{-1}})$
∞	3174.91773
2000	3174.91776
1500	3174.92183
1000	3175.56485
500	3249.39749

Table 4.1: Variation of Δ with a) T' and b) h_c

The question, then, is how low does the base of the rise in temperature need to be to generate any effect? Table 4.1b shows the values of Δ calculated once again for the isothermal limit, $d \to \infty$, and then for various values of d. In each of these cases, the temperature gradient is taken as $10^6\mathrm{KMm^{-1}}$. We see that the base of the temperature rise must lie below 1000km if that feature is to have any effect on mode frequencies. As this is inconsistent with the model of Ulrich, and with the observed form of temperature variation in the solar chromosphere, we are left with the conclusion that the steep rise in temperature at the top of the chromosphere has no significant effect on mode frequencies.

4.4.3 Summary

In this sections we have studied the effect on frequency shift curves of chromospheric temperature gradients, in an attempt to find better agreement with the observed form of such curves. Simultaneously increasing the temperature and magnetic field strength of an isothermal chromosphere gives turnover, but as a gradual effect, rather than the observed precipitous drop in frequency shift. We have seen in this section that the presence of a temperature gradient in the lowest part of the chromosphere has the effect of 'sharpening' the turnover effect. An increase in chromospheric temperature gradient, along with increases in base temperature and magnetic field strength, further encourages this behaviour. Temperature gradients in the highest part of the chromosphere, however, have no significant effect.

Unlike Jain and Roberts (1993), we here make no attempt to match the observed data exactly, for the following reasons. Firstly, the results of Libbrecht and Woodard (1991) are averaged over a number of modes of varying degree and order; the result of this averaging is very sensitive to the particular set of modes chosen, and the precise method of averaging

used. Secondly, given the simplicity of our model, and the fact that an approximate method is used to calculate frequency shifts, it is unlikely that we could exactly reproduce the observed data. The best we can hope to achieve is to recreate the trend of the observed data, for example by producing a turnover curve. We can then investigate the effect on that form of some additional feature in the model; for example, that a chromospheric temperature gradient makes turnover occur more sharply.

4.5 Physical considerations

In the previous section we used the modified Bohr-Sommerfeld condition (4.40) to investigate a particular p-mode problem. However, in this investigation we were basically carrying out a numerical experiment, as we could have done to greater accuracy without ever deriving our condition. What then is the point of our condition?

What we hope to gain from our approach is a greater physical understanding of and insight into the various processes operating. The modified Bohr-Sommerfeld condition (4.40) is a compact result, with all the influence of the chromosphere contained in the single term ϕ; that term itself depends on the quantity Δ, which depends only on the physics of the chromosphere. We should, then, be able to separate out the physical effects operating in this problem, by studying the influence of the chromosphere on the value of Δ, and the influence of the value of Δ on the mode frequency. Carrying out this procedure should give us greater insight into the problem of chromospheric effects on p-mode frequencies; we would also hope to gain a simple physical picture of the workings of this problem, which could potentially be of more general interest in the field of helioseismology.

We look first at the relationship between Δ and ν, the frequency of an individual mode, and consider an analogous physical problem to inspect the physical processes at work.

4.5.1 Relationship between Δ and ν

We have seen in section 4.2.2 that a phase term ϕ, dependent on a quantity Δ provided by our chromospheric model, can modify mode frequencies through a form of the Bohr-Sommerfeld condition. An analogous physical problem is that of sound waves in a organ pipe. Such waves form normal modes at frequencies largely selected by the dimensions of the pipe. However, an additional phase term is introduced by the possibility of one end of the pipe being either open or closed. To illustrate this analogy, we set up a

much simplified system based on the p-mode problem, and examine the physics operating behind the selection of mode frequencies for such a system.

We consider again the wave equation (1.21) for v_z in a general plane-parallel atmosphere. To simplify the problem, we set both the magnetic field strength, B_0, and the gravitational acceleration, g, to zero, and also specify that the temperature is uniform throughout the atmosphere. We also restrict attention to waves which have no horizontal component of propagation, implying that k_x is identically zero. The wave equation for this situation is thus

$$\frac{d^2 v_z}{dz^2} + \frac{\omega^2}{c_I^2} v_z = 0, \tag{4.56}$$

where c_I is the isothermal sound speed throughout the atmosphere. The general solution of equation (4.56) is

$$v_z = a_0 \sin\left(\frac{\omega z}{c_I}\right) + b_0 \cos\left(\frac{\omega z}{c_I}\right). \tag{4.57}$$

We construct a model as follows. We place a solid wall at $z = L$, and consider the behaviour of wave motions in $[0, L]$, which we can consider to be our mode cavity for this problem. The solid wall at $z = L$ imposes the condition

$$v_z\Big|_{z=L} = 0. \tag{4.58}$$

We have a choice of conditions at $z = 0$; it is this choice which will determine the form of the eigenvalue condition for this problem. Firstly, let us consider the atmosphere to be 'closed' at $z = 0$, requiring that

$$v_z\Big|_{z=0} = 0. \tag{4.59}$$

The conditions (4.58) and (4.59) yield the eigenvalues

$$\frac{\omega L}{c_I} = n\pi, \tag{4.60}$$

where n is a positive integer describing the order of the mode.

We can also look at the behaviour when the atmosphere is 'open' at $z = 0$. In the case of a organ pipe, we would expect an open pipe to display a pressure node at $z = 0$, since the gas at that point should have the same unchanging value of pressure as the region unaffected by the wave motion. Thus to represent an open pipe our condition is that the Lagrangian pressure perturbation p_L is zero at $z = 0$. In this problem, $p_{Lt} = -\rho_0 c_I^2 \nabla . \boldsymbol{v}$

and $\nabla.\boldsymbol{v}$ is simply $\frac{dv_z}{dz}$, so our condition representing an 'open' atmosphere is simply

$$\left.\frac{dv_z}{dz}\right|_{z=0} = 0. \tag{4.61}$$

Conditions (4.58) and (4.61) give the eigenvalues

$$\frac{\omega L}{c_I} = (n - \frac{1}{2})\pi. \tag{4.62}$$

We can also look at a more general situation where we specify the value of v_z/p_{Lt} at $z = 0$; this value will fulfil the definition of Δ given in section 4.2.3. The condition at $z = 0$ will then be

$$-\left.\frac{1}{\rho_0 c_I^2}\frac{v_z}{dv_z/dz}\right|_{z=0} = \Delta. \tag{4.63}$$

Conditions (4.58) and (4.63) then give the eigenvalue equation

$$\frac{\omega L}{c_I} = n\pi + \tan^{-1}[\rho_0 c_I \omega L \Delta]. \tag{4.64}$$

This relation can reproduce either the 'closed' atmosphere ($\Delta \rightarrow 0$) result, or the 'open' atmosphere ($\Delta \rightarrow -\infty$) result.

Equation (4.64) is analogous to the modified Bohr-Sommerfeld condition (4.40), except that the $(n - \frac{1}{2})\pi$ in that result appears as $n\pi$ in this condition. This is because the Langer solution used in the derivation of the modified Bohr-Sommerfeld condition introduces a phase shift of $\pi/4$ at each turning point.

We now examine further the behaviour of equation (4.64). Figure 4.15 shows the variation of the mode frequency, calculated from equation (4.64), with Δ, for modes of order 10. All quantities are in non-dimensional units. We see that the mode frequency lies between two extremes, defined by the limiting values as $\Delta \rightarrow \pm\infty$.

Figure 4.16 shows the variation of v_z with z for the $n = 1$ mode, for Δ equal to -1, 0 and 1. We see that for the $\Delta = 0$ case there is precisely one half-wavelength contained in the cavity $[0, L]$, as implied by equation (4.60). This corresponds to the case of the closed organ pipe. For $\Delta = -1$, the phase term $\tan^{-1}[\rho_0 c_I \omega L \Delta]$ will be negative, and so less phase will be contained in the region $[0, L]$. This results in a decrease in mode frequency. The limit $\Delta \rightarrow -\infty$ leads us to the case described by equation (4.62), which corresponds to a completely open pipe.

For $\Delta = 1$, an interesting situation occurs. An additional amount of phase has been introduced into $[0, L]$, and this results in an increase in frequency. This situation does

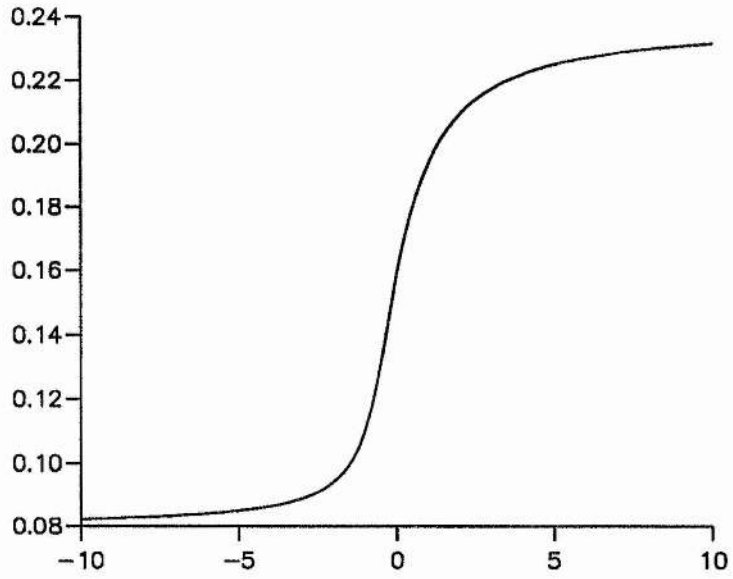

Figure 4.15: Mode frequency (in non-dimensional units) vs. Δ (in non-dimensional units).

not correspond exactly the organ pipe analogy, since in such a situation we cannot physically generate a positive value at the end of the pipe. A closed pipe has $\Delta = 0$; opening the pipe reduces its value. For our general problem, however, we may include this case; we may consider it as the extreme case of closure of the atmosphere.

Thus our physical picture runs as follows. In stipulating the value of Δ at $z = 0$, we are specifiying the position of the pressure and velocity nodes of the wave motion in $[0, L]$; when we vary Δ, we are thus altering how 'open' or 'closed' the atmosphere is, and thus altering the frequency at which a normal mode will be formed in the cavity. Similarly, in the p-mode problem, the value of Δ found from the chromospheric model will specify the pressure and velocity node form of the wave motion in the solar interior cavity, without having any effect on the form or position of the cavity itself. Thus the value of Δ plays a part in fixing the frequency at which a p-mode is formed.

Before we leave this subject, let us briefly examine the relationship of Δ to the frequency of a mode in the actual p-mode problem. Allowing Δ to vary from -4000$\mathrm{m^2 s^2 kg^{-1}}$ to 4000$\mathrm{m^2 s^2 kg^{-1}}$, Figure 4.17 shows the frequency calculated from our modified Bohr-Sommerfeld condition (4.40) for the $l = 50$, $n = 30$ mode. We see that the behaviour is very similar to that shown in Figure 4.15.

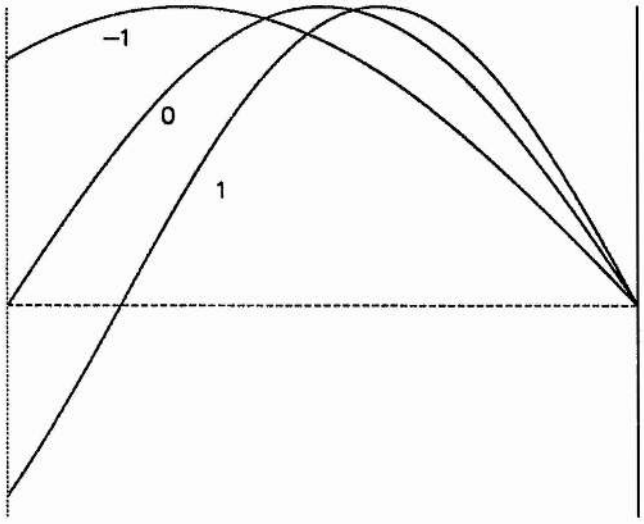

Figure 4.16: v_z vs. z for various values of Δ

In Figure 4.17, we chose an apparently arbitrary range of Δ. Indeed, in this section, we have not been concerned with how the chromospheric model picks a particular value of Δ. It is to this topic we now turn.

4.5.2 Relationship of Δ to the chromospheric model

The value of Δ supplied by the chromospheric model is defined by

$$\Delta = \left.\frac{v_z}{p_{Lt}}\right|_{z=0^-}, \tag{4.65}$$

where p_{Lt} is given in general by

$$p_{Lt} = -\rho_0 \left[v_A^2 \frac{dv_z}{dz} + c_s^2 \nabla . \boldsymbol{v} \right], \tag{4.66}$$

and $z = 0^-$ represents the base of the chromosphere. What chromospheric features will influence the value of this quantity?

Let us examine the typical values of Δ produced by some of the models we have considered. Figure 4.18 shows the variation of Δ with chromospheric temperature for the isothermal non-magnetic chromospheric model, for a frequency of 4.5mHz. We see that an

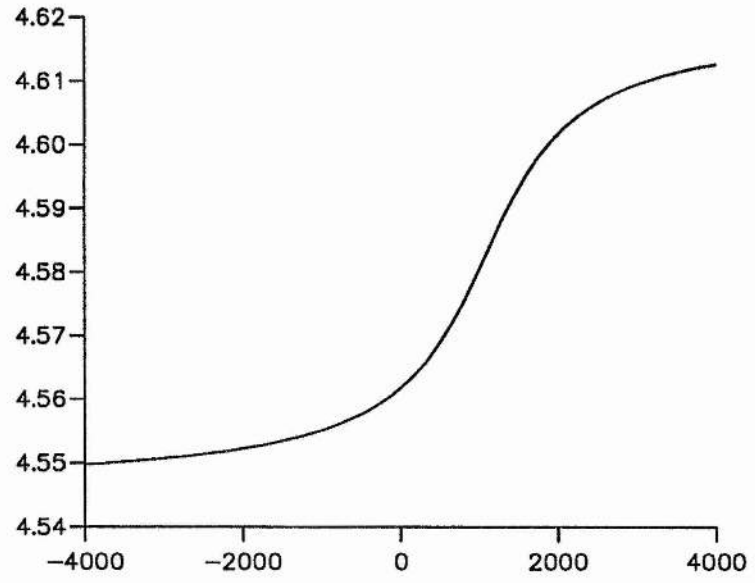

Figure 4.17: Mode frequency (in mHz) vs. Δ (in $\mathrm{m^2 s^2 kg^{-1}}$) calculated from the modified Bohr-Sommerfeld condition for the $l = 50$, $n = 30$ mode.

increase in chromospheric temperature reduces the value of Δ. By Figure 4.17, this should then result in a drop in mode frequency, and this is indeed what we have already seen.

Figure 4.19 then shows the variation of Δ with B_0 for our isothermal model with a uniform horizontal field; the temperature is fixed at 4170K. We see that Δ increases with increasing magnetic field, and that this is again consistent with previous results.

What physical grasp can we gain on the process by which the value of Δ is selected? To help us pick out the important effects, we make the following approximations. Firstly we utilise the fact that for the group of p-modes we are considering (high-n, medium-l), it is generally true that

$$\omega^2 \gg k_x^2 c_s^2, \tag{4.67}$$

where c_s is a typical sound speed in the chromosphere. Since we are considering only high-n modes, it is also true that

$$\omega^2 \gg g k_x. \tag{4.68}$$

Armed with these two observations, we look again at equation (4.26), which is the general relationship between the function Q, defined by $Q = \rho_0^{1/2} c_s^2 \nabla . \boldsymbol{v}$, and the ratio

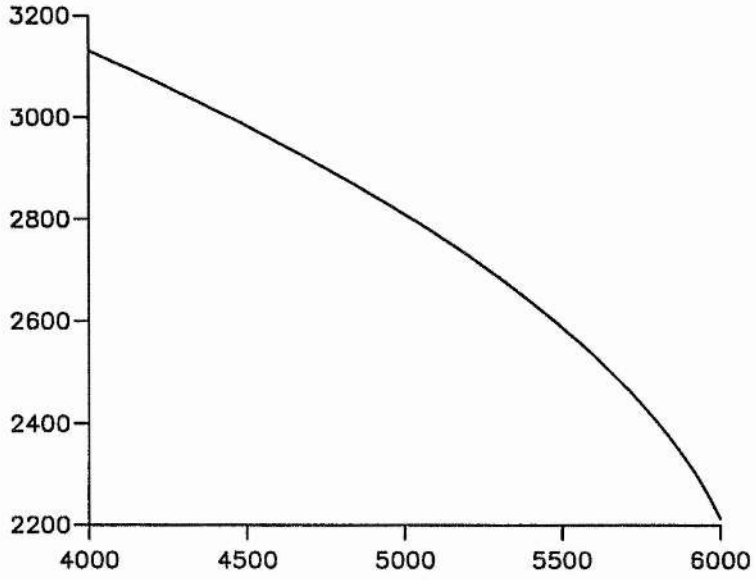

Figure 4.18: Δ (in $\mathrm{m^2 s^2 kg^{-1}}$) vs. temperature (in K) for the isothermal non-magnetic model.

v_z/p_{Lt}, in the absence of a magnetic field:

$$\frac{Q'(z)}{Q(z)} = \left[-\frac{1}{2}\frac{\rho_0'}{\rho_0} + \frac{gk_x^2}{\omega^2}\right] + \frac{\rho_0}{\omega^2}\left[\omega^4 - g^2k_x^2\right]\frac{v_z(z)}{p_{Lt}(z)}. \tag{4.69}$$

Let us consider the first term in square brackets in equation (4.69). In an isothermal atmosphere, this will reduce to

$$-\frac{\gamma g}{2c_0^2} + \frac{gk_x^2}{\omega^2}.$$

When condition (4.67) holds, this expression will be dominated by its first term, $-\gamma g/2c_0^2$. The second term in square brackets in equation (4.69) will obviously reduce to ω^4 when condition (4.68) holds. Thus, under these approximations, equation (4.69) can be written in the form

$$\frac{v_z}{p_{Lt}} = \frac{1}{\rho_0\omega^2}\left[\frac{Q'}{Q} + \frac{\gamma g}{2c_0^2}\right]. \tag{4.70}$$

This is a useful result because Q is the variable of the canonical wave equation (1.24). Thus it proves relatively easy to deduce the form of Q, and thus the behaviour of Q'/Q. We can then use equation (4.70) to make observations about the behaviour of v_z/p_{Lt}, and thus the value of Δ.

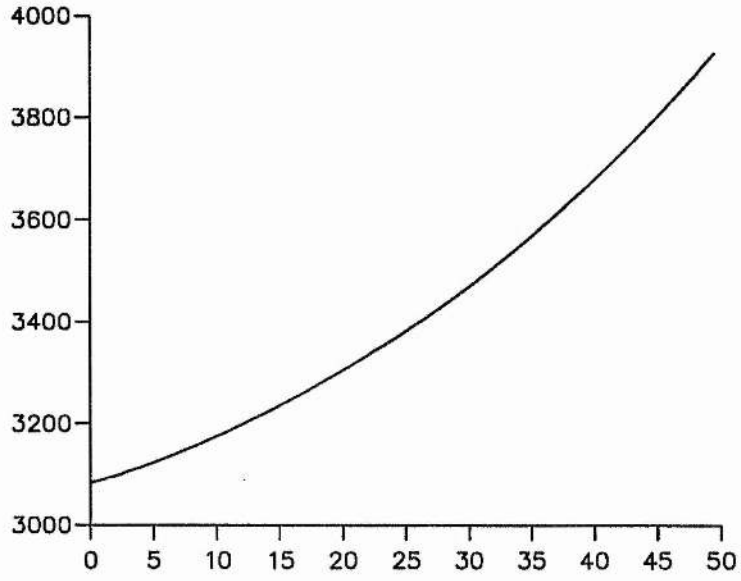

Figure 4.19: Δ (in $m^2s^2kg^{-1}$) vs. magnetic field strength (in G) for the isothermal chromosphere with a uniform horizontal magnetic field.

For example, in the case of an isothermal non-magnetic chromosphere, we find that Q'/Q is given exactly by $\sqrt{-\kappa_0^2}$, which is positive. This implies that the scale height of the decay of the Q solution is $1/\sqrt{-\kappa_0^2}$. For this model, we can write that

$$\Delta = \frac{1}{\rho_0 \omega^2}\left[\sqrt{-\kappa_0^2} + \frac{\gamma g}{2c_0^2}\right].$$

Thus Δ is positive, with implications for the mode frequency as discussed in section 4.5.1. Under the approximations (4.67) and (4.68), κ_0^2 can be written as

$$\kappa_0^2 \sim \frac{\omega^2}{c_0^2} - \frac{\gamma^2 g^2}{c_0^4}. \tag{4.71}$$

At frequencies such that κ_0^2 is negative, increasing the chromospheric temperature acts to increase the term $-\gamma^2 g^2/c_0^4$ in equation (4.71). The term ω^2/c_0^2 decreases, but by a lesser amount, since $\omega^2 < \gamma g/c_0^2$. Thus κ_0^2 increases, and $\sqrt{-\kappa_0^2}$ decreases, making Q decay less rapidly with height. This reduces the value of Δ, and thus of ν.

If, on the other hand, the temperature becomes very small, such that $\kappa_0^2 \to -\infty$, then Δ will become very large; this acts to increase the mode frequency. In such a situation, Q is very rapidly evanescent.

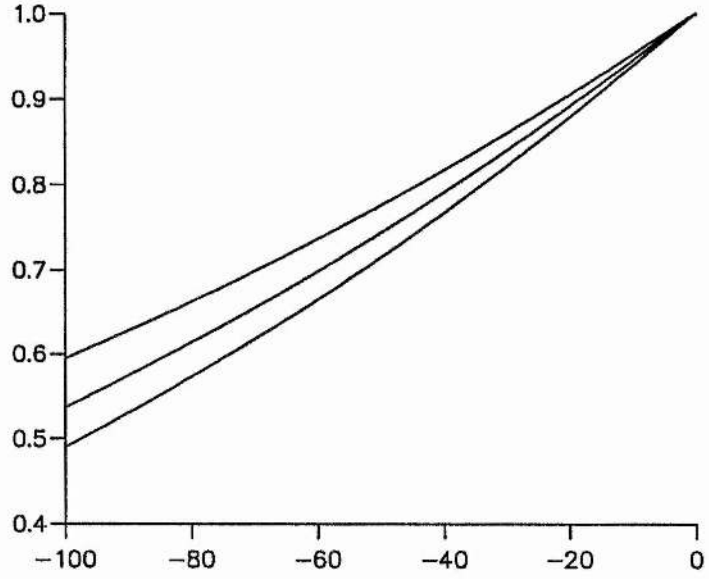

Figure 4.20: Q (in non-dimensionalised units) vs. z (in km) for magnetic field strength of 10G (top curve), 20G and 30G.

Thus we can see that in this case it is the form of Q'/Q near $z = 0^-$ which determines the interface condition at $z = 0$. If Q is very rapidly evanescent, we find that $\Delta \to \infty$; this corresponds to the case of a completely 'closed' organ pipe discussed in section 4.5.1. Smaller values of $\sqrt{-\kappa_0^2}$, with less steeply decaying forms of Q, give lower values of Δ, and thus of ν. It is reasonable that motions which extend further into the chromosphere produce a more 'open' interface condition.

When there is a magnetic field present, it is impossible to derive a simple relationship like equation (4.70), even for the approximations given. However, the same empirical rule is seen to operate; more swiftly evanescent forms of Q result in higher values of Δ. Figure 4.20 shows numerically calculated normalised values of Q near $z = 0^-$ for magnetic field strengths of 10G, 30G and 50G; the steepest curve is that for a field strength of 50G. We saw in Figure 4.19 that the value of Δ is higher for stronger magnetic fields, so a more steeply evanescent form of Q is again associated with higher values of Δ in this case.

Can we associate the rate of evanescence of Q with κ^2 in this case? If we assume that the Q solution is not radically altered by the presence of a magnetic field, we can form

a WKB solution near $z < 0$. This solution will be of the form

$$Q \sim \frac{1}{[-\kappa^2(z)]^{1/4}} \exp\left[\int \sqrt{-\kappa^2(s)}ds\right];$$

for cases when $[\kappa^2(z)]' \ll \kappa^2(z)$, we can then write that

$$\frac{Q'}{Q} \sim \sqrt{-\kappa^2(z)}.$$

We again see that the quantitative behaviour of Q'/Q is governed by the behaviour of $\kappa^2(z)$.

We may now consider the approximate form of κ^2 given in Chapter 2, that is

$$\kappa^2 \approx \frac{\omega^2}{c_s^2 + v_A^2} - \frac{1}{4H^2}. \tag{4.72}$$

Increasing the value of B_0 will decrease the value of κ^2, and thus increase the value of $\sqrt{-\kappa^2}$. Thus increasing the magnetic field strength has the effect of increasing the rate of evanescence of Q in the chromospheric model; we would thus expect that the values of both Δ and the mode frequency would increase along with the magnetic field strength.

Thus for frequencies at which wave motions are evanescent in our chromospheric model, an increase in temperature makes waves 'less evanescent', by reducing the influence of the cut-off term. An increase in magnetic field strength, on the other hand, makes motions 'more evanescent', by reducing the contribution from the first term in κ^2.

4.5.3 Summary

We can summarise our physical picture of the effect of the chromosphere on p-modes as follows. The effect of the chromosphere may be viewed in terms of how 'open' or 'closed' the mode cavity is. This influences the positions of the velocity and pressure nodes and antinodes within the cavity, and thus the frequencies at which modes will form. The more open the cavity, the lower the mode frequencies.

In the chromosphere, the important factor is the rate of evanescence of wave motions. A chromosphere in which motions die out very rapidly with height gives a closed cavity, while less rapidly evanescent motions give a more open cavity.

Chapter 5

High-frequency p-modes

5.1 Introduction

In Chapters 3 and 4 we described investigations into modes lying in the classical p-mode frequency range of 1–5mHz. For such modes, motions are evanescent throughout the chromosphere, and a standing wave is formed whose upper boundary is set by the process of reflection at the solar surface. Such modes have comprised the main subject of p-mode research for several decades.

In recent years, however, observers have reported the apparent existence of modes at frequencies above the acoustic cut-off frequency of around 5.3mHz (Duvall Jr. et al., 1991; Fernandes et al., 1992; Ronan and LaBonte, 1993). These modes, which we describe as high-frequency modes, have been observed at frequencies of up to about 10mHz, and it is anticipated this upper limit may rise further with improved observations. Figure 5.1 shows the familiar frequency-degree parabolae of p-modes, now extending to a frequency of over 8mHz.

Several theories have been put forward to explain the formation of p-modes above the acoustic cut-off frequency. Balmforth and Gough (1990) have suggested that modes may be allowed to form by the trapping of waves at the sharp temperature discontinuity in the transition region. Kumar and Lu (1991) have alternatively suggested that actual normal modes are *not* formed, but that the peaks in power at high frequencies are due to the interference of propagating waves in the chromosphere. The subject remains open for further theoretical explanations.

The improved quality of high-frequency mode observations has recently encouraged

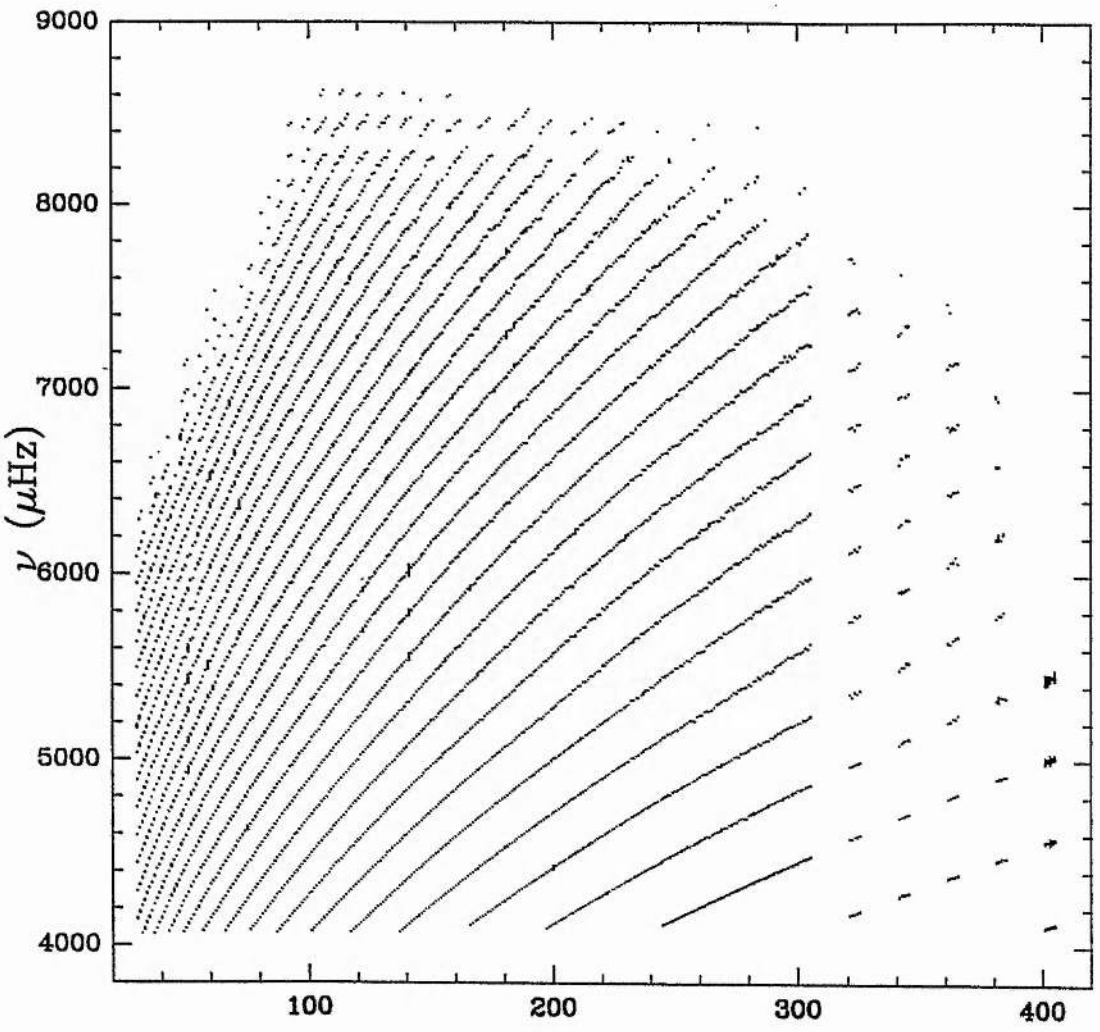

Figure 5.1: Observed mode frequencies (in mHz) vs. degree l (reproduced from Ronan, Cadora and LaBonte, 1993).

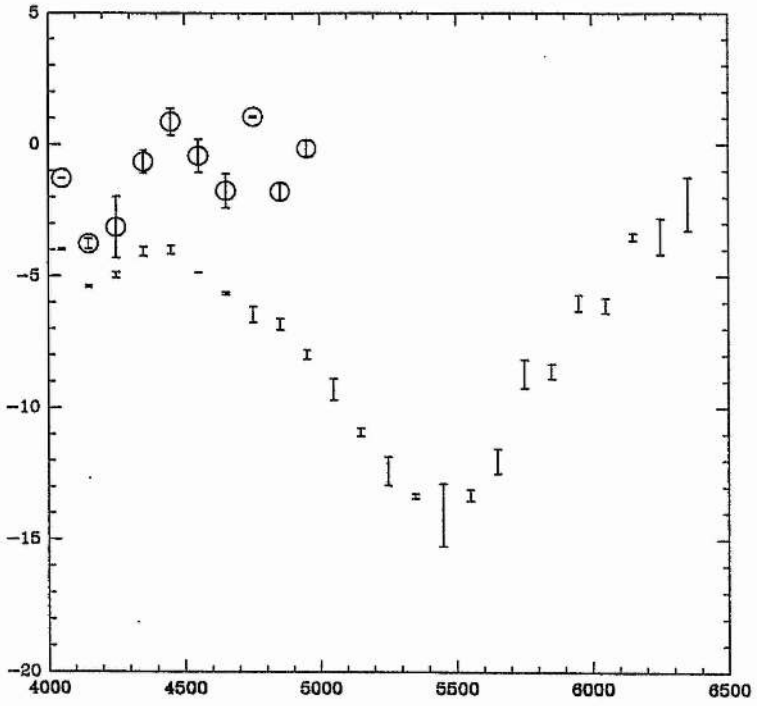

Figure 5.2: Observed frequency shift (in nHz) vs. original frequency (in mHz) (reproduced from Ronan, Cadora and LaBonte, 1993).

observers to consider frequency shifts for these modes. In particular, Ronan et al. (1993) have considered two pairs of datasets in the range 4–6.5mHz, and produced frequency shift curves for this frequency range. These are reproduced in Figure 5.2. Of greatest interest are the uncircled data points, which represent the averaged change in mode frequencies between observing sessions in 1987 and 1991. We see that over that period, many mode frequencies have decreased significantly. For modes of around 4.5mHz, there is virtually no shift, but at higher frequency, we see large negative frequency shifts beginning to occur. At around 5.5mHz, the averaged mode frequency shift is about -13μHz, much larger than shifts observed in the sub-cutoff frequency range. At higher frequencies still, the frequency shift curve 'turns over', and the negative frequency shift starts to decrease in magnitude. We might expect a second zero frequency shift at around 6.5mHz.

Thus we have a situation where modes above the acoustic cut-off frequency appear to exist, but for which no method of mode formation has yet been confirmed. We have already seen in Chapter 2 that a chromospheric magnetic field could supply the missing

mechanism. In the system described in Chapter 2, which included a chromospheric model with a uniform horizontal magnetic field, we found that modes could theoretically form at all frequencies, including those at which high-frequency p-modes are observed. The crucial physical effects are reflection (as influenced by the magnetic field), and refraction (which could trap waves by means of the increasing fast magnetoacoustic speed in the model). Thus we may seek a formulation of the problem which allows us to calculate normal modes for this system above as well as below the acoustic cut-off frequency.

Is this a reasonable physical description of high-frequency p-mode formation? It is expected that a sound wave propagating almost vertically upwards into the chromosphere will manifest itself as a fast magnetoacoustic wave; such a wave could certainly be trapped by a chromospheric magnetic field which gives rise to a monotonically increasing fast speed profile, as occurs in the uniform magnetic field case. Our earlier investigation has shown that, for modes of 10mHz for example, a turning point in the vertical motions of the atmosphere will occur at a height of around 1000km for a 30G field. A field of such an extent and strength in the chromosphere is not implausible. Thus the process of wave trapping we have described for this system could represent the actual mechanism for the formation of high-frequency p-modes.

The frequency shift data described above can be considered as an extension of previously considered frequency shift data, as shown in Figure 1.6 (Libbrecht and Woodard, 1991). This data was produced by comparing mode frequencies measured in 1986 and again in 1989. We attempted to explain the form of the frequency shift curve by modelling the chromosphere as described above, and found that a simultaneous change in temperature and magnetic field strength produces the desired turnover effect. We now propose to follow a similar procedure in the case of high-frequency modes.

In this chapter, we will calculate mode frequencies for the system previously investigated, that is a linear polytrope overlain by an isothermal chromospheric model containing a uniform horizontal magnetic field. Having done so, we then consider the changes induced in mode frequencies by various changes in the equilibrium properties of the chromospheric model.

5.2 Mode frequencies

The method of calculation of mode frequencies is identical to that used in Chapter 4. In the chromospheric model, we numerically integrate the wave equation for v_z as described in section 4.3.2. This allows us to determine the value of Δ, which is then used to calculate the mode frequency through the modified Bohr-Sommerfeld condition, which is

$$\int_{z_1}^{z_2} \kappa(z)\, dz = (n - \frac{1}{2})\pi - \phi, \tag{5.1}$$

where ϕ is a phase angle evaluated from

$$\tan\phi = -\frac{X(0)\mathrm{Ai}[t_1(0)] + \left[-\frac{\kappa^2(0)}{t_1(0)}\right]^{1/2}\mathrm{Ai}'[t_1(0)]}{X(0)\mathrm{Bi}[t_1(0)] + \left[-\frac{\kappa^2(0)}{t_1(0)}\right]^{1/2}\mathrm{Bi}'[t_1(0)]}. \tag{5.2}$$

All variables in equations (5.1 and (5.2) are as defined in section 4.2. Iteration will be required to find the mode frequency. Note also that in this range of frequencies we cannot consider the non-magnetic chromospheric model, since in the absence of a magnetic field modes do not form above the acoustic cut-off frequency.

Figure 5.3 shows mode frequencies calculated using this method. The degree l is allowed to vary from 1 to 200, and the three curves are for modes of order 10, 20 amd 30. The chromospheric magnetic field strength is set at 30G and the temperature at 4170K. We have stopped the curves at l=200 and ν=10mHz; in practice, we could extend them indefinitely. We again see the familiar form of p-mode parabolae. As mentioned in earlier investigations, this is not surprising since the parabolic form is the signature of the interior mode cavity, which operates in the same way whatever the choice of chromospheric model or indeed frequency range. It is in the form of frequency *shifts* that we expect the effect of the chromosphere to manifest itself.

5.3 Frequency shifts

The following procedure is used to calculate frequency shifts. We consider modes of degree l=50, and allow the order n to vary from 1 to 150; the mode l=50, n=150 is found to have a frequency of about 10mHz. We calculate the mode frequencies for one set of the chromospheric model parameters (B_0, T_c), corresponding to a chromospheric magnetic field strength B_0 and temperature T_c. We then repeat the calculation for a different set of

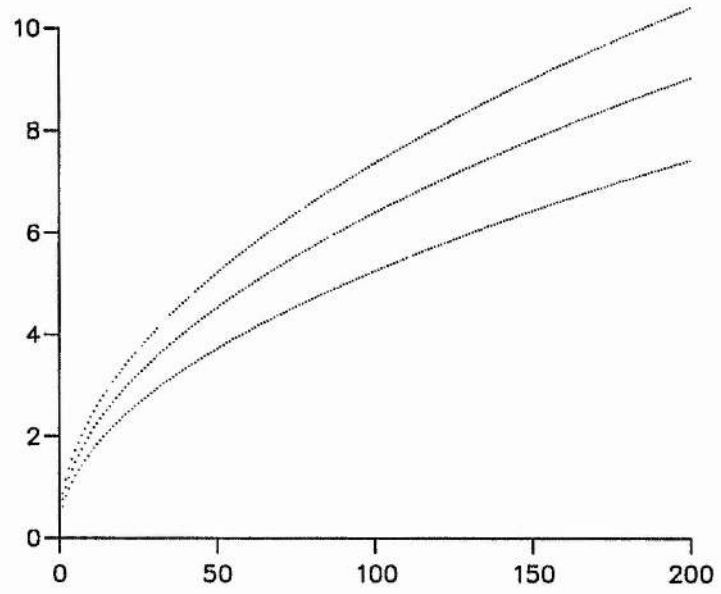

Figure 5.3: Mode frequency (in mHz) vs. degree l for modes of order n=10 (lowest curve), 20 and 30. The chromospheric temperature is taken as 4170K, the magnetic field strength as 30G

parameters, and so determine the change in frequency of each mode. The frequency shift is plotted against the original frequency.

Figure 5.4 shows the frequency response to a change in magnetic field strength in the atmosphere. We set the temperature to 4170K, and specify an initial magnetic field strength of 20G. We then increase the field strength to 30G (the lower curve) and 40G (the upper curve). We see that frequencies generally increase as a result of an increase in field strength, and that the larger change in magnetic field strength results in a larger frequency shift. There is a maximum frequency shift for an initial mode frequency of around 8.5mHz. Thus we see a new feature in the behaviour of the frequency shift curve in the high-frequency mode range, the occurence of a maximum.

Figure 5.5 shows the change in frequency induced by a change in temperature. We set the magnetic field strength to 30G, and impose an initial temperature of 4170K; we then increase the temperature to 5000K (the top curve), 5500K and 6000K (the bottom curve). Frequency shifts are generally negative, and are of greatest magnitude for the largest change in temperature, but again there is a maximum in the magnitude of the frequency shift, in

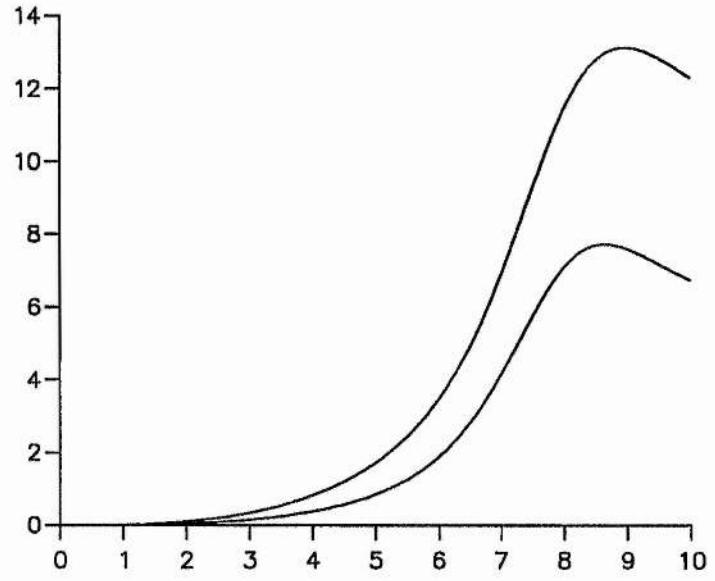

Figure 5.4: Frequency shift (in μHz) vs. original frequency (in mHz) induced by an increase in magnetic field strength from 20G to 30G (giving the lower curve) and 40G (giving the upper curve). The chromospheric temperature is held at 4170K. Modes considered are of degree l=50 and varying order n.

this case for mode frequencies in the range 7–8mHz. This is a feature which is not present in, or even suggested by, the frequency shift curves in the low frequency range.

We can also consider the effect of changing the magnetic field strength and the temperature simultaneously; in doing so, we expect to recover the turnover curves in the 1–5mHz range which we have studied in Chapters 3 and 4. Figure 5.6 shows the effect of increasing the magnetic field strength from 10G to 30G, while simultaneously altering the temperature in the chromosphere from an initial value of 4170K. The topmost curve is for no increase in temperature; subsequent curves are for increases from 4170K to 5000K, 6000K, 7000K and 8000K (the lowest curve). We see an increasingly complex behaviour of the frequency shift curves. The main features are as follows.

All of the curves in Figure 5.6 show a positive frequency shift in the low frequency range; the positive shift is smaller for the larger temperature increases. In the case of small temperature increases, frequency shifts remain positive for frequencies of up to 10mHz. However, when the temperature is increased to 6000K or more, turnover occurs and we find

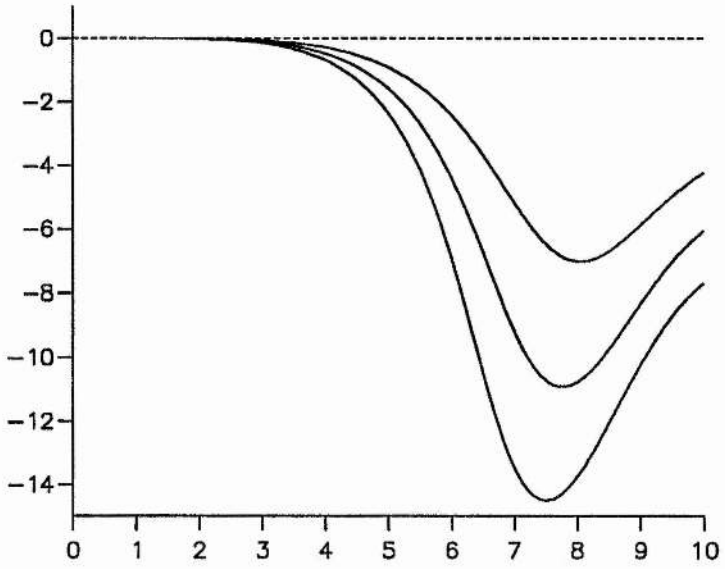

Figure 5.5: Frequency shift (in μHz) vs. original frequency (in mHz) induced by an increase in chromospheric temperature from 4170K to 5000K (top curve), 5500K and 6000K (bottom curve). The magnetic field strength is held at 30G.

a zero in the frequency shift. The larger the temperature change, the lower the frequency at which the zero of frequency shift occurs. We thus have a range of frequency for which frequency shifts are negative. In such cases, we always find a secondary turnover in the frequency shift: that is, the magnitude of the frequency shift reaches a maximum before decreasing once more as the frequency increases further. For these sets of parameters, the secondary turnover occurs at a frequency of between 6 and 6.5mHz. For larger changes in temperature, the magnitude of the frequency shift at secondary turnover is larger. We then generally find a second zero of frequency shift; the frequency at which this occurs is higher for larger temperature increases.

It is helpful to examine one particular frequency shift curve in each of the frequency ranges separately. Consider the middle curve of Figure 5.6, corresponding to a magnetic field strength increase from 10G to 30G along with a temperature increase from 4170K to 6000K. Figure 5.7a shows the classical, sub-cutoff range of frequency we have considered in Chapters 3 and 4. We see in general a positive frequency shift, displaying the turnover effect. The maximum frequency increase is around 100nHz, at a frequency of around 3mHz,

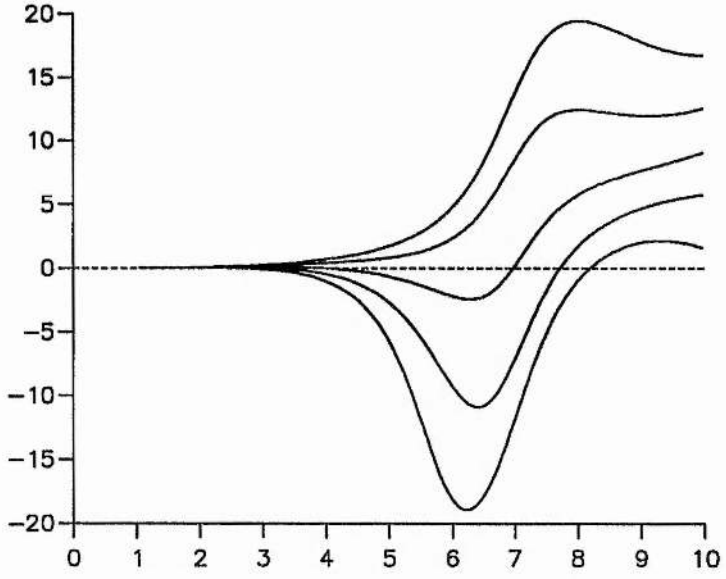

Figure 5.6: Frequency shift (in μHz) vs. original frequency (in mHz) induced by an increase in magnetic field strength from 10G to 30G, with a simultaneous increase in chromospheric temperature from 4170K. Curves displayed are firstly for no increase in temperature (top curve), then for increases to 5000K, 6000K, 7000K and 8000K (bottom curve). Modes considered are of degree l=50 and varying order n.

and there is a zero of frequency shift at around 4mHz.

Figure 5.7b shows the same curve in a higher frequency range, from about 4 to 7mHz; note the change of scale in the frequency shifts. In this range we see in general a negative frequency shift, with another turnover effect apparent. The maximum negative frequency shift for these parameters is around 2.5μHz, at around 6.3mHz, and there is a second zero of frequency shift at around 7mHz.

Figure 5.8 shows frequency shift curves for the same changes in magnetic field strength and temperature as Figure 5.6, but now for a different set of modes. We consider modes of degree 150, and allow the order to range from 1 to 50. Understandably, the l=50, n=150 mode forms at almost exactly the same frequency as the l=150, n=50 mode, so we are again considering frequencies up to 10mHz. We see that the same form of frequency shift curves results, but with the magnitudes of shifts increased approximately threefold.

Figure 5.9 shows the same modes as in Figure 5.6, but now for a different change

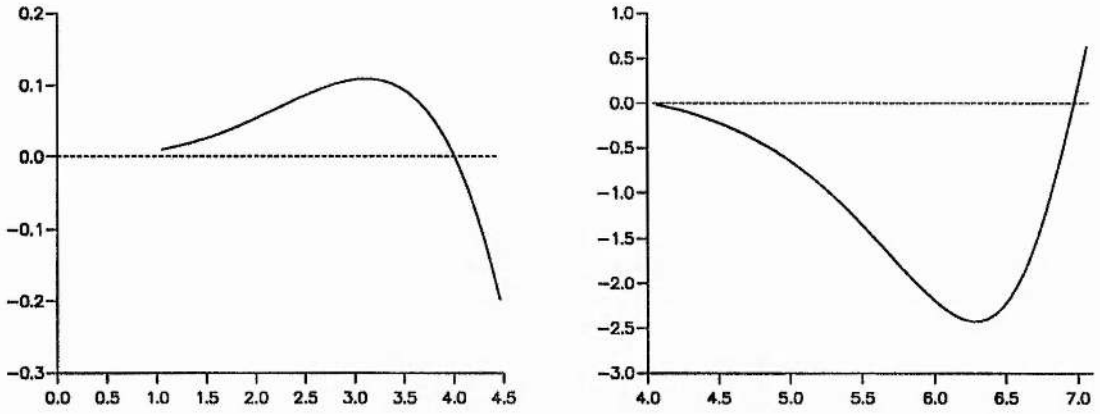

Figure 5.7: Frequency shift (in μHz) vs. original frequency (in mHz) induced by simultaneous increases in chromospheric temperature from 4170K to 6000K and magnetic field strength from 10G to 30G. The frequency range is separated into a) the low frequency range (1–4.5mHz) and b) the high frequency range (4–7mHz).

in magnetic field strength; we now increase the field strength from 20G to 40G, for the same changes in temperature. Again, the basic behaviour is reproduced, but we find that the major features of the curves (for example, points of turnover or zero frequency shift) now occur at higher frequencies than for the 10G to 30G change.

5.4 Physical considerations

What is the cause of these forms of frequency shift curves? This a very large question, which we will not be able to answer fully here. However, we can look at one aspect of the problem as follows. We have seen in section 4.5 that the influence of the chromosphere is expressed through the value of the quantity Δ, as defined in equation (4.25). We plotted the variation of Δ as a function of B_0, the magnetic field strength, and T_c, the chromospheric temperature for a mode of frequency 4mHz; we can now do the same for a mode above the acoustic cut-off frequency.

Figure 5.10 shows the variation of Δ with T_c for a mode of frequency 8mHz and a magnetic field strength of 30G. We see that a singularity in Δ occurs at around T_c=7000K; Δ tends to $-\infty$ as T_c tends to this value from below, and to $+\infty$ as T_c tends to this value from above. Figure 5.11 then shows the variation of Δ with B_0 for an 8mHz mode and a

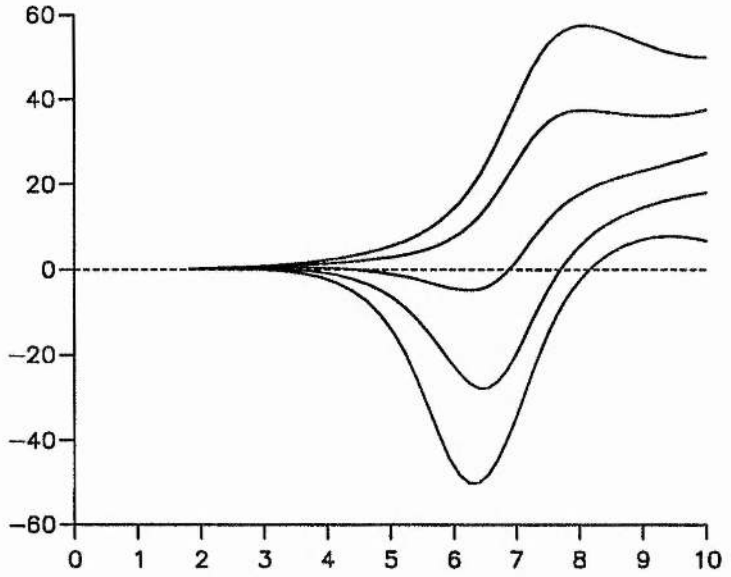

Figure 5.8: Frequency shift (in μHz) vs. original frequency (in mHz) induced by simultaneous increases in chromospheric temperature and magnetic field strength as described in Figure 5.6. Modes considered are of degree l=150 and varying order n.

magnetic field strength of 4170K. Again we see a singularity in Δ, here at around B_0=10G.

Why do such singularities occur? To see this, it is helpful to consider the variation of the vertical velocity, v_z, with height in the chromospheric model, as calculated by our numerical routine. Figure 5.12 shows the normalised value of v_z plotted against height in the model, for a mode of 8mHz, a magnetic field strength of 30G and a variety of chromospheric temperatures. The upper curve is for T_c=4170K, and the others are for T_c=6000K, 8000K and finally 10000K. As the temperature is increased, we see that the form of v_z becomes increasingly 'oscillatory' in z. At a certain temperature, v_z will be zero at $z = 0^-$, that is we will have a node of v_z at $z = 0^-$. This will be the temperature for which $\Delta = 0$. At higher temperatures still, there will be an anti-node of v_z at $z = 0$. Near the anti-node of v_z will exist a node of p_{Lt}, that is a height at which p_{Lt} is zero; thus at a temperature near that for which v_z has an anti-node at $z = 0^-$, p_{LT} will be zero at $z = 0^-$. For this temperature, we will have an infinite value of Δ. As the temperature increases beyond this value, Δ will be finite once more, but of a different sign to the value of Δ on the other side of the singularity. Eventually we will reach another node of v_z, Δ will once more be zero

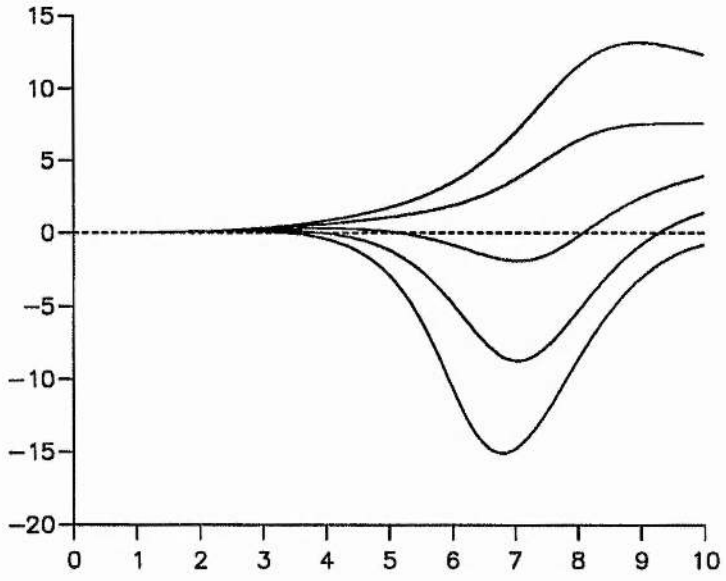

Figure 5.9: Frequency shift (in μHz) vs. original frequency (in mHz) induced by simultaneous increases in magnetic field strength from 20G to 40G and in chromospheric temperature as described in Figure 5.6. Modes considered are of degree l=50 and varying order n.

and the process will repeat itself.

This effect must be taken into account when we calculate mode frequencies for such high-frequency modes. When a node of v_z exists in the chromospheric model, calculation of the frequency of, say, the $n = 30$ mode using the modified Bohr-Sommerfeld condition, with Δ as calculated from the chromospheric model and $n = 30$, will actually give the frequency of the $n = 31$ mode, since the n-value appearing in the condition actually represents the number of nodes of v_z in $z > 0$. Thus our formulation must also take into account the number of nodes of v_z in $z < 0$, as well as the value of Δ. Alternatively, we can still calculate the mode frequency using $n = 30$ in this case, but the value of ϕ must be corrected to include additional integral multiples of π to represent the phase removed from $z > 0$.

In our physical description in Chapter 4, Figure 4.17 showed the response of the mode frequency to the value of Δ; a decrease in Δ results in a decrease in frequency. This picture is still true for this problem, but not complete. Now, Δ can jump across a singularity from, say, a large negative value to a large positive value. In terms of Figure 4.17, what is happening here is that the ω-Δ curve for a mode of order n jumps onto another branch,

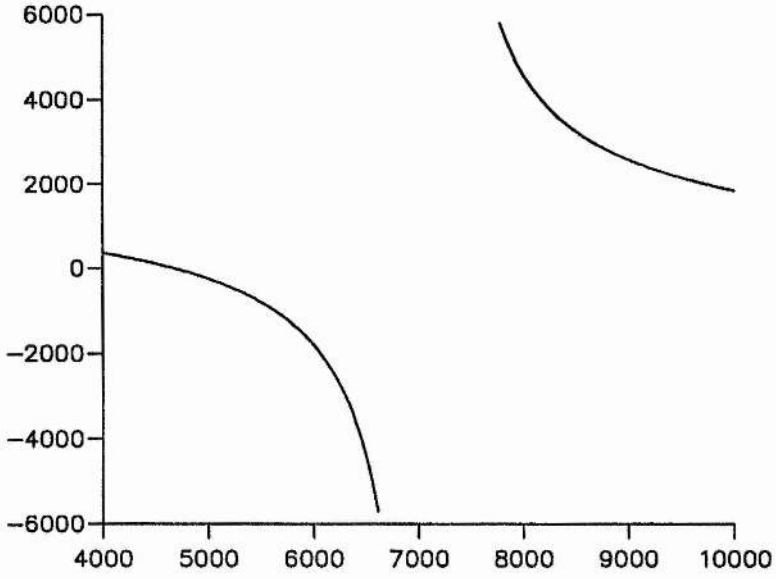

Figure 5.10: Δ vs. chromospheric temperature at a frequency of 8mHz.

that corresponding to the mode of order $n-1$. Thus as Δ passes through a singularity, the mode frequency continues to decrease as a result.

Our physical picture is thus that a more oscillatory form of v_z in $z < 0$ results in a lower value for the mode frequency. Now we have seen that the nature of the v_z solution and the value of Δ depend upon the values of B_0 and T_c. But why do changes in these quantities then yield the forms displayed in Figures 5.6–5.9? This is a complex question, involving the physical processes of reflection and refraction described in section 2.3, and the changes in the operation of these processes brought about by changes in the model; a fully comprehensive physical description of the form of frequency shift curves in the high-frequency range does not yet exist. The physical description of section 4.5 describes only the case where motions are evanescent in $z < 0$, and so is not applicable here. For modes above the acoustic cut-off frequency, we need to consider the effect of chromospheric parameter changes on oscillatory solutions. Further investigation is thus required into the behaviour of high-frequency modes.

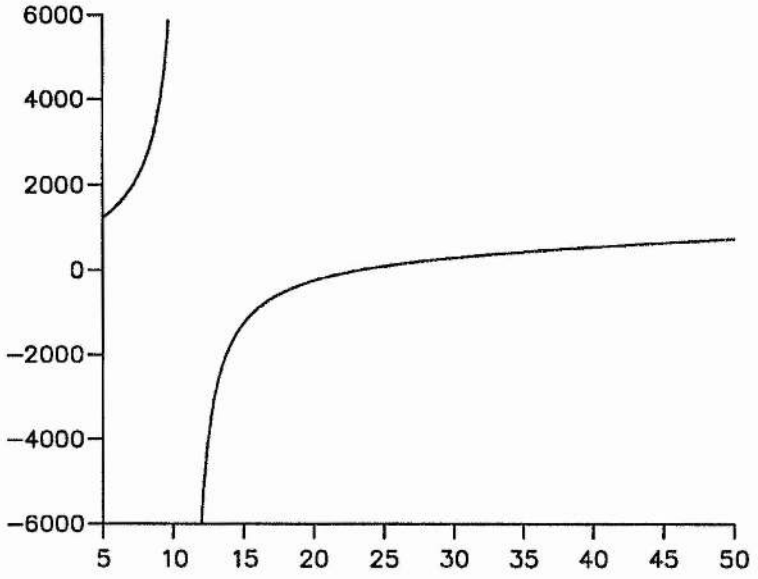

Figure 5.11: Δ vs. magnetic field strength at a frequency of 8mHz.

5.5 Discussion

We now turn to a comparison of our results with the observations. In the low frequency range, we have already seen that the general form of observations (Libbrecht and Woodard, 1991) is reproduced by our model as a consequence of an increase in chromospheric magnetic field strength and temperature (see section 4.1 and also Jain and Roberts (1993)). In the high frequency range, we can compare our theoretical results with the averaged observed frequency shift curve shown in Figure 5.2 (Ronan et al., 1993). We again see that the observed form is successfully reproduced in our theoretical frequency shift curves for an increase in magnetic field strength and temperature. The general form matches the form of the observed curves remarkably well.

So much for the form, but what about the actual numerical values of the frequency shifts and of the frequencies at which various features of the curve occur? A precise matching of our curves to the observations is in fact very difficult. Some of the problems we encounter are similar to those we have already discussed in section 4.4.3. For example, we must decide on realistic values of and changes in B_0, taken to represent the magnetic canopy field strength, and T_0, representing the temperature in the chromosphere. This choice is

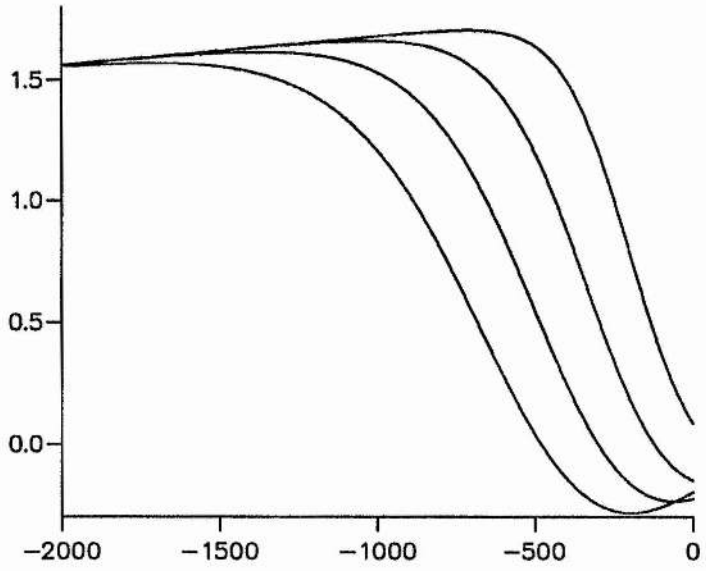

Figure 5.12: Vertical velocity v_z (in dimensionless units) vs. z (in km). Curves displayed are for a mode of frequency 8mHz and chromospheric temperatures of 4170K (top curve), 6000K, 8000K and 10000K (botom curve). the magnetic field strength is 30G.

speculative. We see from Figures 5.6 and 5.9, however, that the precise values of frequencies at which such features as turnover, secondary turnover and zeros of frequency shift occur are very sensitive to the precise change in magnetic field strength considered.

A second element of uncertainty is the averaging procedure used to produce a single observational averaged frequency shift curve. Both Libbrecht and Woodard (1991) and Ronan et al. (1993) use such an averaging procedure. The form of the averaged curve depends on the particular set of modes being considered, since the magnitude of frequency shifts are in general proportional to l: Figure 5.8 shows the dramatic effect on frequency shifts of considering modes of different degree, even for curves of similar form. We would prefer to see averaged curves which removed the l-dependence, as we have done for a limited dataset in section 1.2, or curves presented for narrow bands of l (for example, l=45–55).

A further area of uncertainty is the limitations of our model and the mathematical formulation through which we calculate mode frequencies. For example, one limitation in our treatment of high-frequency modes given here is that we are considering an isothermal chromosphere. The results of Chapter 4 show that temperature gradients in the chromo-

sphere can have a significant effect on mode frequencies; we would expect this to be all the more true at high frequencies. Thus we cannot realistically expect that our simple model will give exact agreement with the observed frequency shift curves, in either the sub-cutoff frequency range or the high frequency range.

The useful conclusions we *can* make from our work are as follows. Firstly, the proposed theory of mode formation above the acoustic cut-off through trapping of waves by the chromospheric magnetic field produces modes of a similar character to p-modes. Secondly, even for our simple chromospheric model, a change in chromospheric parameters can produce the observed forms of mode frequency shift curves in both the sub-cutoff and high-frequency ranges. This is the most we could expect our simple model to do.

There is a final comment we can make on this problem. The agreement of the form of theoretically computed mode frequency shift curves in the 1–5mHz range was a significant achievement (Evans and Roberts, 1990; Jain and Roberts, 1993). However, other authors (Goldreich, Murray, Willette and Kumar, 1991) have produced a similar form, with *better* numerical agreement, by considering altogether different chromospheric effects. Indeed, there might be a number of effects which yield a turnover curve in the 1–5mHz range. Thus, although a turnover curve has been produced, there is no guarantee that we have found the actual cause of the observed frequency shift curve.

We have taken the same model, with the same changes in atmospheric parameters, and extended the frequency shift curve into a new frequency range, and compared the results with a new set of observations. We find good agreement in form with these observations. The same point can indeed be made, that we cannot be sure that we have pin-pointed the dominant physical mechanism which produces such frequency shifts, but with the demonstration of a *second* area of agreement it becomes increasingly unlikely that some different process is responsible for the shifts. However, further investigation is obviously required, both on the theoretical and observational side. A less simple model, perhaps featuring a non-isothermal chromosphere, for which the exact form of wave motions is determined (either analytically or numerically), would be an advance. The basis of such a model is described in Chapter 4. More detailed observations, analysed so as to facilitate comparison with theoretical results, perhaps by not averaging over an extensive range of degree l, would also help. For the moment, our conclusion must be that the influence of the chromosphere, and in particular its magnetic field, is the major influence on p-mode frequency variations over the solar cycle.

Chapter 6

Modes of degree zero

6.1 Introduction

In Chapter 1 we gave the classical description of p-mode formation by successive reflection at the solar surface and refraction within the solar interior. We have earlier investigated a situation whereby the first of these processes, reflection at the solar surface, does not occur (Chapter 5). We now look at a case where the second process, refraction within the solar interior, does not occur.

In our description of p-mode formation, we considered a wave propagating at an oblique angle to a radius of the Sun, and thus being refracted by the increasingly high temperatures nearer the centre of the Sun. We modelled this by a wave propagating in a plane-parallel stratified atmosphere with a linearly increasing temperature. By comparing the radial equation of wave motion, equation (1.48), with that for our plane-parallel atmosphere, we concluded that this 'flattening out' of the Sun would provide a good approximation for modes of high degree, whose cavities are confined to near the solar surface. Dispersion relations were then calculated to yield mode frequencies for such a model, and the inclusion of a chromospheric atmosphere allowed the study of frequency shifts due to chromospheric changes. Asymptotic expansions of the dispersion relations implied frequency shifts which were proportional to the degree l (Evans and Roberts, 1992), and indeed observed p-mode frequency shifts do appear to increase linearly with degree (Libbrecht et al., 1990).

However, these asymptotic expansions imply zero frequency shift for zero-degree modes, whereas observed frequency shifts for zero-degree modes are non-zero (Elsworth et

al., 1990). In fact, no conclusions as to low-degree mode frequency shifts, or indeed to mode frequencies themselves, should be drawn from these dispersion relations or their asymptotic expansions, since the plane-parallel model for which they were derived is invalid at low degree.

Thus the task remained to deal with low-degree modes, and to demonstrate how frequency shift curves could occur for such modes. Low-l modes are in general difficult to treat mathematically, since spherical effects must be taken into consideration. For one special type of low-l mode, however, progress is rather more straightforward. This is the set of modes for which $l = 0$.

How do we understand zero-degree modes? These are radial modes for which no nodal lines exist on the surface of the Sun, implying that the whole Sun is oscillating in phase. We may form a similar description to the wavefront picture given in section 1.2.1 as follows. Here we will encounter a spherical wavefront, each point on which will be travelling towards the centre of the Sun at the same phase speed. After passing through the centre of the Sun, the spherical wavefront will expand outwards again towards the surface, where we will assume for the moment that the wavefront is reflected by similar processes to those described in section 1.2.1.

In terms of wave motion, we can describe this process in terms of a wave propagating radially towards or away from the centre of the Sun. Such a radial wave will not undergo refraction, but will pass straight through the centre of the Sun. The wave will, however, be trapped by reflection at the solar surface. For such modes, then, the cavity in which modes form is the entire Sun, and reflection is the only process acting to form a cavity. A new model is obviously required to calculate mode frequencies in this problem.

In this chapter, we construct a model for this process, and derive a dispersion relation for modes formed in this model. We then consider further the process of reflection at the solar surface by incorporating a chromospheric atmosphere, and examine frequency shifts for the simplest case.

6.2 Mode frequencies

How then do we model the process of zero degree mode formation described above? Since the wave is propagating radially for the $l = 0$ case, the position of a disturbance can be written in terms of a single one-dimensional variable, the depth z. If a mode is to form,

the standing wave solution must be symmetric about the centre of the Sun. Thus we need only consider one half of the wave's transit across any solar diameter. We thus consider the range of z defined by $[0, z_d]$, where z_d is some finite depth. The point $z = 0$ corresponds to the solar surface, and the point $z = z_d$ corresponds to the centre of the Sun.

In this range of z, we will attempt to find solutions to the differential equations governing the wave motions. Since the direction of propagation is purely entirely one-dimensional, we can use our general differential equations as described in section 1.3, but with the horizontal wavenumber k_x set to zero. We consider first the differential equation in the vertical velocity, v_z, equation (1.21), which with $k_x = 0$ and $v_A^2 = 0$ gives

$$\frac{d}{dz}\left[\rho_0 c_s^2 \frac{dv_z}{dz}\right] + \rho_0 \omega^2 v_z = 0. \tag{6.1}$$

Consider again the variation of temperature in $[0, z_d]$ to be given by the linear polytrope model described in section 1.4.1:

$$T = T_0(1 + z/z_0), \qquad 0 \leq z \leq z_d, \tag{6.2}$$

where T_0 is the temperature at $z = 0$ and z_0 is the temperature scale height. The model parameters we will use here are as given in Tables 1.1 and 1.2; note that the polytropic index, m, again takes the value $3/2$. We have assumed that the gravitational acceleration g is constant throughout the relevant range of z. This is not true for spherical stratification; however this should serve as a reasonable first approximation to the true behaviour.

For this model, equation (6.1) takes the form

$$\frac{d^2 v_z}{dz^2} + \frac{m+1}{z_0(1+z/z_0)}\frac{dv_z}{dz} + \frac{\omega^2}{c_{0L}^2(1+z/z_0)}v_z = 0. \tag{6.3}$$

To solve this equation, we introduce a number of transformations. Firstly, we set

$$s = 1 + z/z_0, \tag{6.4}$$

yielding

$$s\frac{d^2 v_z}{ds^2} + (m+1)\frac{dv_z}{ds} + \frac{\omega^2 z_0^2}{c_{0L}^2}v_z = 0. \tag{6.5}$$

The transformation

$$r = \frac{2\omega z_0}{c_{0L}} s^{1/2} \tag{6.6}$$

then gives the differential equation

$$r^2\frac{d^2 v_z}{dr^2} + (2m+1)r\frac{dv_z}{dr} + r^2 v_z = 0, \tag{6.7}$$

which under the further transformation

$$v_z = r^{-m} X \tag{6.8}$$

becomes

$$r^2 \frac{d^2X}{dr^2} + r\frac{dX}{dr} + (r^2 - m^2)X = 0. \tag{6.9}$$

This is the Bessel differential equation (Abramovitz and Stegun, 1967: 9.1.1). Thus our general solution to equation (6.9) is

$$X = c_1 \mathrm{J}_m(r) + c_2 Y_m(r), \tag{6.10}$$

where $\mathrm{J}_m(r)$ and $\mathrm{Y}_m(r)$ are Bessel functions of the first and second kind.

Hence,

$$v_z = r^{-m} \left[c_1 \mathrm{J}_m(r) + c_2 Y_m(r)\right], \tag{6.11}$$

where

$$r = \frac{2\omega z_0}{c_{0L}}(1 + z/z_0)^{1/2}.$$

This solution is equivalent to the asymptotic solution for v_z in the limit of small $k_x z$ found by Goldreich, Murray and Kumar (in press).

We may also calculate the forms of dv_z/dz and $\nabla.\boldsymbol{v}$ in $[0, z_d]$. Since (Abramovitz and Stegun, 1967: 9.1.30)

$$\frac{d}{dz}\left[z^{-m}\mathrm{J}_m(z)\right] = -z^{-m}\mathrm{J}_{m+1}(z), \tag{6.12}$$

and

$$\frac{d}{dz}\left[z^{-m}\mathrm{Y}_m(z)\right] = -z^{-m}\mathrm{Y}_{m+1}(z), \tag{6.13}$$

we find from the solution (6.11) that

$$\frac{dv_z}{dr} = -r^{-m}\left[c_1 \mathrm{J}_{m+1}(r) + c_2 Y_{m+1}(r)\right]. \tag{6.14}$$

Noting that

$$\frac{dr}{dz} = \frac{2\omega^2 z_0}{c_{0L}^2}\frac{1}{r},$$

we find that

$$\frac{dv_z}{dz} = -\frac{2\omega^2 z_0}{c_{0L}^2} r^{-(m+1)}\left[c_1 \mathrm{J}_{m+1}(r) + c_2 Y_{m+1}(r)\right]. \tag{6.15}$$

Furthermore, we see from equation (1.18) that for $k_x \equiv 0$,

$$\nabla.v = \frac{dv_z}{dz}. \tag{6.16}$$

Thus $\nabla.v$ is also given by equation (6.15).

Let us now attempt to form a dispersion relation by applying some boundary conditions on the v_z solution. We specify that

$$v_z\Big|_{z=z_d} = 0. \tag{6.17}$$

Thus, we are effectively placing a 'wall' at $z = z_d$.

From the form of the v_z solution given in equation (6.11), we find that

$$c_1 \mathrm{J}_m(r_d) + c_2 \mathrm{Y}_m(r_d) = 0, \tag{6.18}$$

where

$$r_d = \frac{2\omega z_0}{c_{0L}}(1 + z_d/z_0). \tag{6.19}$$

This condition describes the relationship between the constants c_1 and c_2. The value of z_d will generally be taken to be the solar radius.

What condition may we impose at $z = 0$? In general, we would like to impose a condition related to a chromospheric solution. For now, however, we will merely state that the atmosphere is 'open' at $z = 0$, requiring that

$$\nabla.v\Big|_{z=0} = 0. \tag{6.20}$$

The significance of this boundary condition is discussed in section 4.5. From our solution in $\nabla.v$, equation (6.16), we then find that

$$c_1 \mathrm{J}_{m+1}(r_0) + c_2 \mathrm{Y}_{m+1}(r_0) = 0, \tag{6.21}$$

where

$$r_0 = \frac{2\omega z_0}{c_{0L}}.$$

Finally, we can eliminate c_1 and c_2 between the two expressions (6.18) and (6.21) to obtain the dispersion relation

$$\mathrm{J}_{m+1}(r_0)\mathrm{Y}_m(r_d) - \mathrm{Y}_{m+1}(r_0)\mathrm{J}_m(r_d) = 0. \tag{6.22}$$

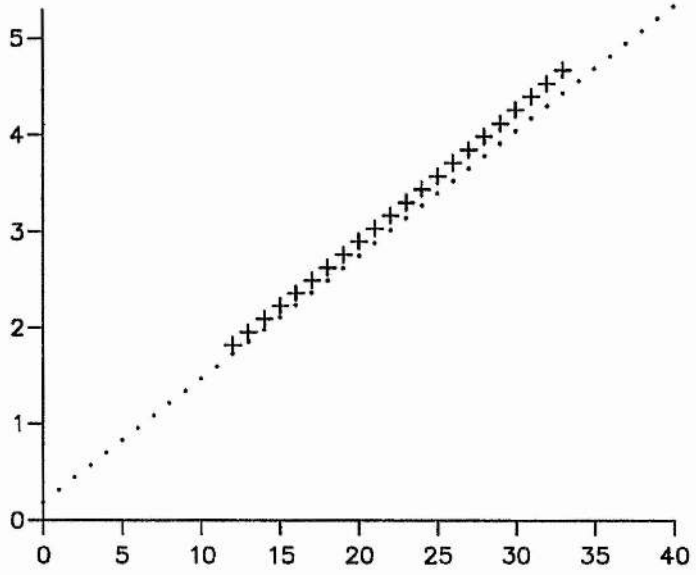

Figure 6.1: Mode frequency (in mHz) vs. order n for modes of zero degree (l=0). Dots depict mode frequencies calculated from our dispersion relation, crosses depict the observed mode frequencies (Libbrecht, Woodard and Kaufman, 1990).

This dispersion relation describes modes formed in a linear polytrope model with a 'wall' at a depth of $z = z_d$ and an open boundary at $z = 0$.

We can calculate mode frequencies from the dispersion relation (6.22). We use the standard linear polytrope parameters given in Tables 1.1 and 1.2, and set $z_d = 6.96 \times 10^8$m (the solar radius). There is a sequence of solutions to equation (6.22), which we identify as a set of modes of integer order n, with n increasing from zero. The dots in Figure 6.1 show the frequencies calculated for these modes, for n going from 0 to 40, plotted against n. The crosses show the observed mode frequencies (Libbrecht et al., 1990) for p-modes of degree zero and order 12–33, also plotted against order. We see that even for such a simple model, there is good agreement with the observed frequencies.

We also see an apparent linear dependence of frequency with order n; this is different to the observed and theoretical behaviour of $l \neq 0$ modes, for which the frequency is approximately proportional to $n^{1/2}$. In the most common physical situations where normal modes arise, for example in a guitar string of finite length fixed at both ends, we expect mode frequency to be proportional to the overtone number, or order, n. The

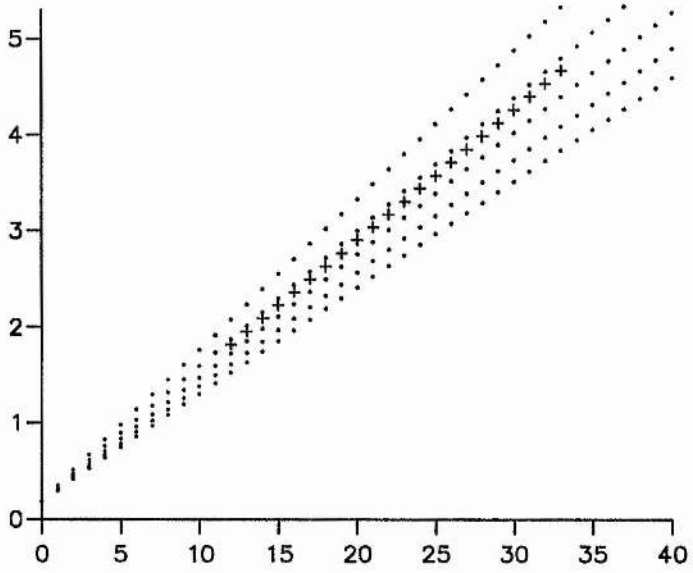

Figure 6.2: Mode frequency (in mHz) vs. order n for varying polytropic index m. Sets of dots depict theoretical mode frequencies for m=1.0 (highest frequencies), 1.25, 1.5, 1.75 and 2.0. Crosses again depict observed mode frequencies (Libbrecht, Woodard and Kaufman, 1990).

reason that $l \neq 0$ p-modes depart from this behaviour is that the depth of the cavity itself increases with frequency, with the resultant effect that the frequency of higher order modes is proportional to $n^{1/2}$. For zero-degree modes, the depth of the cavity is the same for modes of all frequencies, and so mode frequencies scale linearly with order.

Many factors can affect the precise gradient of the theoretically calculated ω-n graph plotted in Figure 6.1, but in terms of the dispersion relation (6.22) they express themselves through two parameters. The first factor is the value taken for z_d; the solar radius is the only justifiable value for this parameter. The second factor is the value taken for the polytropic index m; in Figure 6.1 it is taken to be 3/2, the value appropriate for marginal stability to g-modes in the general treatment of the problem. Figure 6.2 shows various sets of theoretical mode frequencies calculated for various values of m. The set producing the highest frequencies on Figure 6.2 is that for $m = 1$; other sets are for m=1.25, 1.5, 1.75 and 2. We see that the best fit with the observational data (the crosses on Figure 6.2) occurs for $m \approx 1.35$. However, since the agreement is reasonably good for $m = 1.5$, we shall use

this value when calculating mode frequency shifts, to maintain consistency with previous studies.

Thus our simple one-dimensional model, with a 'wall' placed at a depth of the solar radius and a boundary condition of an 'open' atmosphere at $z = 0$, gives good agreement with observed zero-degree p-mode frequencies. We would now like to consider frequency shifts for such modes, which will require some form of chromospheric model. It is to this problem we now turn.

6.3 Frequency shifts

We consider first an isothermal non-magnetic chromospheric atmosphere in $z < 0$, and investigate the effect on mode frequencies of a change in the temperature of the model. This is the model described in section 1.5.2; the forms of v_z and $\nabla.\boldsymbol{v}$ are as given there, but with k_x now zero.

From equation (1.80) we thus find that solutions in terms of $\nabla.\boldsymbol{v}$ can be written as

$$Q = c_3 \exp\left[\sqrt{-\kappa_0^2}\, z\right], \qquad z < 0, \tag{6.23}$$

where

$$Q = \rho_0^{1/2} c_0^2 \nabla.\boldsymbol{v} \tag{6.24}$$

and

$$\kappa_0^2 = \frac{\omega^2}{c_0^2} - \frac{\gamma^2 g^2}{4c_0^4}. \tag{6.25}$$

Thus, we again find a cut-off effect: modes will only be able to form at frequencies such that

$$\omega^2 < \frac{\gamma^2 g^2}{4c_0^2}. \tag{6.26}$$

Thus, in $z < 0$,

$$\begin{aligned} \nabla.\boldsymbol{v} &= \frac{c_3}{\rho_0^{1/2} c_0^2} \exp\left[\sqrt{-\kappa_0^2}\, z\right] \\ &= \frac{c_3}{\rho_{00}^{1/2} c_0^2} \exp\left[\left(\sqrt{-\kappa_0^2} - \frac{\gamma g}{2c_0^2}\right) z\right], \end{aligned} \tag{6.27}$$

since

$$\rho_0(z) = \rho_{00} \exp\left[\frac{\gamma g}{c_0^2} z\right],$$

where ρ_{00} is the equilibrium density at $z = 0^-$. Also, we find from equation (1.83) that the form of v_z in $z < 0$ is given by

$$v_z = -\frac{c_3}{\rho_{00}^{1/2}\omega^2}\left[\sqrt{-\kappa_0^2} + \frac{\gamma g}{2c_0^2}\right]\exp\left[\left(\sqrt{-\kappa_0^2} - \frac{\gamma g}{2c_0^2}\right)z\right]. \tag{6.28}$$

We must now consider our interface conditions at $z = 0$, as introduced in section 1.5.1. In this non-magnetic problem, these demand continuity across $z = 0$ of the equilibrium pressure p_0, the vertical velocity v_z and the time-derivative of the Lagrangian pressure perturbation p_{Lt}, which for this case is simply equal to $\rho_0 c_s^2 \nabla.\boldsymbol{v}$. The condition on continuity of p_0 tells us that

$$\rho_{0L} c_{0L}^2 = \rho_{00} c_0^2. \tag{6.29}$$

From the forms of v_z in $z > 0$ and $z < 0$ given in equations (6.11) and (6.28), the condition on continuity of v_z implies that

$$c_1 r_0^{-m}\left[\mathrm{J}_m(r_0)\mathrm{Y}_m(r_d) - \mathrm{Y}_m(r_0)\mathrm{J}_m(r_d)\right] = -\frac{c_3}{\rho_{00}^{1/2}\omega^2}\left[\sqrt{-\kappa_0^2} + \frac{\gamma g}{2c_0^2}\right]\mathrm{Y}_m(r_d). \tag{6.30}$$

From equations (6.16) and (6.27), continuity of $\rho_0 c_s^2 \nabla.\boldsymbol{v}$ across $z = 0$ implies that

$$-2c_1\rho_{0L}\omega^2 z_0 r_0^{-(m+1)}\left[\mathrm{J}_{m+1}(r_0)\mathrm{Y}_m(r_d) - \mathrm{Y}_{m+1}(r_0)\mathrm{J}_m(r_d)\right] = c_3\rho_{00}^{1/2}\mathrm{Y}_m(r_d). \tag{6.31}$$

Finally, we can eliminate c_1 and c_3 between equations (6.30) and (6.31) to obtain the dispersion relation

$$2\frac{\rho_{0L}}{\rho_{00}}\left[\sqrt{-\kappa_0^2} + \frac{\gamma g}{2c_0^2}\right]\frac{z_0}{r_0}\left[\mathrm{J}_{m+1}(r_0)\mathrm{Y}_m(r_d) - \mathrm{Y}_{m+1}(r_0)\mathrm{J}_m(r_d)\right]$$

$$= \left[\mathrm{J}_m(r_0)\mathrm{Y}_m(r_d) - \mathrm{Y}_m(r_0)\mathrm{J}_m(r_d)\right]. \tag{6.32}$$

Taking into account the condition (6.29) and performing some rearrangement, equation (6.32) becomes

$$\frac{c_0}{c_{0L}}\left[\left(\mathcal{C}^2 - 1\right)^{1/2} + \mathcal{C}\right]\left[\mathrm{J}_{m+1}(r_0)\mathrm{Y}_m(r_d) - \mathrm{Y}_{m+1}(r_0)\mathrm{J}_m(r_d)\right]$$

$$- \left[\mathrm{J}_m(r_0)\mathrm{Y}_m(r_d) - \mathrm{Y}_m(r_0)\mathrm{J}_m(r_d)\right] = 0 \tag{6.33}$$

where

$$\mathcal{C} = \frac{\gamma g}{2\omega c_0} > 1. \tag{6.34}$$

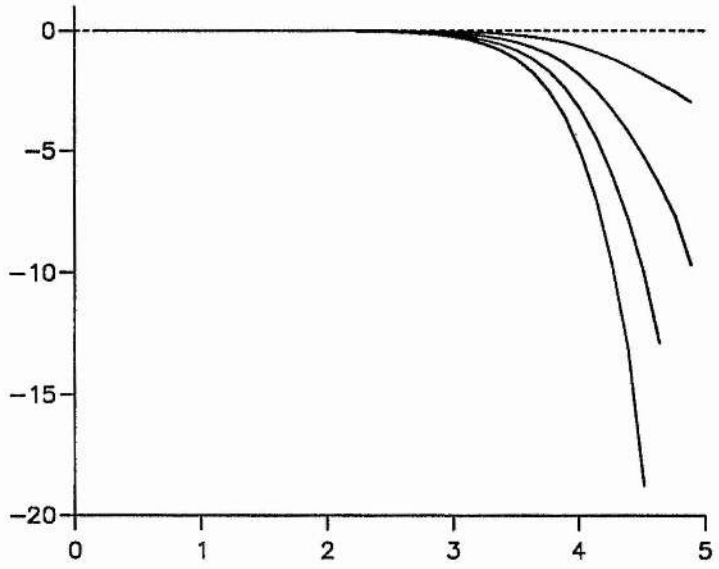

Figure 6.3: Frequency shift (in nHz) vs. original frequency (in mHz) induced by an increase in chromospheric temperature from 4170K to 4500K (smallest shifts), 5000K, 5500K and 6000K (largest shifts).

The limit $C \to \infty$ brings us back to the dispersion relation (6.22).

Equation (6.33) is the dispersion relation for modes formed in the system comprising a linear polytrope model extending from $z = 0$ to a wall at $z = z_d$, overlain by an isothermal non-magnetic atmosphere. We can calculate mode frequencies from the dispersion relation (6.33); these modes display a similar form to those calculated from dispersion relation (6.22).

We can also calculate the changes in mode frequency introduced by a change in the temperature of the chromospheric model. Figure 6.3 shows the change in mode frequency induced by an increase in temperature from 4170K to 4500K, 5000K, 5500K and finally 6000K; the largest shifts are for the largest increase in temperature. To produce the curves, we allow n to vary from 0 to the highest possible value such that the mode frequency is less than the cut-off frequency, and plot the frequency shift against the original frequency.

We see that the effect of an increase in temperature on zero-degree modes is similar in form to that found for $l \neq 0$ modes, but that the magnitude of shifts is much smaller. This is understandable, since the influence of the chromosphere on modes occupying the

whole solar interior is expected to be less significant than its influence on modes confined to the outermost layers of the Sun, as is the case for high-degree modes.

This is the only chromospheric model which has as yet been applied to this problem. We conclude this chapter by summarising its findings, and suggesting some further applications of this approach.

6.4 Discussion

We have seen that a simple linear polytrope model can reproduce the linear dependence on n observed in actual zero-degree p-modes, and can give the mode frequencies reasonably close to those observed. Different values of the polytropic index m can alter the mode frequencies found; this feature could be exploited to give better agreement with the observations. We have also been able to calculate mode frequency shifts for a simple chromospheric model. We see that for an increase in temperature in the model, frequency shifts are of a similar form to those found in the study of $l \neq 0$ modes; the magnitude of the frequency shifts is, however, much smaller than for $l \neq 0$ modes.

It should now be possible to study the effect on zero-degree modes of several different chromospheric and solar interior features; some of these possibilities are discussed in section 7.2.

Chapter 7

Conclusions and further work

In this Chapter, we summarise the main findings of the thesis. We conclude with a brief description of some possibilities for further work suggested this thesis.

7.1 Conclusions

We now summarise the findings of the thesis, taking each Chapter in turn.

Chapter 2

For an isothermal chromosphere with a uniform horizontal magnetic field, the cut-off frequency is infinite, implying that modes may form at all frequencies.

The critical frequency for plasma motions in such a chromosphere depends on the particular wave variable being considered. The processes of reflection and refraction both operate to trap waves at frequencies above the acoustic cut-off.

In the special case of vertical propagation, a singular form of behaviour described as 'evanescent propagation' occurs. Again, there is no unique critical frequency, contrary to the findings of Musielak et al. (1992) and Stark and Musielak (1993); the latter paper apparently contains an error in its derivation of the critical frequency.

Chapter 3

The effect of frequency shift turnover observed in the 1–5mHz range can be reproduced by simultaneous increases in temperature and magnetic field strength in an isothermal chromosphere with a uniform horizontal magnetic field.

Chapter 4

The presence of a temperature gradient in the chromosphere can significantly modify the form of frequency shift curves, compared to those found for an isothermal chromosphere. In particular, the turnover effect is enhanced by an increase in temperature gradient along with simultaneous increases in chromospheric magnetic field strength and base temperature.

The effect of the chromosphere on p-mode frequencies may be viewed in terms of how 'open' or 'closed' the mode cavity is. Rapidly evanescent forms of wave motion in the chromosphere give a closed cavity, less rapidly evanescent motions give a more open cavity, and thus lower mode frequencies.

Chapter 5

Wave trapping by the increasing Alfvén speed in an isothermal chromosphere with a uniform magnetic field does allow the formation of high-frequency modes, that is, modes above the acoustic cut-off frequency.

Frequency shifts of these modes induced by simultaneous increases in chromospheric temperature and magnetic field strength agree well in form with observed frequency shifts.

Chapter 6

A simple linear polytrope model can yield mode frequencies which agree well with observed l=0 mode frequencies. We may use the same model to investigate the influence of the chromosphere on such modes.

7.2 Further work

Of the areas of study considered in this thesis, two are particularly suitable to further investigation: high-frequency modes (Chapter 5) and modes of zero degree (Chapter 6).

High-frequency modes

Our study has used an approximate eigenvalue condition to determine mode frequencies and thus frequency shifts in this high frequency range. It should be possible to develop an exact mathematical formulation of this problem. Instead of using Langer solutions in the interior, we may find exact solutions to the wave equation. These may be in the form of the confluent hypergeometric function solutions given in section 1.4.5, or we may find simpler solutions by considering regions of the interior where certain approximations are valid, and then matching the asymptotic limits of these solutions.

We should continue to use a numerical treatment of the chromosphere. However, further investigation of the behaviour of the canonical equation in $\nabla.v$, equation (1.24), may prove helpful, particularly since it has already given insight into the behaviour of chromospheric wave motions below the acoustic cut-off frequency. This may lead to a full physical explanation for the form of frequency shift curves in the high-frequency range. We should also consider the form of wave motions in the chromosphere in an attempt to make comparisons with observations of wave motions in that region.

It may prove useful to consider the effect of a non-isothermal chromosphere on high-frequency modes. This may assist in finding better numerical agreement with observed averaged frequency shift curves, particularly if the observational curves were presented in a way which took into account the l-dependence of p-mode frequency shifts.

Modes of zero degree

A model has been developed describing zero-degree modes, and which has been used to study the effect of an isothermal non-magnetic chromosphere. We may now study the effect on these modes of various other chromospheric and solar interior features.

Prime candidates are the chromospheric magnetic field and the strong magnetic field thought to reside at the base of the convection zone; both of these effects could be investigated using this approach. We could model the first feature by using our familiar isothermal chromospheric model with a uniform horizontal magnetic field; in this study the results of our investigation into vertical propagation would be particularly relevant. We could model the interior magnetic field by specifying a magnetic region somewhere in $[0, z_d]$; it may be simplest mathematically to specify an isothermal region containing a uniform horizontal magnetic field in the range $[z_m, z_d]$, where $0 < z_m < z_d$. Such investigations

should help assess the relative importance of chromospheric and interior magnetic fields in low-degree p-mode frequency shifts.

Appendix A

Evaluation of integrals in Bohr-Sommerfeld condition

In this Appendix we give further details of the evaluation of various integrals arising through the use of the Bohr-Sommerfeld condition. Our procedure is to present the integral requiring evaluation, give the transformation which yields an integrable form, and give the integral form used.

Derivation of simple WKB dispersion relation (section 1.4.4).

Here we consider the equation

$$\int_{z_1}^{z_2} \kappa(z)\, dz = (n - \frac{1}{2})\pi, \tag{A.1}$$

where

$$\kappa^2 = k_x^2 \left(\frac{A^2}{1 + z/z_0} - \frac{B^2}{(1 + z/z_0)^2} - 1 \right), \tag{A.2}$$

where

$$A^2 = \frac{\omega^2}{k_x^2 c_{0L}^2}, \qquad B^2 = \frac{m(m+2)}{4k_x^2 z_0^2}, \tag{A.3}$$

and where z_1 and z_2 are the zeros of κ^2. We wish to evaluate the integral

$$I = \int_{z_1}^{z_2} \kappa(z)\, dz. \tag{A.4}$$

Make the transformation

$$s = 1 + z/z_0. \tag{A.5}$$

Then we may write equation (A.4) as

$$I = k_x z_0 \int_{s_1}^{s_2} \left(\frac{A^2}{s} - \frac{B^2}{s^2} - 1 \right)^{1/2} ds, \tag{A.6}$$

where s_1 and s_2 are the roots of

$$A^2 s - B^2 - s^2 = 0. \tag{A.7}$$

Now

$$\int \left(\frac{A^2}{s} - \frac{B^2}{s^2} - 1 \right)^{1/2} ds = \left(A^2 s - s^2 - B^2 \right)^{1/2}$$

$$+ \frac{1}{2} A^2 \sin^{-1} \left[\frac{2s - A^2}{(A^4 - 4B^2)^{1/2}} \right] - B \sin^{-1} \left[\frac{A^2 s - 2B^2}{s(A^4 - 4B^2)^{1/2}} \right] \tag{A.8}$$

$$= F(s); \tag{A.9}$$

thus

$$\begin{aligned} I &= F(s_2) - F(s_1) \\ &= k_x z_0 \left[\frac{1}{2} A^2 - B \right] \pi. \end{aligned} \tag{A.10}$$

Equations (A.1) and (A.10) then yield the dispersion relation displayed as equation (1.63).

Derivation of dispersion relation for isothermal magnetic chromosphere (section 3.4).

Here we consider the equation

$$(n + \alpha)\pi = \mathrm{I}_1 + \mathrm{I}_2. \tag{A.11}$$

The integral I_1 is given by

$$I_1 = \int_{z_1}^{0} \kappa(z)\, dz, \tag{A.12}$$

where

$$\kappa^2 = \frac{\omega^2}{c_0^2 + v_0^2 \exp(-z/H)} - k_x^2, \tag{A.13}$$

and z_1 is the zero of κ^2 in $z < 0$.

The integral I_2 is given by

$$I_2 = \int_0^{z_2} \kappa(z)\, dz, \tag{A.14}$$

where

$$\kappa^2 = \frac{\omega^2}{c_{0L}^2(1 + z/z_0)} - k_x^2, \tag{A.15}$$

and z_2 is the zero of κ^2 in $z > 0$.

Let us evaluate I_2 first. This is a simplified case of the integration carried out above. Under the transformation (A.5), equation (A.14) becomes

$$I_2 = k_x z_0 \int_1^{s_2} \left(\frac{A^2}{s} - 1\right)^{1/2} ds, \tag{A.16}$$

where $A^2 = \omega^2/k_x^2 c_{0L}^2$ and $s_2 = A^2$.

Now

$$\int \left(\frac{A^2}{s} - 1\right)^{1/2} ds = s^{1/2}(A^2 - s)^{1/2} - \frac{1}{2}\sin^{-1}\left(1 - 2s/A^2\right). \tag{A.17}$$

Thus, from equation (A.16),

$$I_2 = k_x z_0 A^2 \left[\frac{\pi}{4} + \frac{1}{2}\sin^{-1}(1 - 2/A^2) - (A^2 - 1)^{1/2}\right]. \tag{A.18}$$

To evaluate I_1, make the substitution

$$\frac{v_0^2}{c_0^2}\exp(-z/H) = \frac{1}{s}, \tag{A.19}$$

Equation (A.12) then becomes

$$I_1 = k_x H \int_{s_1}^{s_2} \left(\frac{C^2 s}{1 + s} - 1\right)^{1/2} \frac{1}{s}\, ds, \tag{A.20}$$

where

$$C^2 = \frac{\omega^2}{k_x^2 c_0^2}, \tag{A.21}$$

and

$$s_1 = \frac{1}{C^2 - 1}, \qquad s_2 = \frac{c_0^2}{v_0^2}. \tag{A.22}$$

Now

$$\int \left(\frac{C^2 s}{1 + s} - 1\right)^{1/2} \frac{1}{s}\, ds = -\sin^{-1}\left[\frac{C^2 s - 2s - 2}{C^2 s}\right] + (C^2 - 1)^{1/2}\log \mathcal{G}, \tag{A.23}$$

where

$$\mathcal{G} = 2(C^2-1)^{1/2}(1+s)^{1/2}(C^2 s - s - 1)^{1/2} + 2C^2 s - 2s + C^2 - 2. \tag{A.24}$$

Thus, from equation (A.20),

$$I_1 = \frac{r^{1/2}}{\gamma}(\Omega^2 - r)^{1/2}\log X - \frac{r}{\gamma}\left[\frac{\pi}{2} + \sin^{-1}\left(1 - \frac{2r(1+\sigma)}{\Omega^2}\right)\right], \tag{A.25}$$

where $r = \gamma k_x H$, $\sigma = v_0^2/c_0^2$ and

$$X = \frac{2}{\sigma\Omega^2}(\Omega^2 - r)^{1/2}[\Omega^2 - r(1+\sigma)]^{1/2}(1+\sigma)^{1/2} + \frac{2}{\sigma\Omega^2}(\Omega^2 - r)(1+\sigma/2) - \frac{r}{\Omega^2}.$$

Equations (A.11), (A.18) and (A.25) then give the dispersion relation displayed as equation (3.18).

Derivation of dispersion relation for the algebraic fast speed profile (section 3.5).

For this problem we again consider equation (A.11), but with a different form for the integral I_1. Here,

$$I_1 = \int_{z_1}^{0} \kappa(z)\, dz, \tag{A.26}$$

where

$$\kappa^2(z) = \frac{\omega^2}{c_{f\infty}^2[1 - A^2/(1 - z/B^2)]} - k_x^2, \tag{A.27}$$

and z_1 is the zero of κ^2 in $z < 0$. Under the transformation

$$s = 1 - z/B^2, \tag{A.28}$$

equation (A.26) becomes

$$I_1 = B^2 k_x (1 - D^2)^{1/2} \int_1^{s_1} \left[\frac{A^2 D^2/(1-D^2)}{s - A^2} - 1\right]^{1/2} ds, \tag{A.29}$$

where $D^2 = \omega^2/k_x^2 c_{f\infty}^2$ and $s_1 = A^2/(1 - D^2)$.

Now

$$\int \left[\frac{A^2 D^2/(1-D^2)}{s - A^2} - 1\right]^{1/2} ds = \frac{A^2 D^2}{2(1-D^2)} \sin^{-1}\left[\frac{2(s - A^2)}{A^2 D^2/(1-D^2)} - 1\right]$$

$$+ (s - A^2)^{1/2}\left[\frac{A^2 D^2}{1 - D^2} - (s - A^2)\right]^{1/2}. \tag{A.30}$$

Thus we find that

$$I_1 = B^2 k_x (1-D^2)^{1/2} \left\{ \frac{A^2 D^2}{1-D^2} \frac{\pi}{4} - \frac{A^2 D^2}{2(1-D^2)} \sin^{-1} \left[\frac{2(1-A^2)}{A^2 D^2/(1-D^2)} - 1 \right] \right.$$

$$\left. - (1-A^2)^{1/2} \left(\frac{A^2}{1-D^2} - 1 \right)^{1/2} \right\}. \quad \text{(A.31)}$$

After some rearrangement, equations (A.11), (A.18) and (A.31) give the dispersion relation displayed as equation (3.28).

Derivation of dispersion relation for the hyperbolic tangent fast speed profile (section 3.6).

For this problem we again consider equation (A.11), but with a different form for the integral I_1. Here,

$$I_1 = \int_{z_1}^{0} \kappa(z)\, dz, \quad \text{(A.32)}$$

where

$$\kappa^2(z) = \frac{\omega^2}{c_I^2 + c_P^2 \tanh(-z/B^2 - D^2)} - k_x^2, \quad \text{(A.33)}$$

and z_1 is the zero of κ^2 in $z < 0$. Under the transformation

$$s = 1 + \frac{c_P^2}{c_I^2} \tanh(-z/B^2 - D^2), \quad \text{(A.34)}$$

equation (A.32) becomes

$$I_1 = \frac{k_x B^2}{F^2} \int_{s_1}^{s_2} \left(\frac{E^2}{s} - 1 \right)^{1/2} \frac{1}{F^4 - (s-1)^2}\, ds, \quad \text{(A.35)}$$

where

$$E^2 = \omega^2/k_x^2 c_I^2, \qquad F^2 = c_P^2/c_I^2, \quad \text{(A.36)}$$

and

$$s_1 = E^2, \qquad s_2 = 1 - F^2 \tanh D^2. \quad \text{(A.37)}$$

Now

$$\int \left(\frac{E^2}{s} - 1 \right)^{1/2} \frac{1}{F^4 - (s-1)^2}\, ds = \frac{F^2 + E^2 - 1}{2F^2(F^4 - E^2 + E^2F^2 - 2F^2 + 1)^{1/2}} \sin^{-1} \mathcal{H}$$

$$+ \frac{F^2 - E^2 + 1}{2F^2(F^4 - E^2 - E^2F^2 + 2F^2 + 1)^{1/2}} \sin^{-1} \mathcal{J}, \quad \text{(A.38)}$$

where

$$\mathcal{H} = \frac{(E^2+2F^2-2)(F^2+s-1)-2F^4+2E^2-2E^2F^2+4F^2-2}{(F^2+s-1)E^2}$$

and

$$\mathcal{J} = \frac{(-E^2+2F^2+2)(F^2-s-1)-2F^4+2E^2+2E^2F^2-4F^2-2}{(F^2-s+1)E^2}$$

Thus after some lengthy algebra we find that

$$I_1 = k_x F^2 H_i \left\{ \frac{(F^2+E^2-1)^{1/2}}{(F^2-1)^{1/2}} \left[\frac{\pi}{4} - \frac{1}{2}\sin^{-1} X_1 \right] \right.$$
$$\left. - \frac{(F^2-E^2-1)^{1/2}}{(F^2+1)^{1/2}} \left[\frac{\pi}{4} - \frac{1}{2}\sin^{-1} X_2 \right] \right\}, \qquad \text{(A.39)}$$

where

$$X_1 = 1 + \frac{2(F^2-1)}{E^2} - \frac{2(F^2-1)(F^2+E^2-1)}{E^2F^2(1-\tanh D^2)},$$

and

$$X_2 = 1 - \frac{2(F^2-1)}{E^2} + \frac{2(F^2+1)(F^2-E^2+1)}{E^2F^2(1+\tanh D^2)}.$$

Equations (A.11), (A.18) and (A.39) then give the dispersion relation displayed as equation (3.32).

Evaluation of Langer solution variable $t_1(0)$ (section 4.2.5).

We wish to determine the value of the variable $t_1(z)$ at the point $z = 0$. The form of $t_1(z)$ depends on the sign of z_1 as follows:

$$\frac{2}{3}[t_1(0)]^{3/2} = \int_0^{z_1} [-\kappa^2(w)]^{1/2}\, dw, \qquad z_1 > 0, \qquad \text{(A.40)}$$

$$\frac{2}{3}[-t_1(0)]^{3/2} = \int_{z_1}^{0} \kappa(w)\, dw, \qquad z_1 < 0, \qquad \text{(A.41)}$$

where

$$\kappa^2 = k_x^2 \left(\frac{A^2}{1+z/z_0} - \frac{B^2}{(1+z/z_0)^2} - 1 \right), \qquad \text{(A.42)}$$

where

$$A^2 = \frac{\omega^2}{k_x^2 c_{0L}^2}, \qquad B^2 = \frac{m(m+2)}{4k_x^2 z_0^2}, \qquad \text{(A.43)}$$

and where z_1 is the zero of κ^2 near $z = 0$.

Let us consider the case where $z_1 < 0$. In this case we may use the transformation (A.5) and the integral (A.8) to find

$$\frac{2}{3}[-t_1(0)]^{3/2} = k_x z_0 \left\{ \left(\frac{A^2}{2} - B \right) \frac{\pi}{2} + (A^2 - B^2 - 1)^{1/2} \right.$$

$$\left. - \frac{1}{2} A^2 \sin^{-1} \left[\frac{2 - A^2}{(A^4 - 4B^2)^{1/2}} \right] + B \sin^{-1} \left[\frac{A^2 - 2B^2}{(A^4 - 4B^2)^{1/2}} \right] \right\}. \tag{A.44}$$

When $z_1 > 0$ we must evaluate the integral

$$I = \int_0^{z_1} \left[-\kappa^2(z) \right]^{1/2} dz. \tag{A.45}$$

Under the transformation (A.5) equation (A.45) becomes

$$I = k_x z_0 \int_1^{s_1} \left(1 - \frac{A^2}{s} + \frac{B^2}{s^2} \right)^{1/2} ds. \tag{A.46}$$

Now

$$\int \left(1 - \frac{A^2}{s} + \frac{B^2}{s^2} \right)^{1/2} ds = (s^2 - A^2 s + B^2)^{1/2}$$

$$- \frac{1}{2} A^2 \log \left[2(s^2 - A^2 s + B^2) + 2s - A^2 \right]$$

$$- B \log \left[\frac{2B(s^2 - A^2 s + B^2)^{1/2} - A^2 s + 2B^2}{s} \right]. \tag{A.47}$$

After some algebra, we find from equation (A.46) that

$$\frac{2}{3}[t_1(0)]^{3/2} = k_x z_0 \left\{ -\frac{1}{4}(A^2 + 2B) \log(A^4 - 4B^2) - (1 - A^2 + B^2)^{1/2} \right.$$

$$+ \frac{1}{2} A^2 \log \left[A^2 - 2 - 2(1 - A^2 + B^2)^{1/2} \right]$$

$$\left. + B \log \left[2B(1 - A^2 + B^2)^{1/2} - A^2 + 2B^2 \right] \right\}. \tag{A.48}$$

We use equations (A.44) and (A.48) to evaluate $t_1(0)$ for use in the modified Bohr-Sommerfeld condition.

Bibliography

Abramovitz, M. J. and Stegun, I. A. (1967). *Handbook of Mathematical Functions*, Dover.

Adam, J. A. (1975). PhD thesis, University of London.

Adam, J. A. (1977). *Solar Phys.* **52**: 293.

An, C.-H., Musielak, Z. E., Moore, R. L. and Suess, S. T. (1989). *Ap. J.* **345**: 597.

Balmforth, N. and Gough, D. O. (1990). *Ap. J.* **362**: 256.

Bender, C. M. and Orszag, S. A. (1987). *Advanced Mathematical Methods for Scientists and Engineers*, McGraw Hill.

Bogdan, T. J. (1987). *Ap. J.* **318**: 889.

Bogdan, T. J. (1989). *in* E. Leer and P. Maltby (eds), *Workshop on Flux Tubes in the Solar Atmosphere*, University of Oslo, p. 101.

Bogdan, T. J. and Cattaneo, F. (1989). *Ap. J.* **342**: 545.

Bogdan, T. J. and Zweibel, E. G. (1985). *Ap. J.* **298**: 867.

Campbell, W. R. (1989). PhD thesis, University of St. Andrews.

Campbell, W. R. and Roberts, B. (1988). *in* J. Christensen-Dalsgaard and S. Frandsen (eds), *IAU Symposium 123: Advances in Helio- and Asteroseismology*, Dordrecht, p. 161.

Campbell, W. R. and Roberts, B. (1989). *Ap. J.* **338**: 538.

Christensen-Dalsgaard, J. (1980). *M.N.R.A.S.* **190**: 765.

Christensen-Dalsgaard, J., Duvall, T. L., Gough, D. O., Harvey, J. W. and Rhodes, E. J. (1985). *Nature* **315**: 378.

Cowling, T. G. (1941). *M.N.R.A.S.* **101**: 367.

Deubner, F.-L. (1975). *Astron. and Astrophys.* **371**: 44.

Deubner, F.-L. and Gough, D. O. (1984). *Ann. Rev. Astron. Astrophys.* **22**: 593.

Duvall Jr., T. L., Harvey, J. W., Jefferies, S. M. and Pomerantz, M. A. (1991). *Ap. J.* **373**: 308.

Elsworth, Y., Howe, R., Isaak, G. R., McLeod, C. P. and New, R. (1990). *Nature* **345**: 322.

Evans, D. J. (1991). PhD thesis, University of St. Andrews.

Evans, D. J. and Roberts, B. (1990). *Ap.J.* **356**: 704.

Evans, D. J. and Roberts, B. (1991). *Ap.J.* **371**: 387.

Evans, D. J. and Roberts, B. (1992). *Nature* **355**: 230.

Fernandes, D. N., Scherrer, P. H., Tarbell, T. D. and Title, A. M. (1992). *Ap. J.* **392**: 736.

Giovanelli, R. G. (1980). *Solar Phys.* **68**: 49.

Giovanelli, R. G. and Jones, H. P. (1982). *Solar Phys.* **79**: 267.

Goedblood, J. P. (1971). *Physica* **53**: 512.

Goldreich, P., Murray, N. and Kumar, P. (in press). *Ap. J.*

Goldreich, P., Murray, N., Willette, G. and Kumar, P. (1991). *Ap.J.* **370**: 752.

Jain, R. (1992). PhD thesis, University of St. Andrews.

Jain, R. and Roberts, B. (1993). *Ap. J.* **414**: 898.

Jones, H. P. and Giovanelli, R. G. (1983). *Solar Phys.* **87**: 37.

Kumar, P. and Lu, E. (1991). *Ap. J.* **373**: 308.

Lamb, H. (1932). *Hydrodynamics*, Cambridge University Press.

Langer, R. E. (1934). *Trans. Am. Math. Soc.* **36**: 90.

Leibacher, J. W. and Stein, R. F. (1971). *Astrophys. Lett.* **7**: 191.

Leighton, R. B. (1960). *Proc. IAU Symp.*, Vol. 12, p. 321.

Libbrecht, K. G. (1988). *Ap. J.* **334**: 510.

Libbrecht, K. G. and Woodard, M. F. (1990). *Nature* **345**: 779.

Libbrecht, K. G. and Woodard, M. F. (1991). *Ap.J.* **374**: L61.

Libbrecht, K. G., Woodard, M. F. and Kaufman, J. M. (1990). *Ap.J. Suppl.* **74**: 1129.

Musielak, Z. E., An, C.-H., Moore, R. L. and Suess, S. T. (1989). *Ap. J.* **344**: 478.

Musielak, Z. E., Fontenla, J. M. and Moore, R. L. (1992). *Phys. Fluids B* **4**: 13.

Nayfeh, A. H. (1983). *Introduction to Perturbation Techniques*, Wiley.

Nye, A. H. and Thomas, J. H. (1976). *Ap. J.* **204**: 573.

Priest, E. R. (1982). *Solar Magnetohydrodynamics*, Reidel.

Roberts, B. (1985). Magnetohydrodynamic waves, *in* E. R. Priest (ed.), *Solar System Magnetic Fields*, Reidel.

Roberts, B. and Campbell, W. R. (1986). *Nature* **323**: 603.

Ronan, R. S. and LaBonte, B. J. (1993). *in* T. Brown (ed.), *GONG 1992: Seismic Investigation of the Sun and Stars*, Vol. 42 of *Astron. Soc. Pacific Conf. Series*, p. 93.

Ronan, R. S., Cadora, K. M. and LaBonte, B. J. (1993). *Solar Physics (Letters).* (in press).

Spruit, H. C. and Roberts, B. (1983). *Nature* **304**: 401.

Stark, B. A. and Musielak, Z. E. (1993). *Ap. J.* **409**: 450.

Thomas, J. H. (1982). *Ap. J.* **262**: 760.

Ulrich, R. K. (1970). *Ap. J.* **162**: 993.

Ulrich, R. K. (1993). Personal communication.

Wright, A. N. and Thompson, M. J. (1992). *Astron. and Astrophys.* **264**: 701.

Zweibel, E. G. and Bogdan, T. J. (1986). *Ap. J.* **308**: 401.

Zweibel, E. G. and Däppen, W. (1989). *Ap.J.* **343**: 994.